Universidad Autónoma de Madrid

Instituto de Física teórica

Study of Mesonic Observables from a Mixed Action Lattice QCD Formalism

Author
Jose A. Romero Jurado

Supervisor
Gregorio Herdoiza

A thesis submitted in fulfillment of the requirements for the degree of Doctor of Philosophy

in

Theoretical physics

Instituto de Física Teórica
UAM-CSIC

Abstract

We propose a Lattice QCD mixed-action approach in with sea quarks regularize using $N_f = 2 + 1$ non-perturbatively $\mathcal{O}(a)$-improved Wilson fermions with open boundary conditions in the time direction, while a Wilson twisted mass action at maximal twist is used for valence quarks. In this setup, fermionic observables are free from $\mathcal{O}(a)$ lattice artifacts proportional to the valence quark masses.

Two alternative procedures for the matching of sea and valence quark masses are discussed. We perform a universality check by comparing continuum limit extrapolations of the quark masses and of the pseudoscalar meson decay constants obtained with two setups: the mixed action and the standard approach where Wilson fermions are used in sea and valence sectors.

We use the gradient flow scale t_0 and physical input from the pion and kaon decay constants to carry out a scale setting procedure. This is applied to the determination of the light and strange quark masses. A particular attention is given to the statistical analysis of the lattice data and to the assessment of the systematic uncertainties.

Abstract

Presentamos una acción mixta para QCD en el retículo donde los fermiones del sector del mar son discretizados mediante una acción $N_f = 2+1$ no perturbativa sin efectos de discretización $\mathcal{O}(a)$. Asimismo, los fermiones de valencia son rotados quiralmente a un punto donde la masa de quark tiene únicamente componente quiral y la masa estándar se anula.

Se discuten dos alternativas para hacer la correspondencia entre las masas de los quarks del sector del mar y de valencia. Llevamos a cabo un control de la validez de la acción mixta mediante una comparación de la extrapolación al continuo de las masas de quarks y de los factores de decaimiento mesonicos de dicha acción con la acción unitaria Wilson.

Se implementa un método para fijar la escala reticular y determinar las masas de quarks del sector ligero y extraño. Se presta particular atención al análisis estadístico de los resultados y a la estimación del error sistemático.

Contents

Chapter 1

Introduction

In our current understanding of Nature, there are four fundamental forces corresponding to the gravitational, electromagnetic, weak and strong interactions. The Standard Model (SM) is built on a combination of relativistic Quantum Field Theories (QFT), the electro-weak theory, which unifies the electromagnetic and weak forces, and Quantum Chromodynamics (QCD), describing the strong interactions. Although it cannot fully explain many features observed in Nature, such as gravity, the SM has successfully predicted a vast number of experimental results over the years. It is, therefore, widely accepted to behave as an effective theory able to describe the laws of physics up to an energy scale above which a more fundamental theory is required.

QFT is the mathematical framework that combines the laws of Quantum Mechanics with the relativistic classical field theory. Matter particles are defined as excited states of their underlying dynamical fermionic fields. In this framework, interactions arise naturally from gauge symmetries, i.e., local transformations that leave the Lagrangian invariant. In most gauge theories the set of possible transformations is a finite-dimensional Lie Group, with bosonic force carriers belonging to the adjoint representation.

QCD is a gauge theory whose charge, called color, is carried by elementary particles, the quarks and the gluons. The properties of these particles can be described by representations of the Lie algebra. The non-abelian $SU(3)$ Lie Group is the one associated to QCD. In this theory, each quark flavour belongs to the fundamental representation ($\mathbf{3}$) of the Lie Algebra $su(3)$, while gluons pertain to the adjoint representation ($\mathbf{8}$) [1–5]. Such gluon fields are represented by the field $A_\mu(x)$, and can be decomposed in terms of the Gell-Mann matrices λ_c acting in color space

$$A_\mu(x) = \sum_{c=1}^{8} \lambda_c A_{\mu,c}(x), \qquad T_c = \frac{\lambda_c}{2}, \tag{1.1}$$

where T_c are the generators of the $su(3)$ algebra. The dynamics of QCD can be derived from its Lagrangian, which is defined as follows

$$\mathcal{L} = \sum_{f=1}^{N_f} \left[\overline{\psi}^f \left(iD_0 - m_{0,f}\right) \psi^f\right] + \frac{1}{4} F_{\mu\nu} F_{\mu\nu}, \tag{1.2}$$

up to gauge-fixing terms. The fermion field corresponding to the flavor f is denoted by $\psi^f(x)$, N_f is the number of fermion flavors and $F_{\mu\nu}$ is the gluonic field strength tensor. [1]

The invariance of the Lagrangian under local $SU(3)$ transformations, leads to the appearance of an interaction term in the Dirac operator [2]

$$D_0 = \sum_{\mu=0}^{3} \gamma_\mu \left(\partial_\mu + iA_\mu(x)\right) \equiv \sum_{\mu=0}^{3} \gamma_\mu \nabla_\mu, \tag{1.3}$$

where ∇_μ is the gauge covariant derivative.

The SM is a renormalized gauge theory defined by the local $SU(3) \times SU(2) \times U(1)$ gauge symmetry. With respect to the electro-weak theory, $SU(2) \times U(1)$, QCD shows specific features that require different techniques in order to compute physical observables. In particular, QCD is a non-abelian theory that contains gluonic fields that do not commute, leading to the following expression for the gluonic field strength tensor

$$F_{\mu\nu}(x) = \partial_\mu A_\nu(x) - \partial_\nu A_\mu(x) + i\left[A_\mu(x), A_\nu(x)\right]. \tag{1.4}$$

This induces non-trivial self-interations between gluons. This feature gives rise to non-perturbative (NP) effects, which are a major difference with respect to Quantum Electrodynamics (QED).

Furthermore, QCD is an *asymptotically free* theory [6,7] for the $N_f = 6$ number of flavors observed in Nature. This means that quarks and gluons interact very weakly at high energies, *i.e.*, short distances. This property is proved through the high-energy behavior of the beta function

$$\beta(g) = \frac{\mathrm{d}g(\mu)}{\mathrm{d}\left(\log\mu\right)}, \tag{1.5}$$

that measures the variation of the strong coupling constant g with respect to the energy scale μ. A perturbative expression of the beta function reads

$$\beta(g) = -\frac{g^3}{(4\pi)^2}\left(11 - \frac{2}{3}N_f\right) + \mathcal{O}(g^5). \tag{1.6}$$

[1] Dirac or spin indices are represented by the first Greek alphabet letters while Latin letters refer to color indices. These indices may be suppressed as appropriate. Lorentz indices will be represented by μ and ν.

[2] The 0 subindex in the Dirac operator will refer to the massless Dirac operator.

Since $\beta(g)$ is shown to be negative for the $SU(3)$ group with $N_f = 6$, quarks tend to behave asymptotically as free particles as the energy increases. In this regime, an expansion in the coupling constant can be performed and the convergence properties of perturbation theory (PT) improve as the energy scale increases.

On the other hand, one observes that the coupling constant grows logarithmically as the energy scale decreases. In this regime another important feature of QCD, known as *confinement*, appears. Quarks or any combination of them, that carry a colored charge, are not observed in Nature, only color singlet states appear as physical observables. Mesons and baryons are the most common QCD bound states, formed by a quark and an anti-quark and by three different quark fields, respectively, but any other color singlet state may exist. Recent experimental results have also provided evidence of the existence of tetraquarks [8] and pentaquarks [9].

At the QCD scale, others non-perturbative phenomena appear, as the spontaneous breaking of chiral symmetry. In this regime where the coupling constant is not small enough to apply perturbation theory, non-perturbative methods are required. The only method derived from first principles to explore this regime is Lattice QCD (LQCD). Efective Field Theories (EFTs) are also a useful tool to explore a particular range of energies. In the context of EFTs, QCD can be matched to another field theory that respects the symmetries of QCD while containing only a subset of its degrees of freedom. However, effective theories rely on a number of couplings depending on the energy scale, which must be estimated either experimentally or through LQCD computations. Chiral Perturbation Theory (ChPT) and Heavy Quark Effective Theory (HQET) are examples of effective field theories describing the massless and the heavy quark limit, respectively.

LQCD is based on a discretization of Euclidean space-time into a hypercubic grid whose distance between sites is given by the lattice spacing, a. Subsequently, a discretized version of the QCD action in terms of gluonic and fermionic fields can be constructed. LQCD computations require neither model assumptions nor additional physical parameters than those of the continuum theory.

The lattice regularization was originally introduced by Wilson [5] in the seventies. In recent years, we have witnessed a number of developments due to the increase of computing resources and the improvement of the algorithms. Simulating quark masses in the sea requires the inversion of the Dirac operator, which is a demanding task specially for the lightest quark masses. Despite the progress in this field, dynamical simulations at physical quark masses are still very demanding and additional information from an extrapolation employing heavier masses is often used.

In Chapter 2, we review some concepts of LQCD, emphasizing in the development of a discretized version of the QCD action and its renormalization properties. In Chapter 3, we develop a setup, based in a mixed action, with the aim of re-

moving some of the leading discretization effects in the computation of physical observables. The algorithms involved in the dynamical simulation of the gauge configurations, as well as the strategy followed for the statistical analysis, are detailed in Chapter 4. Finally in Chapter 5, we present the results for the scale setting and the physical quark masses, in both Wilson and the mixed action regularizations.

Chapter 2

Lattice QCD

In this Chapter, we review some of the main theoretical elements of LQCD, from the discretization of the fields and action to the implementation of the renormalization factors in a discretized space-time. We also describe the basic steps required to perform a LQCD computation.

Observables on the lattice are computed through the path integral formalism, as shown in Section 2.2. In this formulation, the functionals that represent the fields are weighted by a Boltzmann factor depending on the action. To avoid an imaginary argument in the exponential that would lead to large fluctuations of the integrand, the Minkowski space-time metric is transformed into a Euclidean space by applying a *Wick rotation*, where the time coordinate becomes imaginary $x_0 = i\tau$. Consequently, the volume element becomes [1]

$$d^4x^{(M)} = d\tau dx_1 dx_2 dx_3 \quad \longrightarrow \quad d^4x^{(E)} = i dx_0 dx_1 dx_2 dx_3. \tag{2.1}$$

The discretization of space-time by the lattice spacing a in a finite volume involves a redefinition of the coordinates in terms of a label $n \in \Lambda$

$$\Lambda = \{n_0, n_1, n_2, n_3 \mid n_0 = 0, ..., N_t - 1,\ n_i = 0, ..., N_s - 1\ \ \forall i = 1, 2, 3\}\,, \tag{2.2}$$

where the spatial lattice size is given by $L = aN_s$ and the Euclidean time range from 0 to $T = aN_t$. In these terms, the position coordinates are discretized as follows

$$x = (x_0, x_1, x_2, x_3) = a(n_0, n_1, n_2, n_3). \tag{2.3}$$

The theory is built in a way that the broken symmetries are recovered when a vanishes and the lattice volumen, V, goes to infinity. Gauge symmetry is specifically preserved, but other symmetries, such as the translational invariance and

[1] The upper index M and E in brackets denotes Minkowski and Euclidean space-time, respectively.

continuous rotations, are broken and recovered only once the extrapolation to the continuum limit is carried out.

This regularization has the advantage that the inverse of the lattice spacing acts as a maximum energy, suppressing the ultra-violet divergences that appears in loop integrals, while the finite volume gets rid of the infrared divergences. On the other hand, LQCD computations receive finite volume and discretization effects that need to be addressed.

In Section 2.1, we explain how to formulate gluonic and fermionic fields on the lattice. In Sections 2.4 and 2.5, we describe how to construct a discretized version of the QCD action. In Section 2.2, the path integral is then introduced as the standard lattice approach to estimate expectation values of physical observables, and will be related to the Euclidean correlators in Section 2.3. In Section 2.6, we describe the techniques used to reduce the discretization effects. Sections 2.7 and 2.8 address the discretized version of the Ward-Takahashi identities and the renormalization of quark bilinears, respectively.

2.1 Fields on the lattice

On the lattice, gluon fields are elements of the Lie Group $SU(3)$ unlike the vector potential $A_\mu(x)$, which belongs to the Lie Algebra $su(3)$ in the continuum theory. In contrast to the Lie Algebra, elements of the Lie group are allowed to carry out non-infinitesimal transformations between neighboring positions of the lattice. Such a construction allows to preserve gauge symmetry.

Gluon fields, as $SU(3)$ elements, must leave the action invariant under local rotations in color space. These rotations are performed by the matrices, $\Omega_i(x) \in SU(3)$, of the defining representation corresponding to a set of 3×3 complex matrices that are unitary [2] and whose determinant is 1.

By construction, quarks are constrained to occupy the sites of the lattice grid, while gluons, connect neighboring sites. The quarks fields are described on the lattice by Dirac 4-spinors whose Dirac, color and flavor indices are represented by $\alpha = 1, 2, 3, 4$, $c = 1, 2, 3$ and $f = u, d, s, \ldots$ respectively

$$\overline{\psi}^f(x)_{\substack{\alpha \\ c}}, \quad \psi^f(x)_{\substack{\alpha \\ c}}. \tag{2.4}$$

The spinor $\overline{\psi}$ denotes the antiparticle of ψ and x is the position in the space-time lattice. Notice that unlike what happens in the Minkowski metric, where ψ and $\overline{\psi}$ are related by γ_0, in the Euclidean space-time they must be treated as independent variables.

[2] A matrix Ω is unitary iff $\Omega\Omega^\dagger = \mathbb{1}$.

The quark spinors transform as follows

$$\begin{aligned}\psi'^f(x)_\alpha &= \Omega(x)\psi^f(x)_\alpha,\\ \overline{\psi}'^f(x)_\alpha &= \overline{\psi}^f(x)_\alpha\Omega^\dagger(x),\end{aligned} \tag{2.5}$$

under a color transformation. Since quarks are half-integer spin particles, they behave according to the Fermi-Dirac statistics, meaning that two quarks are not allowed to occupy the same energy state. This results in anti-commuting fields, that can be interpreted as *Grassmann* variables.

As a discrete version of the gluon fields A_μ, a set of fields $U_{\mu,c_1c_2}(x)$ defined as *links*, are proposed for every connection between sites of the lattice. The position of a site on the lattice is denoted by x, whereas $\mu = 0, 1, 2, 3$ points out the orientation in the Euclidean space. Color indices are c_1 and c_2, which are frequently not explicitly displayed. These fields, belonging to the fundamental representation of $SU(3)$, connect the sites x and $x+\hat{\mu}$, where $\hat{\mu}$ is the unitary vector pointing in the μ direction. By contrast, the adjoint operator, $U^\dagger_\mu(x)$, links the site x to the site $x-\hat{\mu}$, such that $U_{-\mu}(x) = U_\mu(x-\hat{\mu})^\dagger$. A random set of link variables placed over complete lattice volume is commonly denominated as the *gauge configuration*.

The gauge transformations act on the gluon fields as follows

$$\begin{aligned}U'_\mu(x) &= \Omega(x)U_\mu(x)\Omega(x+\hat{\mu})^\dagger,\\ U'^\dagger_\mu(x) &= \Omega(x+\hat{\mu})U_\mu(x)\Omega(x)^\dagger.\end{aligned} \tag{2.6}$$

Strictly speaking, link variables are the lattice counterparts of the continuum gauge transporters of the gluon fields A_μ. Gauge transporters, $G(a,b)$, are defined as the path-ordered exponential of a given field, A, along a curve $\mathcal{C}$ between the points a and b

$$G(a,b) = P\text{exp}\left(i\int_{\mathcal{C}} A\cdot ds\right). \tag{2.7}$$

The link $U_\mu(x)$ acts as a discrete gauge transporter between the sites x and $x+\hat{\mu}$

$$U_\mu(x) = \exp\left(iaA_\mu(x)\right), \tag{2.8}$$

$$= \exp\left(ia\sum_{c=1}^{8}\lambda_c A_{\mu,c}(x)\right), \tag{2.9}$$

where the path is approximated by its length a.

Neither the links nor the quark lattice fields are gauge invariant by themselves, but the action and lattice operators can be constructed by gauge invariant combinations of them. The fermionic spinor field contains 24 degrees of freedom, coming from the product of the possible choices of the color, spin and electromagnetic charge [3]. The gluon field contains 32 degrees of freedom as a combination of

[3]Note, however, that electromagnetic effects will be neglected in this work.

8 different possible colors and 4 components of the Lorentz indices. The number of degrees of freedom of such fields, together with the number of space-time points of the lattice, require specific algorithms optimized to perform numerical simulations.

In the next section, we introduce the path integral formalism.

2.2 Path integral

The expectation value of a physical observable can be computed through a lattice formulation of the path integral that allows to calculate time-ordered products of fields, known as correlators [10]

$$\langle T\left(O_1(x_1)O(x_2)...O_N(x_N)\right)\rangle = \frac{1}{Z}\int \mathcal{D}[\psi,\overline{\psi},U]O_1(x_1)O(x_2)...O_N(x_N)e^{-S}, \quad (2.10)$$

$$Z = \int \mathcal{D}[\psi,\overline{\psi},U]e^{-S}. \quad (2.11)$$

The integration measure $\mathcal{D}[\psi,\overline{\psi},U]$ is the product of integration measures of all link and quark fields, defined in Section 2.1, over all their internal components and lattice positions. The partition function Z is also defined as a path integral ensuring the proper normalization. It can be identified as the vacuum to vacuum amplitude of the Euclidean space-time. The time-ordering operation T orders the operators according to descending time. The Wick rotation performed on the lattice in eq. (2.1) allows the action, defined as the integral over the Lagrangian density

$$S = S_G + S_F = \int d^4x\mathcal{L}_G + \int d^4x\mathcal{L}_F, \quad (2.12)$$

to act as a Boltzmann weight factor. The gluonic and fermionic part of the action are $S_G[U]$ and $S_F[\psi,\overline{\psi},U]$, respectively, and will be introduced in Sections 2.4 and 2.5.

The path integral is evaluated over all field configurations and space-time positions in order to consider the quantum fluctuations around the classical trajectory. Each integral is performed over a compact domain and, considering that the number of integrals is finite, the entire path integral becomes a high dimensional integral. As the lattice spacing becomes smaller the computation cost of the integral grows and demands the application of specific techniques as the ones described in Section 4.1.

As stated in Section 2.1, the anti-commuting nature of the fermion fields implies that they must be treated as Grassmann variables during the integration. The path

integral can be split into a fermion integral nested within a pure gauge integral

$$\langle O \rangle = \frac{1}{Z} \int \mathcal{D}[\psi, \overline{\psi}, U] O e^{-S_G[U] - S_F[\psi, \overline{\psi}, U]}, \tag{2.13}$$

$$\langle\langle O \rangle\rangle_U = \frac{1}{Z} \int \mathcal{D}[U] e^{-S_G[U]} Z_F[U] \left[\frac{1}{Z_F[U]} \int \mathcal{D}[\psi, \overline{\psi}] O e^{-S_F[\psi, \overline{\psi}, U]} \right]. \tag{2.14}$$

To integrate out the fermionic part, let us employ a generalization of the *Matthews-Salam* formula [11, 12] in the presence of two external anti-commuting sources $\overline{\eta}$ and η

$$\mathcal{Z}[\overline{\eta}, \eta] = \int \mathcal{D}[\psi, \overline{\psi}] e^{\left(\overline{\psi} A \psi + \overline{\eta} \psi + \overline{\psi} \eta\right)} = \det(A) e^{-\left(\overline{\eta} A^{-1} \eta\right)}. \tag{2.15}$$

The equation above is known as the *generating functional* for fermion fields, and has several applications. For instance, the fermionic partition function, Z_F, becomes a product of the Dirac operator determinants of the various quark flavors [4] when the sources are imposed to be zero

$$Z_F = \int \mathcal{D}[\psi, \overline{\psi}] \exp\left(\sum_{f=1}^{N_f} \overline{\psi}^f D^f \psi^f \right) = \prod_f^{N_f} \det(D^f). \tag{2.16}$$

Besides, operating with Grassmann variables implies to deal with non-positive definite matrices, leading to poor importance sampling and large variance in the observables. As detailed in Section 4.1, the fermions are integrated out and reintroduced in terms of bosonic *pseudofermion* fields by rewriting the resulting determinant through an analogous generating functional for bosonic fields. The formula shown in eq. (2.15), together with the properties of Grassmann variables, allows to derive the expression for any correlator. In particular, for the two-point function of fermion fields we find

$$\left\langle \overline{\psi}^{f_1}(x)_{c_1}^{\alpha_1} \psi^{f_2}(y)_{c_2}^{\alpha_2} \right\rangle = \frac{1}{a^4} \delta_{f_1 f_2} {D^{f_1}}^{-1}(x, y)_{c_1 c_2}^{\alpha_1 \alpha_2}, \tag{2.17}$$

corresponding to the propagator of a quark flavor f_1.

2.3 Euclidean correlator

The path integral formalism allows to relate the Euclidean correlator – initially defined in the QFT formalism and expressed in terms of the Hilbert operators $\hat{O}_i$ – to the integral of functionals O_i, which relies on the statistical field theory and can be numerically estimated.

[4] The discrete version of the Dirac operator will be defined in Section 2.5.

2.3.1 Euclidean correlator: Quantum Field Theory

The Euclidean correlator is defined in QFT as the expectation value of a product of normal ordered operators evaluated at different positions. These objects are expressed in terms of the Hilbert-space operators $\hat{O}_i$, and of the Hamiltonian $\hat{H}$, which measures the energy of the system and is responsible for the time evolution. A suitable choice of the operators allows to determine the energy spectrum and the matrix elements of the physical states with definite quantum numbers.

In particular, a correlator of two Hilbert space operators at different Euclidean times x_{0_1} and x_{0_2} is written as [5]

$$\langle O_2(x_{0_2})O_1(x_{0_1})\rangle_T = \frac{1}{Z}\mathrm{tr}\left[e^{-(T-x_{0_2})\hat{H}}\hat{O}_2 e^{-(x_{0_2}-x_{0_1})\hat{H}}\hat{O}_1 e^{-x_{0_1}\hat{H}}\right], \tag{2.18}$$

where the time dependent operators are rewritten as $\hat{O}(t) = e^{it\hat{H}}\hat{O}e^{-it\hat{H}}$, conforming to the Heisenberg picture, as long as the Hamiltonian does not vary with time. Z is called normalization factor and has a similar role to the partition function in statistical mechanics:

$$Z = \mathrm{tr}\left[e^{-T\hat{H}}\right]. \tag{2.19}$$

In the QFT formalism, the operator $\hat{O}_p$ annihilates a state with the quantum numbers of the particle p. On the other hand, the adjoint [6] operator $\hat{O}_p^\dagger$ creates a state with the quantum numbers of p. In this regard, the two-point correlator defined in eq. (2.18) can be understood as a function that creates or annihilates a particle defined by $\hat{O}_1$ at a given time x_{0_1} and does the equivalent at x_{0_2} with $\hat{O}_2$. In particular, the two-point function allows to extract masses and matrix elements from meson states on the lattice.

Hadronic matrix elements emerge by inserting the unit operator $\mathbb{1} = \sum_n |n\rangle\langle n|$ between the time-ordered operators, in any orthonormal basis $|n\rangle$ of the Hamiltonian

$$\langle O_2(x_{0_2})O_1(x_{0_1})\rangle_T = \frac{\sum\limits_{m,n,n'} \langle m|\, e^{-(T-x_{0_2})\hat{H}}\hat{O}_2\,|n\rangle\,\langle n|\, e^{-(x_{0_2}-x_{0_1})\hat{H}}\hat{O}_1\,|n'\rangle\,\langle n'|\, e^{-x_{0_1}\hat{H}}\,|m\rangle}{\sum\limits_{m'}\langle m'|\, e^{-T\hat{H}}\,|m'\rangle}. \tag{2.20}$$

The energy spectrum of the system is extracted by evaluating the Hamiltonian over the dual eigenvector basis. The vacuum energy can be removed from the exponentials so the energies are redefined in terms of their relative values. Applying

[5] The trace of a Hilbert operator is defined as $\mathrm{tr}\left[\hat{O}\right] = \sum\limits_n \langle n|\,\hat{O}\,|n\rangle$, where $|n\rangle$ is an orthonormal basis of the Hilbert space.

[6] The adjoint operator $\hat{O}_p^\dagger$ is defined such that $\langle n|\,\hat{O}_p\,|n'\rangle = \langle n'|\,\hat{O}_p^\dagger\,|n\rangle^*$.

then the inner product of the orthonormal basis, the two-point correlator simplifies as follows,

$$\langle O_2(x_{0_2})O_1(x_{0_1})\rangle_T = \frac{\sum\limits_{m,n} e^{-(T-\Delta x_0)\Delta E_m} e^{-\Delta x_0 \Delta E_n} \langle m|\hat{O}_2|n\rangle \langle n|\hat{O}_1|m\rangle}{\sum\limits_{m} e^{-T\Delta E_m}}, \quad (2.21)$$

becoming exclusively dependent of the time separation between the operators, $\Delta x_0 = x_{0_2} - x_{0_1}$.

The above expression can be used to isolate the ground state mass from the large Euclidean time separations Δx_0 where excited state contaminations are exponentially suppressed.

This procedure can be similarly applied to n-point correlation functions in order to study more complex processes. For instance, processes that involve an initial and a final hadron together with the insertion of an electromagnetic or a weak current.

2.3.2 Euclidean correlator: Path integral

The path integral formalism, introduced in Section 2.2, provides a well defined numerical method to estimate expectation values on the lattice. We define the hadron interpolators, $O\left[\psi, \overline{\psi}, U\right]$, as the functionals of gluon and quark fields which play a similar role to the creator and annihilation Hilbert operators.

In general, the interpolators create a wave function whose quantum numbers overlap with the ground state, but also with a complete set of excited states or multi-particle states that share those quantum numbers. The choice of the interpolator is not unique, and various alternatives may give rise to the same set of particles. Looking for different choices for the interpolators may be useful to isolate the ground state. As stated in Chapter 1, only color singlet states can be observed in Nature. In particular, we will be interested in mesonic states, constructed by interpolators made up of a quark and an antiquark.

The fermion fields used to define a given interpolating operator can be placed in the same site of the lattice, a situation known as *local interpolator*, or they can be located at separated spatial positions connected by gauge link variables. The latter is known as a *non-local* or *extended interpolator*.

Discrete symmetries can be incorporated in the definition of the interpolating field in such a way that it reproduces the quantum numbers of the target hadron. Transformations under parity and charge conjugation for gauge fields, as well as for quark and anti-quark fields, are described in Appendix C.

In a generic expression for a mesonic interpolation field

$$O_M(x_0, \boldsymbol{x}) = \sum_{\boldsymbol{y},\boldsymbol{z}} \overline{\psi}^{f_1}(x_0, \boldsymbol{y})^{\alpha_1}_{c_1} F(\boldsymbol{x}, \boldsymbol{y}, \boldsymbol{z})^{\alpha_1\alpha_2}_{c_1c_2} \psi^{f_2}(x_0, \boldsymbol{z})^{\alpha_2}_{c_2}, \quad (2.22)$$

a distribution function F characterizes the spatial distribution of the operator. The local meson interpolator is obtained by a particular choice of F

$$F(\boldsymbol{x},\boldsymbol{y},\boldsymbol{z})^{\alpha_1\alpha_2}_{c_1c_2} = \delta(\boldsymbol{x}-\boldsymbol{y})\delta(\boldsymbol{x}-\boldsymbol{z})\delta_{c_1c_2}\Gamma_{\alpha_1\alpha_2}, \tag{2.23}$$

that reduces eq. (2.22) to a single spatial point. Such a choice leads to the expression for the local interpolators:

$$O_{M,L}(x_0,\boldsymbol{x}) = \overline{\psi}(x_0,\boldsymbol{x})^{\alpha_1}_{c_1} T\Gamma_{\alpha_1\alpha_2}\psi(x_0,\boldsymbol{x})^{\alpha_2}_{c_1}, \tag{2.24}$$

where T is a matrix in flavor space. The equation above allows to construct the complete set of mesonic states. First of all, the flavor valence content is carried by the fermionic spinor ψ, which is now a vector in flavor space. The flavor matrix T controls the flavor structure, as defined in Appendix B. The matrix Γ is a product of gamma matrices chosen so that the interpolator acquires the proper spin and parity of the target state. A set of common values of Γ is given in Table A.1.

An approach that allows to enhance the overlap to the desired state considers a spatially extended interpolator at a fixed time slice. For this purpose, the function F is factorized in terms of the *smearing* function S,

$$F(\boldsymbol{x},\boldsymbol{y},\boldsymbol{z})^{\alpha_1\alpha_2}_{c_1c_2} = \sum_{\substack{\alpha_0,\alpha_0'\\c_0}} S_{\mathrm{sm}}(\boldsymbol{x},\boldsymbol{y})^{\alpha_0\alpha_1}_{c_0c_1}\Gamma_{\alpha_0\alpha_0'}S_{\mathrm{sm}}(\boldsymbol{x},\boldsymbol{z})^{\alpha_0'\alpha_2}_{c_0c_2}. \tag{2.25}$$

Considering an extended operator allows to incorporate the spatial distribution of the desired hadronic state over distances of the order of the inverse of its mass. Spinors are commonly redefined in order to absorb the non-local character of F,

$$\overline{\psi}^{f_1}_{\mathrm{sm}}(x_0,\boldsymbol{x})^{\alpha_0}_{c_0} = \sum_{\boldsymbol{y}} S_{\mathrm{sm}}(\boldsymbol{x},\boldsymbol{y})^{\alpha_0\alpha_1}_{c_0c_1}\overline{\psi}^{f_1}(x_0,\boldsymbol{y})^{\alpha_1}_{c_1}, \tag{2.26}$$

$$\psi^{f_2}_{\mathrm{sm}}(x_0,\boldsymbol{x})^{\alpha_0}_{c_0} = \sum_{\boldsymbol{z}} S_{\mathrm{sm}}(\boldsymbol{x},\boldsymbol{z})^{*\,\alpha_0\alpha_2}_{c_0c_2}\psi^{f_2}(x_0,\boldsymbol{z})^{\alpha_2}_{c_2}, \tag{2.27}$$

leading to an expression of the extended meson interpolator equivalent to eq. (2.24), in terms of the smeared fermionic fields

$$O_{M,E}(x_0,\boldsymbol{x}) = \sum_{\substack{\alpha_0,\alpha_0'\\c_0}} \overline{\psi}^{f_1}_{\mathrm{sm}}(x_0,\boldsymbol{x})^{\alpha_0}_{c_0}\Gamma_{\alpha_0\alpha_0'}\psi^{f_2}_{\mathrm{sm}}(x_0,\boldsymbol{x})^{\alpha_0}_{c_0}. \tag{2.28}$$

Smearing of the interpolating fields is particularly relevant for heavy-light mesons, since the time interval where the ground state shows a clear signal becomes shorter. The smearing function S employed in the heavy sector will be introduced in Section 4.3.

We express a meson correlator in terms of the quark propagators D^{-1}, defined in eq. (2.17). The generic notation for the fermions fields in eqs. (2.26) and (2.27) ensures that the following derivation holds for local and non-local interpolators

$$\begin{aligned}
\left\langle O_2(x_2)\overline{O}_1(x_1)\right\rangle &= \left\langle \overline{\psi}^{f_i}(x_2)_{\substack{\alpha_1\\c_1}}\Gamma_{\alpha_1\alpha_2}T_{ij}\psi^{f_j}(x_2)_{\substack{\alpha_2\\c_1}}\overline{\psi}^{f_k}(x_1)_{\substack{\beta_1\\c_2}}\Gamma'_{\beta_1,\beta_2}T'_{kl}\psi^{f_l}(x_1)_{\substack{\beta_2\\c_2}}\right\rangle, \\
&= T_{ij}T'_{kl}\Gamma_{\alpha_1\alpha_2}\Gamma'_{\beta_1,\beta_2}\left(\left\langle \psi^{f_j}(x_2)_{\substack{\alpha_2\\c_1}}\overline{\psi}^{f_i}(x_2)_{\substack{\alpha_1\\c_1}}\right\rangle\left\langle \psi^{f_l}(x_1)_{\substack{\beta_2\\c_2}}\overline{\psi}^{f_k}(x_1)_{\substack{\beta_1\\c_2}}\right\rangle\right. \\
&\qquad \left. - \left\langle \psi^{f_j}(x_2)_{\substack{\alpha_2\\c_1}}\overline{\psi}^{f_k}(x_1)_{\substack{\beta_1\\c_2}}\right\rangle\left\langle \psi^{f_l}(x_1)_{\substack{\beta_2\\c_2}}\overline{\psi}^{f_i}(x_2)_{\substack{\alpha_1\\c_1}}\right\rangle\right), \\
&= \mathrm{Tr}\left[T\right]\mathrm{Tr}\left[T'\right]\mathrm{Tr}\left[D^{-1}(x_2,x_2)\Gamma\right]\mathrm{Tr}\left[D^{-1}(x_1,x_1)\Gamma'\right] \\
&\qquad - \mathrm{Tr}\left[TT'\right]\mathrm{Tr}\left[D^{-1}(x_2,x_1)\Gamma' D^{-1}(x_1,x_2)\Gamma\right], \qquad (2.29)
\end{aligned}$$

where the trace is performed over the spinor and color indices and the summation over all indices involved is implicit. The negative sign on the second step arises from the anti-commuting nature of the fermion fields while in the third step the flavor indices are contracted by the Dirac delta-function appearing in the propagator definition.

The first term in eq. (2.29) implies the propagation of a quark from a space-time site back to the same point, which leads to the so-called *quark-disconnected* diagrams. This piece vanishes for the flavor non-singlet states, whether they are charged (off-diagonal) or neutral (diagonal), since their flavor matrices are traceless. Those that transport a quark from a single point to another and then propagate back in the opposite direction are known as *quark-connected* diagrams. The computational cost required to compute disconnected diagrams often largely exceeds the one needed for the connected diagrams. For instance, a quark-connected two-point correlation function with definite spatial momentum can be computed from a single inversion for every spin and color component of a local source. On the other hand, the quark-disconnected diagram would require an inversion for every spatial position of the operator at the sink. If the sum over the spatial points is approximated by stochastic noise sources at fixed Euclidean time, the study of disconnected diagrams would still need one inversion per Euclidean time. Moreover, quark-disconnected diagrams tend to have large variance contributions to the noise, which require specific methods to achieve a proper error reduction [13].

We review in the next sections the discretized actions that will be used in our setup.

2.4 Gauge action

The gauge part of the action, in eq. (2.30), governs the gluon dynamics, including their self-interactions

$$S_G = \int d^4x \mathcal{L}_G = \frac{1}{4} \int d^4x F_{\mu\nu}(x) F^{\mu\nu}(x). \tag{2.30}$$

The most simple formulation of the discrete gauge action is made of products of four link variables – known as plaquettes – that close the shortest possible path in a lattice around a lattice site x

$$U_{\mu\nu}(x) = U_\mu(x) U_\nu(x + \hat{\mu}) U_\mu(x + \hat{\nu})^\dagger U_\nu(x)^\dagger, \tag{2.31}$$

whose trace form a gauge invariant object. The so-called *Wilson gauge action* or *plaquette action*, sums all the different plaquettes of a lattice

$$S_G[U_\mu] = \frac{\beta}{3} \sum_p \mathrm{Tr}\left[\mathbb{1} - U_{\mu\nu}(p)\right]. \tag{2.32}$$

By Taylor expanding in the lattice spacing a and using equation (2.8), the lattice action converges towards the QCD gauge action in the limit $a \to 0$. The parameter $\beta = \frac{6}{g_0^2}$ is related to the inverse of the bare coupling g_0. The difference with respect to the continuum action is proportional to $\mathcal{O}(a^2)$.

Other discrete gauge actions differing, for instance, by the size of the expected lattice artifacts, can be considered as long as they converge to the QCD gauge action in the continuum limit. In Subsection 3.1.1, the definition of the gauge action used in our numerical studies will be presented

2.5 Fermionic actions

In this section, various discretizations of the fermionic action are reviewed. The fermionic action in the continuum is defined through the QCD Lagrangian, introduced in eq. (1.2)

$$S_F = \int d^4x \mathcal{L}_F = \int d^4x \sum_{f=1}^{N_f} \sum_{\substack{\alpha_1,\alpha_2 \\ c}} \left[\overline{\psi}^f(x)_{\substack{\alpha_1 \\ c}} \sum_{\mu=0}^{3} \left((\gamma_\mu)_{\alpha_1\alpha_2} \nabla_{\mu,c}(x) + m_{0,f} \right) \psi^f(x)^{\substack{\alpha_2 \\ c}} \right]. \tag{2.33}$$

As we will see, the most straightforward discretization, described in Subsection 2.5.1, leads to the appearance of lattice artifacts that need to be removed by adding extra terms to the action. These terms cannot change the physics and must vanish in the continuum limit. As in the case of the gauge action, a discretized fermionic lattice

action is required to be invariant under gauge transformations and to coincide with eq. (2.33) in the continuum limit.

Chiral symmetry and spontaneous symmetry breaking play a crucial role in QCD. Chiral symmetry is a global symmetry of the group $U(N_f)_L \times U(N_f)_R$ that allows to rotate the fermion fields so that the free propagator remains invariant. Under a proper election of the basis, left-handed and right-handed fermions decouple in the chiral limit, *i.e.*, the limit of vanishing quark masses. The spontaneous symmetry breaking of chiral symmetry in QCD is responsible for various phenomena such as the absence of parity doublings in the hadronic spectrum or the appearance of nearly massless modes. It is crucial that any lattice discretization properly reproduces these properties. A more detailed description of the global symmetries, including chiral symmetry, is presented in Appendix B.

Two different fermionic discretizations are introduced in this section, Wilson fermions and Wilson twisted mass fermions.

2.5.1 Naive fermions

Let us consider the non-interacting case where fermions propagate freely, *i.e.*, the specific case of vanishing gluon fields $A_\mu(x)$ in the Dirac operator in eq. (1.3). The partial derivative of the Dirac operator can be discretized by a Taylor expansion in the lattice size a. We defined the forward and backward lattice derivatives in the direction $\hat{\mu}$

$$\partial_\mu \psi(x) = \frac{1}{a}\left[\psi(x+\hat{\mu}) - \psi(x)\right], \qquad \partial^*_\mu \psi(x) = \frac{1}{a}\left[\psi(x) - \psi(x-\hat{\mu})\right], \tag{2.34}$$

which both hold up to $\mathcal{O}(a)$ effects. We generally use the symmetric derivative evaluated at the adjacent sites, $\widetilde{\partial}_\mu = \frac{1}{2}\left(\partial_\mu + \partial^*_\mu\right)$, to reduce the cut-off effects to $\mathcal{O}(a^2)$. Making use of the previous discretization for the derivative and the fermionic field, the naive free fermion action yields

$$S_F[\psi, \overline{\psi}] = a^4 \sum_x \sum_{f=1}^{N_f} \sum_{\substack{\alpha_1,\alpha_2 \\ c}} \overline{\psi}^f(x)_{\substack{\alpha_1 \\ c}} \left[\sum_{\mu=0}^{3} (\gamma_\mu)_{\alpha_1\alpha_2} \widetilde{\partial}_\mu \psi^f(x)_{\substack{\alpha_2 \\ c}} + m_{0,f} \psi^f(x)_{\substack{\alpha_2 \\ c}} \right]. \tag{2.35}$$

Let us now see how to impose gauge invariance of the fermionic action. Since fermion fields transform as in eq. (2.5), any $SU(3)$ local transformation would break gauge invariance in the partial derivative term appearing in eq. (2.35). The partial derivative can be upgraded to a covariant derivative made up by $SU(3)$ invariant combinations of fermionic and link fields. Considering that links transform as eq. (2.6), non-local combinations of fields such as $\overline{\psi}(x) U_\mu(x) \psi(x+\hat{\mu})$ and

$\overline{\psi}(x)U_{-\mu}(x)\psi(x-\hat{\mu})$ provide suitable definitions for forward and backward covariant derivatives, leading to the following symmetric covariant derivative:

$$\widetilde{\nabla}_{\mu,c_1c_2}\psi^f(x)_{\substack{\alpha\\c_2}} = \frac{1}{2a}\left[U_{\mu,c_1c_2}(x)\psi^f(x+\hat{\mu})_{\substack{\alpha\\c_2}} - U_{-\mu,c_1c_2}(x)\psi^f(x-\hat{\mu})_{\substack{\alpha\\c_2}}\right]. \tag{2.36}$$

Consequently, the naive fermionic action needs to be generalized in the presence of a gluonic field U_μ

$$S_F[\psi,\overline{\psi},U_\mu] = a^4\sum_{x,y}\sum_f\sum_{\substack{\alpha_1,\alpha_2\\c_1,c_2}}\overline{\psi}^f(x)_{\substack{\alpha_1\\c_1}}\left[\sum_\mu(\gamma_\mu)_{\alpha_1\alpha_2}\widetilde{\nabla}_{\mu,c_1c_2} + m_{0,f}\delta_{xy}\delta_{c_1c_2}\delta_{\alpha_1\alpha_2}\right]\psi^f(y)_{\substack{\alpha_2\\c_2}}, \tag{2.37}$$

$$= a^4\sum_{x,y}\sum_f\sum_{\substack{\alpha_1,\alpha_2\\c_1,c_2}}\overline{\psi}^f(x)_{\substack{\alpha_1\\c_1}}D^f(x,y)_{\substack{\alpha_1\alpha_2\\c_1c_2}}\psi^f(y)_{\substack{\alpha_2\\c_2}}. \tag{2.38}$$

In eq. (2.38), the fermionic action is rewritten in terms of the Dirac operator, taking advantage of the bilinearity in the fermionic fields.

The action derived above leads, however, to the *doubling* problem. This means that the massless lattice quark propagator D^{-1} contains additional unphysical singularities beyond the one expected in the continuum limit. Computing the Fourier transform of the Dirac operator in the non-interacting theory, $U_\mu = \mathbb{1}$, for the specific case where $m = 0$, the expression obtained in the 4-momentum representation is proportional to $\sin(ap_\mu)$

$$D_0(p,q)|_{U_\mu=\mathbb{1},m=0} = \delta_{pq}\left(\frac{i}{a}\sum_\mu\gamma_\mu\sin(ap_\mu)\right), \tag{2.39}$$

where the coordinates of the 4-momentum are restricted to live in the first Brillouin zone, $-\frac{\pi}{a} \leq p_\mu \leq \frac{\pi}{a}$.

Taking advantage of the fact that $D(p,q)$ is diagonal in momentum space, the inverse can be easily derived leading to 16 poles in the domain of p. This is in contradiction with the single pole structure of its continuum counterpart, $-i\frac{\not{p}}{p^2}$. According to dispersion relations, singularities in the propagator are related to stable single particles. Therefore, these 15 unphysical states or doublers that appear on the lattice need to be eliminated. According to the No-Go Theorem [14, 15], doublers can only be removed by giving up one of the following properties of QCD: locality, hermiticity or chiral symmetry.

2.5.2 Wilson fermions

To circumvent the doubling problem mentioned in Subsection 2.5.1, Wilson proposed [5] an alternative definition of the action which gives up chiral symmetry

on the lattice. Wilson fermions rely on adding a new term to the Dirac operator in eq. (2.38), in order to give an extra mass to the doublers that allows them to decouple in the continuum limit. Being proportional to the lattice spacing, the Wilson term is constructed to vanish in the continuum limit.

In particular, adding a Laplacian operator to the continuum Dirac operator, proportionally to a, fulfills the previous requirements: [7]

$$-\overline{\psi}(x)\left(\frac{a}{2}\nabla^2_{c_1c_2}\right)\psi(y) \xrightarrow{a>0} \overline{\psi}(x)\left(\frac{4}{a}\delta_{xy} - \sum_{\mu=0}^{3}\frac{U_{\mu,c_1c_2}(x)\delta_{x+\hat{\mu},y} + U_{-\mu,c_1c_2}(x)\delta_{x-\hat{\mu},y}}{2a}\right)\psi(y), \tag{2.40}$$

$$\xrightarrow{\text{F.T.}} \frac{4}{a} - \frac{1}{a}\sum_{\mu=0}^{3}\cos(ap_\mu). \tag{2.41}$$

On the first step, the discretization of the second derivative is performed in an analogous way to the partial derivative in eq. (2.34). Then, the discrete Fourier transform is again applied leading to a cosine that provides an extra mass contribution to the doublers. As the lattice spacing decreases the mass of the doublers increase to a point that they effectively decouple from the theory.

Wilson fermions are defined by the sum of the naive Dirac operator, defined in Subsection 2.5.1, and the Wilson term in eq. (2.40),

$$D(x,y)^{\alpha_1\alpha_2}_{c_1c_2} = \sum_{\mu}(\gamma_\mu)_{\alpha_1\alpha_2}\widetilde{\nabla}_{\mu,c_1c_2} + \left(\delta_{xy}\delta_{c_1c_2}m_{0,f} - \frac{a}{2}\nabla^2_{c_1c_2}\right)\delta_{\alpha_1\alpha_2}. \tag{2.42}$$

In particular, the Wilson term is not invariant under the axial transformation, defined in eq. (B.4). In the absence of the Wilson term, the fact that the chiral symmetry is satisfied in the chiral limit implies that the quark masses can be multiplicatively renormalized (see Section 2.8 for more details). However, on the lattice, the Wilson term shifts the massless quark limit by an additive term given by the *critical mass*, m_{cr}. The *subtracted* bare quark mass is defined by the difference between the bare quark mass $m_{0,f}$ and the critical mass [8]

$$m_{q,f} = m_{0,f} - m_{\text{cr}}. \tag{2.43}$$

The renormalized quark mass can then, in principle, be achieved by multiplicatively renormalizing the subtracted quark mass.

Some considerations are remarkable for the implementation of the Wilson action. The Wilson regularization, as any non-improved action, receives $\mathcal{O}(a)$ discretization errors. In Section 2.6, we discuss the techniques employed to eliminate

[7] F.T. refers to the Fourier transform.

[8] index f denotes quark flavor.

these effects. Furthermore, the fact that the Wilson term breaks chiral symmetry explicitly induces unphysical mixing between operators with wrong chirality. Conversely to the Wilson twisted mass action presented in the next Subsection 2.5.3, the distribution of the low-lying eigenvalues is not protected by an infrared regulator and unphysically small eigenvalues can appear. Note that in the quenched approximation these eigenvalues lead to instabilities, because they are not properly compensated by the fermionic determinant.

A different approach that evades the No-Go theorem was proposed in [16], which implements a discrete version of chiral symmetry while also eliminating the doublers. The anti-commutation relation is replaced on the lattice by

$$\{D, \gamma_5\} = 0 \xrightarrow{a>0} \{D, \gamma_5\} = aD\gamma_5 D, \tag{2.44}$$

where the latter relation is known as the Ginsparg-Wilson (GW) equation. GW fermions fulfill an exact chiral symmetry that differs at $\mathcal{O}(a)$ from the chiral symmetry defined in the continuum. Overlap [17] or Domain wall [18] fermions are examples of successful lattice implementations satisfying the GW relation. These lattice formulations are however significantly more computationally demanding than those based on the Wilson formalism.

2.5.3 Wilson twisted mass fermions

In this section, some general aspects of the *Wilson twisted mass* [19–24] (Wtm) regularization are reviewed, since it will be a fundamental part of our mixed action. We refer to [25] for a more complete discussion.

The twisted mass term was initially defined for two degenerate light quark flavors, $N_f = 2$, where it takes the form

$$\overline{\psi}\left(i\mu_{\ell,0}\gamma_5\tau^3\right)\psi. \tag{2.45}$$

The element τ^3 is the third Pauli matrix acting in the flavor space [9], and will be henceforth combined with $\mu_{\ell,0}$ by defining the twisted mass $\boldsymbol{\mu}_0 = \mathrm{diag}\,(\mu_{\ell,0}, -\mu_{\ell,0})$ through a diagonal matrix in flavor space. The new mass term acts as an infrared cut-off in the spectrum of the Dirac operator that helps to stabilize the computation of the quark propagators.

In the formal continuum limit, the equivalence between twisted mass QCD and QCD can be established since the fermionic actions can be related by a global chiral rotation of the fields. We define the *physical basis* $\left\{\psi, \overline{\psi}\right\}$ to be the one in which the action takes the usual form of the QCD action shown in eq. (2.33), and the *twisted basis* $\{\chi, \overline{\chi}\}$ as the one in which the action exhibits the additional

[9] The Pauli matrices are proportional to the generators of the group $SU(2)$ by $T^a = \tau^a/2$.

twisted mass presented in eq. (2.45). The equivalence becomes more explicit by expressing the sum of the bare and the twisted mass in polar coordinates

$$m_{\ell,0} + i\mu_{\ell,0}\gamma_5\tau^3 = Me^{i\alpha\gamma_5\tau^3}, \tag{2.46}$$

where the M is referred to as the *polar mass* and α to as the *polar angle*. This redefinition leads to the following expression of the action in the twisted basis

$$S_F[\chi,\overline{\chi},U_\mu] = a^4\sum_x \sum_{\substack{\alpha_1,\alpha_2\\ c_1,c_2}} \overline{\chi}^{\alpha_1}_{c_1}(x)\left[D_0(x,y)^{\alpha_1\alpha_2}_{c_1c_2} + Me^{i\alpha\gamma_5\tau^3}\delta_{xy}\delta_{c_1c_2}\delta_{\alpha_1\alpha_2}\right]\chi^{\alpha_2}_{c_2}(y). \tag{2.47}$$

Considering that the massless Dirac operator is invariant under a chiral rotation, the twisted mass can be reabsorbed in the physical basis by an axial rotation

$$\begin{aligned}\psi &= e^{i\omega\gamma_5\frac{\tau_3}{2}}\chi,\\ \overline{\psi} &= \overline{\chi}e^{i\omega\gamma_5\frac{\tau_3}{2}},\end{aligned} \tag{2.48}$$

when the *twisted angle* is matched to the polar angle $\omega = \alpha$. This rotation leaves the integration measure of the path integral invariant, meaning that the change of variables is non-anomalous.

The main motivation to use Wtm fermions is the property of automatic $\mathcal{O}(a)$ improvement of physical observables at maximal twist [22]. Maximal twist is defined as a particular case of Wtm fermions where the quark mass in the complex plane becomes purely imaginary, *i.e.*, the twist angle is $\frac{\pi}{2}$. In the context of the mixed action, in the valence sector, the subtracted quark mass has to be set to zero while the twisted mass requires a matching procedure to the sea quark mass to recover the unitarity of the theory in the continuum. The matching procedure will be explained in Section 3.6.

When using Wtm fermions in the sea and valence sectors, automatic $\mathcal{O}(a)$ improvement can be proved by performing a Symanzik expansion (see Section 2.6) on the fully twisted fermionic action [26]. In doing so, one can identify the relevant $\mathcal{O}(a)$ counterterms of the action which happen to cancel in this setup by imposing the vector symmetry of QCD in the physical basis. In particular, the counterterms cancel out by the subgroup defined by the second generator of $SU_V(2)$, which will be denoted as $[SU_V(2)]_2$. See Appendix B for an introduction to the continuum global symmetries.

The Wtm formalism can be extended to a non-degenerate flavor structure in the valence sector [24, 27] while also preserving the property of automatic $\mathcal{O}(a)$-improvement.

The symmetries in the twisted basis, called *twisted symmetries* hereafter, are a composition operation of the standard symmetries by an axial rotation over a

polar angle. Starting from the vector and axial rotations, described in Appendix B for the physical basis, the analogous transformations for a Wtm Lagrangian at a generic angle ω can be derived through the eq. (2.48)

$$\chi \longrightarrow \chi' = e^{-i\omega\gamma_5\frac{\tau^3}{2}} e^{i\alpha_V^a\frac{\tau^a}{2}} e^{i\omega\gamma_5\frac{\tau^3}{2}}\chi, \qquad \overline{\chi} \longrightarrow \overline{\chi}' = \overline{\chi} e^{i\omega\gamma_5\frac{\tau^3}{2}} e^{-i\alpha_V^a\frac{\tau^a}{2}} e^{-i\omega\gamma_5\frac{\tau^3}{2}}, \tag{2.49}$$

$$\chi \longrightarrow \chi' = e^{-i\omega\gamma_5\frac{\tau^3}{2}} e^{i\alpha_A^a\gamma_5\frac{\tau^a}{2}} e^{i\omega\gamma_5\frac{\tau^3}{2}}\chi, \quad \overline{\chi} \longrightarrow \overline{\chi}' = \overline{\chi} e^{i\omega\gamma_5\frac{\tau^3}{2}} e^{i\alpha_A^a\gamma_5\frac{\tau^a}{2}} e^{-i\omega\gamma_5\frac{\tau^3}{2}}, \tag{2.50}$$

which will be referred as $SU_V(2)_\omega$ and $SU_A(2)_\omega$ for a generic twisted angle. Likewise for Wilson fermions, the twisted vector symmetry $SU_V(2)_\omega$ holds for degenerate quark masses while the $SU_A(2)_\omega$ symmetry is only satisfied in the chiral limit.

The Wtm action also requires for the Wilson term of eq. (2.40) to eliminate the doublers. The Wilson term is not invariant under neither twisted axial rotations nor twisted vector rotations, thus breaking chiral symmetry. Breaking axial symmetry implies that the Wilson and the Wtm theory are not equivalent anymore on the lattice by the transformation in eq. (2.48).

The vector twisted rotation, conversely to the standard vector rotation, is proportional to γ_5. The opposite happens to the axial twisted transformation, which does not depend on the fifth gamma matrix. The quark bilinears in the twisted basis are defined in an analogous way to those in the physical basis, shown in eqs. (B.11) to (B.15). [10] At $\omega = \frac{\pi}{2}$, the twisted mass and the Wilson term are totally misaligned in terms of the generators 1 and 2 of $SU(2)$. The Wilson term breaks the symmetry $\left[U_V(1)_{\frac{\pi}{2}}\right]_{1,2}$ while it preserves $\left[U_A(1)_{\frac{\pi}{2}}\right]_{1,2}$. The opposite happens for the twisted mass at maximal twist. This implies indirectly that the charged vector current in the twisted basis is already renormalized since the axial transformation $[U_A(1)_{\frac{\pi}{2}}]_{1,2}$ behaves as in the continuum, *i.e.*, it is only broken in the massive case. As a consequence, the pseudoscalar decay constant in the Wtm regularization can be reexpressed by using the vector Ward-Takahashi identity (See Section 2.7), so that it is protected from renormalization.

The *discrete twisted symmetries* can be derived in a similar way to the global symmetries starting from the physical basis, as defined in Appendix C. Although the transformation under twisted charge conjugation is conserved in the Wtm regularization, parity and time-reversal are not. Both parity and time-reversal require an extra change of sign of the twisted mass to keep the action invariant, which implies that $\mathcal{CPT}$ symmetry is conserved.

An advantage of the Wtm regularization is the relatively cheap cost of the simulations with respect to *e.g.* Ginsparg-Wilson fermions. Wtm fermions also re-

[10] We will use a calligraphic symbol to denote the quark bilinears in the physical basis.

duce the mixing with wrong chirality operators in the renormalization process [24]. Therefore, at maximal twist, many quantities of interest profit from a simpler renormalization pattern, thus reducing the systematic errors associated with them. Nonetheless, additional lattice artifacts associated to the breaking of flavor symmetry and of parity can appear. For instance, a specific $\mathcal{O}(a^2)$ discretization effect appears in the mass splitting between the charged and neutral pions.

2.6 $\mathcal{O}(a)$-improvement

In LQCD, a physical observable is commonly obtained by an extrapolation to the physical point and to the continuum limit of simulation points from different values of the quark masses and of the lattice spacings. Lattice data is affected by lattice artifacts. While this can in principle be addressed by reducing the value of the lattice spacing, the cost of generating gauge configurations increases significantly as the lattice spacing decreases. The improvement program consists on removing the lattice artifacts at leading order on the lattice spacing in order to reduce deviations from the continuum results, specially from the coarser lattice spacings. This is commonly required for un-improved actions, such as Wilson fermions.

Symanzik's improvement program [28] provides a systematic methodology to describe cut-off effects. It allows to reduce those effects by either tuning counterterms to diminish their contributions or by combining observables in a way that the common cut-off effects cancel. Such counterterms can be computed by either perturbative or non-perturbative methods. The bottom line is to describe the lattice action as a local effective field theory in terms of the continuum Lagrangian and local operators of dimensions $k+4$

$$S_{\text{eff}} = S_0 + \sum_{k=1}^{\infty} a^k S_k = \int d^4x \mathcal{L}_{\text{QCD}}(x) + \sum_{k=1}^{\infty} a^k \int d^4x \mathcal{L}_k(x), \tag{2.51}$$

which are gauge invariant and respect the symmetries of the lattice theory. We refer to the continuum action with a 0 index. Cut-off effects of $\mathcal{O}(a\mathcal{L}^{(k)})$ can be mitigated by adding to the theory the irrelevant operators composing $\mathcal{L}^{(k)}$ with the appropriate coefficients. The procedure can be done order by order in a, however, the number of operators grows very quickly with k. In practice, after classifying all possible $k+4$ valid operators, a subset of them are found not be independent once the equations of motion are applied. In this way, one can distinguish mass-dependent lattice artifacts from those that are present in the chiral limit. The corresponding coefficients of the mass-independent and mass-dependent $\mathcal{O}(a)$ lattice artifacts of a generic operator O will be labelled by c_0 and b_O, respectively.

Improving the action allows to improve the hadronic spectrum, but it is not a sufficient condition to remove $\mathcal{O}(a)$ effects from other fermionic observables. The

improvement program has to be carried out in both the lattice action and the observables. Analogously to the action, a lattice observable can be expanded in a power series of the lattice spacing where the leading term is the continuum value and the successive terms depend on higher-dimensional operators [11]

$$O_{\text{eff}}(x) = O_0(x) + aO_1(x) + a^2O_2(x) + ..., \tag{2.52}$$

where the fields $O_i(x)$ must respect the symmetries of the lattice regularization. As an illustration, we indicate the generic expression for the $\mathcal{O}(a)$-improved 2-point function

$$\begin{aligned} Z_O^2 \langle O(x_2)O(x_1)\rangle = \langle O(x_2)O(x_1)\rangle_0 - a\int d^4x \mathcal{L}_1(x) \langle O(x_2)O(x_1)\rangle_0 \\ + a\sum_{i=1}^{2} \langle O(x_2)O_1(x_i)O(x_1)\rangle_0 + \mathcal{O}(a^2), \end{aligned} \tag{2.53}$$

where the interpolators are placed at different lattice sites $x_1 \neq x_2$.

2.7 Ward identities

Ward-Takahashi identities (WTI) are the quantized version of the Noether's theorem that relates the invariance of expectation values under the transformation of the fermionic fields. The lattice version of the WTI contains higher dimensional operators as a consequence of the breaking of chiral symmetry on the lattice (see Section 2.5 for more details) by the Wilson term. The WTI can provide a way to relate the renormalization factors of operators, as shown in Section 2.8.

WTI are derived by applying a local infinitesimal change of variables to the field functionals in the path integral shown in eq. (2.13)

$$\begin{aligned} \psi(x) \longrightarrow \psi'(x) &= \psi(x) + \delta_X\psi(x), & \overline{\psi}(x) \longrightarrow \overline{\psi}'(x) &= \overline{\psi}(x) + \delta_X\overline{\psi}(x), \quad (2.54) \\ &= (\mathbb{1} + \alpha_X^a\lambda^a)\,\psi(x), & &= \overline{\psi}(x)\left(\mathbb{1} + \alpha_X^a\hat{\lambda}^a\right), \quad (2.55) \end{aligned}$$

where the transformations in the case of axial and vector WTI, are obtained by assuming locality in the eqs. (B.9) and (B.10), *i.e.*,

$$\alpha_X^a \longrightarrow \alpha_X^a(x). \tag{2.56}$$

The coefficients are required to be smooth functions within a bounded region $\mathcal{D}$, outside of which they vanish. The choice of the matrices λ^a and $\hat{\lambda}^a$ will lead to the different WTIs.

[11] Subindex 0 refers to the value of the observable in the continuum.

For non-anomalous transformations $\delta_X(x)$ where the integration measures remains invariant, the integral

$$\int \mathcal{D}[\psi,\overline{\psi},U]\delta_X\left(Oe^{-S}\right)=0, \tag{2.57}$$

cancels for any functional O. This implies, by applying the chain rule, that the following relation

$$0=\langle\delta_X O\rangle-\langle O\delta_X S\rangle\,, \tag{2.58}$$

is fulfilled for a generic observable O. The variation of the action according to eq. (2.55) only acts on the fermionic fields leaving the purely gluonic terms invariant. After neglecting $\mathcal{O}(\alpha_X^2)$ and considering mild assumptions [12], the variation of the action can be written as

$$\delta_X S=i\int_{\mathcal{D}} d^4x\;\alpha_X(x)\left(-\partial_\mu\left(\overline{\psi}\gamma_\mu T\psi\right)+\overline{\psi}\left(\hat{T}M+MT\right)\psi\right), \tag{2.59}$$

where M is the mass matrix. For convenience, we consider the observable O as a product of two operators, one that has only support inside the region $\mathcal{D}$, $O_{\rm i}$, and another that has support outside D, denoted as $O_{\rm e}$

$$\langle(\delta_X O_{\rm i})\,O_{\rm e}\rangle=\langle O_{\rm i}O_{\rm e}\delta_X S\rangle\,. \tag{2.60}$$

Note that $\delta_X O_{\rm e}$ vanishes since, by construction, $\alpha_X(x)$ cancels outside $\mathcal{D}$.

Starting from the vector transformation in eq. (B.9), the WTI in the continuum can be easily derived by setting the parameter λ^a, in eqs. (2.54) and (2.55), according to the generators of $SU(N_f)$, $\lambda^a=-\hat{\lambda}^a=T^a$

$$\delta_V S=-i\int_{\mathcal{D}} d^4x\;\alpha_V(x)\left(\partial_\mu\mathcal{V}^a_\mu+\overline{\psi}\,[T^a,M]\,\psi\right). \tag{2.61}$$

The operator O can be restricted to region external to $\mathcal{D}$, which implies that O_i is set to 1 and $O=O_e$. Such an assumption can be carried out without loss of generality since the region $\mathcal{D}$ can be chosen arbitrarily. Thus, the lhs of eq. (2.60) vanishes while the observable O_e can be introduced within the integral of eq. (2.61). For instance, considering the $SU(2)$ flavor group, with a mass matrix $M=\mathrm{diag}\,(m_u,m_d)$, the vector WTI or PCVC relation links the partial derivative of the vector current in eq. (B.11) with the scalar density in eq. (B.13), proportionally to the mass difference δm_ℓ between the up and down quarks

$$\left\langle\partial_\mu\mathcal{V}^a_\mu(x)\;O\right\rangle=\left\langle\overline{\psi}\,[M,T^a]\,\psi\;O\right\rangle\quad\xrightarrow{M_{2\times2}}\quad i\epsilon_{3ab}\delta m_\ell\left\langle S^b(x)\;O\right\rangle, \tag{2.62}$$

where ϵ_{ijk} is the Levi-Civita symbol and T^a corresponds to $\tau^a/2$. The conservation of the vector current occurs as long as the light quark masses are degenerate.

[12] $\hat{T}^a\gamma_\mu+\gamma_\mu T^a=0$.

The axial WTI or PCAC relation in the light sector can be derived in a similar way by means of the axial transformation in eq. (B.10). Setting $\lambda^a = \hat{\lambda}^a = \gamma_5 \frac{\tau^a}{2}$ and assuming the same reasoning for O as before, the PCAC relation reads

$$\left\langle \partial_\mu \mathcal{A}^a_\mu(x)\, O \right\rangle = \left\langle \overline{\psi}\gamma_5 \left\{ M, \frac{\tau^a}{2} \right\} \psi\, O \right\rangle \quad \xrightarrow{m_u = m_d = m_\ell} \quad 2m_\ell \left\langle P^a(x)\, O \right\rangle . \tag{2.63}$$

Thus, axial current is said to be partially conserved since the rhs of eq. (2.63) vanishes solely in the chiral limit (see Appendix B for more details). In a more general case where the light quark masses are non-zero but degenerate, the partial derivative of the axial current is related to the pseudoscalar density times the quark mass. The mass appearing in the rhs of the relation (2.63) is referred as the PCAC quark mass. On the lattice, dimension 5 operators associated to $\mathcal{O}(a)$ lattice artifacts can appear in both vector and axial WTI, [13] shown in eqs. (2.62) and (2.63), respectively. These discretization effects have direct implications over the renormalization factor of such currents, as detailed in Section 2.8.

Ward identities in the Wtm formalism are derived in a similar way considering that the vector and axial transformations in the physical basis are equivalent to each other in the twisted basis. The action variation introduced in eq. (2.59) presents a new term coming from the twisted mass term in the Lagrangian of eq. (2.45) which leads to additional terms in the WTI. In the case of degenerate quark light masses, the WTI in the Wtm basis is simplified as follows

$$\left\langle \partial_\mu V^a_\mu(x)\, O \right\rangle = -2\mu_\ell\, \epsilon_{3ab} \left\langle P^b(x)\, O \right\rangle + \mathcal{O}(a), \tag{2.64}$$

$$\left\langle \partial_\mu A^a_\mu(x)\, O \right\rangle = 2m_\ell \left\langle P^a(x)\, O \right\rangle + i\mu_\ell\, \delta_{3a} \left\langle S^0(x)\, O \right\rangle + \mathcal{O}(a). \tag{2.65}$$

2.8 Renormalization

In perturbation theory, loop corrections lead to the existence of poles in momentum space, which give rise to ultraviolet divergences. Renormalization arises as a method to obtain finite quantities in the continuum limit, *i.e.* once the UV cut-off is removed, by relating the bare parameters – the coupling constant, the fields and the quark masses – to physical variables. Although discretizing the space-time acts as a cut-off that removes these divergences, the connection between a bare lattice observable and its continuum physical counterpart may involve operators that receive finite, logarithmic and power divergent corrections in the lattice spacing. In the process of renormalization, the operators may inherit a dependence of the renormalization scheme and scale.

[13] The partial derivative of the vector and axial WTI on the lattice becomes a backward derivative.

For instance, an operator O renormalizes multiplicatively through a renormalization factor $Z_O^{\mathcal{S}}$

$$O^{R_{\mathcal{S}}}(a) = Z_O^{\mathcal{S}}(a,\mu)O, \tag{2.66}$$

that depends on the lattice spacing a, the renormalization scale μ and the renormalization scheme $\mathcal{S}$. The lattice computation of the renormalization factors can be hindered by a mixing due to the breaking of continuum symmetries. Discrete symmetries can however be used to simplify the mixing pattern.

Renormalization factors can be computed by perturbative or non-perturbative approaches. For instance, the Schrödinger functional (SF) [29, 30] scheme provides a non-perturbative method to estimate renormalization constants and the renormalization group running of the coupling, quark masses and operators. The Schrödinger functional on the lattice is given by the functional integral

$$Z(C,C') = \int e^{-S[U]}\mathcal{D}\left[U\right], \tag{2.67}$$

where the fields are confined to a cylindric volume system with periodic boundary condition in the spatial directions and Dirichlet boundaries in time. The behavior at the boundaries is given by the continuous functions C and C'. While Dirichlet boundary conditions break translation invariance in the time direction they also provide a mechanism to directly simulate massless fermions on the lattice as required for a mass-independent renormalization scheme.

In this setup, recursive techniques applied to a finite volume lead to a connection between the low-energy scale of QCD with the high-energy regime where PT can be safely applied. In this way, the running of fundamental parameters, such as the strong coupling and the quark masses, can be determined in a non-perturbative fashion. Furhtermore, the conversion to other schemes, such as $\overline{\text{MS}}$ can be performed at high-energies where high-order corrections in perturbation theory are under control. In this work, results from the SF will be used from the renormalization and running of the quark mass and for the determination of $\mathcal{O}(a)$-improvement coefficients [31, 32].

As discussed in Section 2.7, Ward identities provide constrains on the renormalization factors of quark bilinears. In the continuum, WTI proves that vector and axial currents are partially conserved, see eqs. (2.62) and (2.63), meaning that the currents are strictly conserved in the chiral limit. Chiral symmetry guarantees the applicability of the non-renormalization theorem [33] for the partially conserved axial and vector currents, leading to $Z_V = Z_A = 1$ in the continuum limit.

In general, on the lattice, the WTI of the currents are modified with respect to their continuum form. The mixing of the additional terms with lower dimensional operators needs to be analyzed in order to guarantee the recovery of the QCD WTI in the continuum limit. When considering Wilson fermions, for the case

of the vector current a point-split conserved current $\hat{\mathcal{V}}_\mu^a$ exists while for the local counterpart a $Z_V \neq 1$ renormalization factor is required

$$\hat{\mathcal{V}}_\mu^a(x) = \frac{1}{2}\left[\overline{\psi}(x)\left(\gamma_\mu - 1\right)U_\mu(x)T^a\psi\left(x + a\hat{\mu}\right) + \overline{\psi}\left(x + a\hat{\mu}\right)\left(\gamma_\mu + 1\right)U_\mu^\dagger(x)T^a\psi(x)\right]. \tag{2.68}$$

In the case of the axial current both local and the point-split currents require renormalization factors $Z_A \neq 1$. WTI also relate the renormalization factors of the vector and axial currents with the scalar and pseudoscalar currents, respectively.

Chapter 3

Mixed-action setup

We consider a mixed action approach by combining Wilson fermions in the sea sector with Wtm fermions in the valence sector. We design a setup aiming to take advantage from some of the features of the Wtm regularization. Finally we will compare the continuum results of the mixed action to those of the Wilson unitary action. The difference between the physical results for both actions will be used to estimate the systematic uncertainty.

In the sea sector, we consider the gauge configurations on ensembles generated by the CLS initiative [34], listed in Table 3.1. The sea action is built out of a tree-level Lüscher-Weisz gauge action along with an $N_f = 2 + 1$ non-perturbatively improved Wilson fermionic action. In Section 3.1, we provide further information about the sea action in order to complement the description of the gauge and fermionic action previously introduced in Sections 2.4 and 2.5, respectively.

The ensembles have periodic boundary conditions on the spatial directions, while open boundary condition in time are employed to avoid the freezing of the topological charge at the smallest values of the lattice spacing. The lattice spacing of the ensembles considered ranges from 0.087 to 0.050 fm. In order to guarantee a good control of the autocorrelations, the length of the CLS simulations in Monte Carlo time is targeted to be significantly larger than slowest mode of the algorithm, given by exponential autocorrelation time. To get rid of unphysical low-lying eigenvalues of the Wilson-Dirac operator, and thus to stabilize the simulations, a small twisted mass is added to the fermionic determinant, as detailed in Subsection 4.1.1. This approximation can the be removed through a reweighting procedure [35].

In Section 3.3, we will discuss some general principles behind the use of a mixed action, while the used matching procedures will be presented in Section 3.6.

The use of valence Wtm fermions at full-twist, described in Subsection 2.5.3, implies the absence of $\mathcal{O}(a)$ lattice artifacts proportional to the valence quark masses. In Section 3.2, we review the implementation of the Wtm fermions in

β	a [fm]	label	N_s	N_t	κ_ℓ	κ_s	M_π [MeV]	M_K [MeV]	$M_\pi L$
3.40	0.086	H101	32	96	0.13675962	0.1367596200	420	420	5.8
		H102	32	96	0.13686500	0.1365493390	350	440	4.9
		H105	32	96	0.13697000	0.1363407900	280	460	3.9
3.46	0.076	H400	32	96	0.13688848	0.1368884800	420	420	5.2
		H401	32	96	0.13672500	0.1367250000	550	550	7.3
		H402	32	96	0.13685500	0.1368550000	450	450	5.7
3.55	0.064	N202	48	128	0.13700000	0.1370000000	420	420	6.5
		N203	48	128	0.13708000	0.1368402840	340	440	5.4
		N200	48	128	0.13714000	0.1367208600	280	460	4.4
		D200	64	128	0.13720000	0.1366017480	200	480	4.2
3.70	0.050	N300	48	128	0.13700000	0.1370000000	420	420	5.1
		J303	64	192	0.13712300	0.1367546608	260	470	4.1

Table 3.1: List of CLS ensembles. The first two columns denote the β value and the lattice spacing a in fermi for every set of ensembles. The labels identify every ensemble by its geometry, coupling and quark mass combination, respectively. The parameters N_s and N_t refer to the spatial and the time lattice size, introduced in eq. (2.2). In the next columns, it is shown the hopping parameters of the light and the strange quark masses followed by the approximate values for the pion and the kaon masses, expressed in MeV. The product of the lattice size L times the pion mass, shown in the last column, should be large enough to not altering the physics due to volume effects.

the valence sector. In this setup, we expect to profit from good scaling properties without the need to tune operator-dependent improvement coefficients.

3.1 Sea sector

3.1.1 Lattice action

The gauge action described in Section 2.4 does not introduce $\mathcal{O}(a)$ cut-off effects. This means that there are no dimension 5 gauge invariant operators that could be added to the Lagrangian without breaking its symmetries. This can be easily inferred since any gluonic observable must be formed by an even number of multiplicative links in order to respect gauge invariance. By following this, there can only be three independent dimension 6 operators since there are three different unique ways of closing six link variables in a rectangular lattice: planar rectangles,

twisted and L-shaped. The most general gluonic action containing plaquettes and the operators above reads

$$S_G[U_\mu] = \frac{\beta}{3}\left[c_0 \sum_p \mathrm{Tr}\left[\mathbb{1} - U_{\mu\nu}(p)\right] + \sum_{i=1}^{3} c_i \sum_r \mathrm{Tr}\left[\mathbb{1} - U^{(i)}(r)\right]\right], \tag{3.1}$$

where $U^{(i)}(r)$ indicates the three different dimension 6 operators and the coefficients c_i can be computed in perturbation theory or by renormalization group methods. A proper selection of such coefficient can lead to $O(a^2)$ improvement in the gauge action. The gluonic action employed for generating the gauge configurations along this work is known as the three-level improved Lüscher-Weisz action [36, 37], where the values for c_i are given by

$$c_0 = \frac{5}{3}, \qquad c_1 = -\frac{1}{12}, \qquad c_2 = 0, \qquad c_3 = 0. \tag{3.2}$$

Therefore, the only remaining contributions come from the regular plaquette term and the sum over all planar rectangles.

The Wilson fermionic action described in Subsection 2.5.2 is employed in the dynamical simulations that produce the gauge field configurations, defining the fermionic content in the sea sector. This fermionic action contains $O(a)$ errors that can be removed according to the Symanzik expansion in eq. (2.51). The $O(a)$ discretization effects originate from the terms containing operators of dimension 5. Once the equations of motion are used, there is a unique dimension 5 operator that preserves the symmetries of the Lagrangian and is linearly independent from the other dimension 5 operators and from the terms that appear already in the action [38]

$$i\overline{\psi}\sigma_{\mu\nu}\hat{F}_{\mu\nu}\psi, \tag{3.3}$$

where $\hat{F}_{\mu\nu}$ denotes the discretized version of the continuum field strength tensor. A common choice, although not unique, reads

$$\hat{F}_{\mu\nu}(x) \equiv -\frac{i}{8a^2}\left(Q_{\mu\nu}(x) - Q_{\nu\mu}(x)\right), \tag{3.4}$$

$$Q_{\mu\nu}(x) = U_{\mu\nu}(x) + U_{\nu-\mu}(x) + U_{-\mu-\nu}(x) + U_{-\nu\mu}(x), \tag{3.5}$$

where the object $Q_{\mu\nu}(x)$ is defined as the sum of the four closest plaquettes, defined in eq. (2.31). The fermionic Wilson $\mathcal{O}(a)$-improved action is composed by the standard Wilson terms in eq. (2.42) plus the piece defined above in eq. (3.3), usually denominated as the *clover term* [1]

$$S_F^{(I)}\big|_s = S_F|_s + i\frac{a^5}{4}c_{\mathrm{sw}} \sum_x \sum_{\mu<\nu} \overline{\psi}(x)\sigma_{\mu\nu}\hat{F}_{\mu\nu}(x)\psi(x), \tag{3.6}$$

[1] The notation $|_s$ and $|_v$ denote sea and valence sector, respectively.

where c_{sw} is the *Sheikholeslami–Wohlert* improvement coefficient [39]. The fact that there is a large number of dimension 6 operators implies that the expansion of the Symanzik program to $\mathcal{O}(a^2)$ is in practice not carried out in present day lattice calculations.

3.1.2 Open boundary conditions

The main reason to opt for open boundary conditions (OBC) instead of periodic conditions in the time direction is related with the existence of different topological sectors on the lattice. Different topological sectors represent a separate set of elements of the configuration space such that the configurations belonging to a sector cannot be continuously transformed into the configurations pertaining to another sector. The topological sectors can be characterized by the so-called topological charge Q, defined in Appendix E. The topological charge is a quantity related to the axial anomaly, which vanishes in the classical theory where the symmetry is satisfied. The *Index theorem* states that Q is an integer number given by the difference between the zero modes of the Dirac operator with positive and negative chiralities.

The HMC algorithm (see Subsection 4.1.4) with periodic boundary conditions (PBC) in time may struggle to sample the various topological sectors. As the lattice spacing decreases, the Monte Carlo time required to explore the whole configuration space grows. In this case, the probability to freeze the fluctuations of the topological charge are significantly increased. In other words, the ergodicity property of the algorithm can be compromised. This effect not only delay the thermalization process but also leads to an increase of the autocorrelation times of observables measured on the produced configurations [40–44]. This issue becomes specially severe as the lattice spacing drops below 0.05 fm.

Close to the continuum limit where the gauge fields are sufficiently smooth, the space of lattice gauge fields can be proved to be decomposed into topological charge sectors [45,46]. At small values of the lattice spacing, when simulating QCD with the HMC algorithm and PBC in time, the regions of field space separating these topological sectors are heavily suppressed. The simulation is then expected to remain frozen on a given topological sector. The use of OBC in time dissolves the topological sectors and smoothly connects the space of gauge fields [47].

OBC allows to connect the entire field space by allowing the topological charge to move through the boundaries of the lattice, facilitating the variations of observables related to the topology [48, 49]. The scaling of the autocorrelation time as a function of the lattice spacing follows a $1/a^2$ law which is significantly better than the one observed when using PBC. Setting OBC in the time direction leads to the breaking of the time translation symmetry and induces boundary effects. For this reason, observables are measured far from the boundaries and ratios of

correlation functions with common source position are considered to remove the boundary effects on the low-lying states.

In practice, OBC in time are imposed by setting the elements of the field strength tensor involving the time component to be zero at the boundaries,

$$F_{0\nu}\left(x_0 = 0, \boldsymbol{x}\right) = F_{0\nu}\left(x_0 = T - a, \boldsymbol{x}\right) = 0. \tag{3.7}$$

3.2 Valence sector

Wilson twisted mass fermions are implemented in the valence sector by the action shown in eq. (2.47). The Wtm action will include the Sheikholeslami–Wohlert term since this does not compromise the symmetry arguments behind the absence of $\mathcal{O}(a)$ effects coming from the valence sector. In this way, in the massless limit, the same fermionic action is used in the sea and valence and, therefore, the renormalization factors are identical for the sea and valence regularizations. Furthermore, the presence of the clover term has been observed to reduce $\mathcal{O}(a^2)$ lattices artifacts related to Wtm flavor symmetry breaking effects. The Wilson term expressed in eq. (2.40) is added to remove the doublers from the theory, leading to the following valence action:

$$S_F|_v = a^4 \overline{\chi}(x) \left[\sum_\mu \gamma_\mu \widetilde{\nabla}_\mu - \frac{a}{2}\nabla^2 + i\frac{a}{4} c_{\mathrm{sw}} \sum_{\mu<\nu} \sigma_{\mu\nu} \hat{F}_{\mu\nu} + \boldsymbol{m}_0 + i\gamma_5 \boldsymbol{\mu} \right] \chi(x), \tag{3.8}$$

where the flavor content is expressed matricially in the mass parameters and color and Dirac indices are omitted.

The fermion fields χ are not restricted to be in a flavor doublet anymore. They are regularized as Osterwalder-Seiler (OS) fermions [50] in order to incorporate the contributions from the strange and charm quarks

$$\boldsymbol{\mu} = \mathrm{diag}\left(\mu_\ell, -\mu_\ell, \pm\mu_s, \mp\mu_c\right). \tag{3.9}$$

Maximal twist is obtained when the bare standard quark mass is tuned to the critical mass $\boldsymbol{m}_0 = m_{\mathrm{cr}}\mathbb{1}_4$. In this case, the twisted mass matrix $\boldsymbol{\mu}$ carries the information about the desired quark masses. For the light and strange quark this is achieved through the matching procedures described in Section 3.6. As described in Subsection 2.5.3, when using the Wilson twisted mass regularization in the sea and valence sectors, the automatic $\mathcal{O}(a)$ improvement for physical observables can be achieved. In the case of our mixed action, an analysis of the Symanzik expansion [51] reveals that residual $\mathcal{O}(a)$ effects coming from the sea quark masses will remain even after the tuning to maximal twist. For instance, the Symanzik expansion of the renormalized twisted mass is given by:

$$\mu_q^R = Z_\mu(\tilde{g}_0^2, a\mu)\left(1 + a\bar{b}_\mu \mathrm{Tr}\left(M_q|_s\right)\right)\mu_q + \mathcal{O}(a^2), \tag{3.10}$$

where $\tilde{g}_0$ is the modified coupling in eq. (3.14), μ is the renormalization scale and Z_μ is the renormalization constant of the twisted mass. A difference in the Symanzik expansion of the twisted mass μ_q, with respect to both the subtracted and the PCAC quark mass of the unitary Wilson setup, is the absence of cut-off effects proportional to the valence quark masses. This property is expected to be particularly relevant in the heavy quark sector.

The twisted mass renormalization factor is related to that of the pseudoscalar density by the vector WTI in the twisted basis defined in eq. (2.64)

$$Z_\mu(\tilde{g}_0^2, a\mu) = \frac{1}{Z_P(\tilde{g}_0^2, a\mu)}. \tag{3.11}$$

3.3 Mixed action

On the lattice, fermion fields from the sea and valence sectors can be easily separated since they appear at two distinct stages of a computation. The sea quarks are introduced through the fermionic action, commonly integrated out in terms of a matrix determinant, as shown in eq. (4.2). The valence quarks can for instance appear, through Wick contractions, as quark propagators in fermionic observables based on n-point correlation functions. Any difference between the sea and valence masses of a given quark flavor must be proportional to the lattice spacing, so that it vanishes in the continuum limit.

On the lattice, one is allowed to take different masses or even different discretizations of the sea and valence Dirac operators. A mixed action is named partially quenched when the quark masses are distinct while the massless Dirac operator is the same for both the fermionic determinant and the valence quark propagators. The mixed action defined in the previous section is an example of a partially quenched mixed action.

A mixed action allows to simulate fermionic observables for a wide range of masses by varying exclusively the valence quark propagators, which often require less computational resources compared to the cost involved in the generation of the gauge configurations for different sea quark masses. Furthermore, a generic mixed action can allow to combine the advantages of considering a computationally cheap regularization in the sea sector with a more expensive valence discretization with additional properties relevant for the determination of some physical observables. On the other hand, even after the matching procedure of the quark masses, the use of different actions in sea and valence sectors breaks unitarity at finite lattice spacings. An analysis using chiral effective theories shows that the breaking of unitarity induces unphysical double pole structures in the flavor diagonal pseudoscalar two-point correlation function [52]. This can induce subtle lattice

artifacts in quantities such as the isospin zero two pion energy or the non-singlet scalar meson two-point correlation function.

3.4 Renormalized chiral trajectory

Various ensembles at different quark masses need to be generated in order to be able to carry out the extrapolation to the physical point. In the $N_f = 2+1$ theory it is desirable to approach the physical point along a fixed chiral trajectory in the $(m_{q,\ell}, m_{q,s})$ plane. Among the existing CLS ensembles [34], we are interested on those that follow a line of constant trace of the quark mass matrix M_q to approach the physical point

$$\mathrm{Tr}M_q = 2m_{q,\ell} + m_{q,s} = \text{const}, \tag{3.12}$$

where the $m_{q,f}$ is the subtracted quark mass defined in eq. (2.43). In practice the critical mass is not known a priori, so the ensembles are generated following a constant value of the trace of the unsubtracted bare quark masses. This is possible since the critical mass remains constant at a given value of g_0. The renormalized coupling g_R is defined as follows

$$g_R^2 = \tilde{g}_0^2 Z_g\left(\tilde{g}_0^2, a\mu\right), \tag{3.13}$$

where the Symanzik expansion of the improved coupling $\tilde{g}_0$ is

$$\tilde{g}_0^2 = g_0^2\left[1 + \frac{b_g(g_0)}{N_f} a\mathrm{Tr}M_q\right]. \tag{3.14}$$

The leading cut-off effects are thus proportional to $\mathrm{Tr}M_q$. Therefore, the main reason to generate the ensembles along the line defined in eq. (3.12) is to keep the renormalized coupling g_R constant when the sea quark masses are varied at fixed value of the bare coupling g_0.

In practice, it is more advantageous to deal with a chiral trajectory in terms of the pion and kaon masses, that are renormalized quantities without $\mathcal{O}(a)$ effects. Pseudoscalar meson masses are related to the quark masses at lowest order in ChPT

$$m_\pi^2 \propto 2m_\ell, \tag{3.15}$$

$$m_K^2 \propto m_\ell + m_s. \tag{3.16}$$

The dimensionless observables ϕ_4 and ϕ_2 are useful for fixing the chiral trajectory and the extrapolation to the physical point, respectively

$$\phi_4 = 8t_0\left(\frac{1}{2}m_\pi^2 + m_K^2\right), \tag{3.17}$$

$$\phi_2 = 8t_0 m_\pi^2, \tag{3.18}$$

where t_0 is the gradient flow scale, that will be introduced in Subsection 3.5.1.

Notice that, at each value of the lattice spacing, there exist CLS ensembles at the symmetric point, $m_{0,\ell} = m_{0,s}$, with a pion mass $M_\pi = 420$ MeV. Furthermore, at a single value of the lattice spacing, $a = 0.077$ fm, additional ensembles along the symmetric line $m_{0,\ell} = m_{0,s}$ were generated. Among the ensembles considered in Table 3.1, the heavier ensembles are placed in the intersection between the chiral trajectory and the line of symmetric point ensembles.

The achieved value for ϕ_4 may be slightly shifted from the preliminary chiral trajectory when the ensembles are generated. Also, the value chosen for $\phi_4^{\rm ph}$ relies on the physical value of t_0 which cannot be extracted from experiments and therefore requires a previous lattice computation. Although an initial value of $t_0^{\rm ph}$ can be taken from an independent lattice determination [53], the scale setting procedure will result in an independent determination of $\phi_4^{\rm ph}$.

To adjust the trajectory after the generation of the ensembles, we carry out a small correction on the bare quark masses with respect to their initial values considered for the dynamical simulations [54]. Such a small correction is carried out in the observable of interest through a low-order Taylor expansion in the quark masses. For the sake of generalization, let us consider a derived observable f determined through a set of primary variables $\{p^\alpha\}_{\alpha=1}^{N_\alpha}$. We consider as primary observable the quantities derived directly from the Monte Carlo samples

$$p^\alpha \equiv \langle p^\alpha \rangle_c = \frac{1}{N_c} \sum_{c=1}^{N_c} p^{\alpha c}, \tag{3.19}$$

where the index c indicates the Monte Carlo (MC) time of every gauge configuration. Considering a derived observable as any function depending on primary observables $f\left(p^1, p^2, ..., p^{N_\alpha}\right)$, we perform a Taylor expansion up to first order in terms of the light and strange mass [2]

$$f(m'_{q,\ell}, m'_{q,s}) = f(m_{q,\ell}, m_{q,s}) + 2\left(m'_{q,\ell} - m_{q,\ell}\right) \frac{df(m_{q,\ell}, m_{q,s})}{dm_{q,\ell}} + \left(m'_{q,s} - m_{q,s}\right) \frac{df(m_{q,\ell}, m_{q,s})}{dm_{q,s}}, \tag{3.20}$$

where primed masses refer to the target masses lying over the desired chiral trajectory, while unprimed masses indicate the simulated masses. There is some freedom in the way to reach the chiral trajectory when shifting the quark masses in the plane $(m'_{q,\ell}, m'_{q,s})$. We prefer to approach the desired trajectory through the line

$$\left(m'_{q,\ell} - m_{q,\ell}\right) = \left(m'_{q,s} - m_{q,s}\right), \tag{3.21}$$

so that the coefficients of the Taylor expansion remain as smaller as possible.

[2] The dependence on the primary observable will be omitted for simplicity.

The derivatives over the quark masses are determined by applying the chain rule,

$$\frac{df}{dm_{q,f}} = \sum_{\alpha=1}^{N_\alpha} \frac{df}{dp^\alpha} \frac{d}{dm_{q,f}} \left[\frac{1}{Z(m_{q,f})} \int \mathcal{D}\left[\psi, \overline{\psi}, U\right] e^{-S(m_{q,f})} p^\alpha(m_{q,f}) \right]. \tag{3.22}$$

After some algebra, one can easily derive a suitable expression in terms of quantities that can be measured on the lattice

$$\frac{df}{dm_{q,f}} = \sum_{\alpha=1}^{N_\alpha} \frac{\partial f}{\partial \left\langle p^\alpha \right\rangle_c} \left[\left\langle \frac{\partial p^{\alpha c}}{\partial m_{q,f}} \right\rangle_c + \left\langle \left(p^{\alpha c} - \left\langle p^\alpha \right\rangle_c\right) \left(\frac{\partial S(U^c)}{\partial m_{q,f}} - \left\langle \frac{\partial S(U)}{\partial m_{q,f}} \right\rangle_c \right) \right\rangle_c \right]. \tag{3.23}$$

The derivative of the action with respect to the quark mass is responsible for the sea quark mass shifting and can be derived through the eq. (4.3), where the effective fermionic action is related to the trace of the inverse of the Dirac operator

$$\frac{\partial S(U^c)}{\partial m_{q,f}} = -\mathrm{Tr}\left[\left[D_0 + m_{q,f}\right]^{-1} (U^c) \right]. \tag{3.24}$$

The quantity above is observable independent, meaning that it only needs to be evaluated once per ensemble. On the other hand, the first term appearing in the rhs of eq. (3.24) is responsible for the shifting of the valence quark masses. When p^α is a two-point mesonic correlation function, the derivative stems from equation (2.29). Considering $m_{q,1}$ and $m_{q,2}$ as the masses of two distinct valence quark flavors of a generic meson, the derivative reads

$$\frac{\partial p^{\alpha c}}{\partial m_{q,f}} = (-1)^{(1+\delta_{f,1}+\delta_{f,2})} \mathrm{Tr}\left[\left[D_0 + m_{q,1}\right]^{-(1+\delta_{f,1})} (x_2, x_1) \Gamma T \left[D_0 + m_{q,2}\right]^{-(1+\delta_{f,2})} (x_1, x_2) \Gamma T' \right]. \tag{3.25}$$

In the Wilson formalism, applying the contribution to the valence quark masses is required to hold up the unitarity of the setup. However, in the mixed action setup one can do a direct computation with the desired shifted mass without relying on a Taylor expansion in the valence quark masses.

In the following section, we discuss about the computational strategies used to estimate the gradient flow scale t_0 and different fermionic observables on the lattice.

3.5 Lattice observables

In this section, we review the definitions and the procedures applied in the calculation of the lattice observables used in this work. Numerical results for these observables are presented in Chapter 5. The observables considered in this study include

the purely gluonic quantity t_0, employed to set the scale, as well as fermionic observables like the pseudoscalar meson mass and decay constant or the PCAC mass.

3.5.1 Gradient flow scale t_0

The observable t_0 is a purely gluonic quantity derived from the *Wilson flow* or *gradient flow* [55]. The *flow time*, $t_w \geq 0$, is an artificial 5th dimension added to the gauge fields in a way that starting by their original values at $t_w = 0$, the fields evolves with t_w according to the flow equation (3.26).

The gradient flow provides a method to perform a continuous transformation allowing to smooth the gauge fields [56]. The gradient flow profits from various properties that render flowed observables particularly useful for scale setting, the study of topology or determining the strong coupling constant.

The Wilson flow is determined by the flow equation in term of the Wilson action S

$$a^2 \partial_{t_w} V_\mu (x; t_w) = -g_0^2 \left\{ \partial_{x,\mu} S(V_\mu (x; t_w)) \right\} V_\mu (x; t_w) , \tag{3.26}$$

where the initial condition is given by the original gauge configurations

$$V_\mu (x; t_w = 0) = U_\mu (x) . \tag{3.27}$$

Notice that the flow time has the dimension of a length squared.

The action density $E(x_0; t_w)$ is a gauge invariant and flow time dependent observable which does not require renormalization. On the lattice, $E(x_0; t_w)$ is defined in terms of $V_{\mu\nu}$ plaquettes

$$E(x_0; t_w) = 2 \sum_{\boldsymbol{x}} \mathrm{Tr} \left[\mathbb{1} - V_{\mu\nu}(x; t_w) \right] , \tag{3.28}$$

where the plaquette sum is carried out solely in the spatial coordinates, leaving the Euclidean time dependence.

The scale parameter t_0 is then defined by the dimensionless operator

$$\left\langle t_w^2 E(x_0; t_w) \right\rangle_{x_0,c} \Big|_{t_w = t_0} = 0.3, \tag{3.29}$$

obtained after averaging over MC time and Euclidean time consecutively. The specific criteria chosen in eq. (3.29) is due to the good properties observed in terms of statistical precision, lattice artifacts, finite size effects and quark mass dependence observed around this specific point.

In contrast with other scale setting parameters, t_0 cannot be estimated by experiments, although it is well-defined observable in the continuum limit that can be accurately determined on the lattice.

3.5.2 Pseudoscalar meson mass

The pseudoscalar meson masses, computed in the unitary Wilson setup, will play an important role in the matching of the sea and valence quark masses needed in our mixed action approach. Ground state meson masses can be extracted from the two-point correlator function defined in eq. (2.21). Considering a sufficiently large value of the lattice time extent, T, the equation (2.18) simplifies to

$$\lim_{T\to\infty} \langle O_2(x_{0_2}) O_1(x_{0_1})\rangle_T = \sum_n \langle 0|\, \hat{O}_2\, |n\rangle \, \langle n|\, \hat{O}_1\, |0\rangle \, e^{-\Delta x_0 \Delta E_n}. \tag{3.30}$$

Since we will employ pion and kaon masses in the mixed action matching and to define the renormalized chiral trajectory, the meson 2-point functions need to be specified for these pseudoscalar states. For simplicity, the fermionic observables will be described in the flavor basis. In this way, the bilinear flavor content is explicitly expressed in terms of the indices r and s instead of the flavor matrix T^a. For instance, the pseudoscalar density defined in eq. (B.14) becomes

$$\mathcal{P}^{rs}(x) = \overline{\psi}^r(x)\gamma_5\psi^s(x), \tag{3.31}$$

in the flavor basis.

The pseudoscalar correlator is defined as the sum of all pseudoscalar two-point functions over the spatial lattice at a given temporal source x_{0_1} and sink x_{0_2} positions

$$C^{rs}_{\mathrm{pp}}(x_{0_2}, x_{0_1}) = \frac{a^6}{L^3} \sum_{\boldsymbol{x_2},\boldsymbol{x_1}} \langle \mathcal{P}^{rs}(x_2)\mathcal{P}^{sr}(x_1)\rangle \,. \tag{3.32}$$

The correlator is projected to zero-momentum so that the pseudoscalar masses can be extracted from the energies in eq. (3.30). At zero-momentum, the signal to noise ratio of the mass-degenerate pseudoscalar meson correlator remains constant when varying the source-sink separation. In this case, the pseudoscalar meson mass can be isolated from an effective mass analysis with a plateau that extends over large time separations.

The expectation values are computed through the contractions of the quark propagators as derived from eq. (2.29), according to their quantum numbers shown in Table A.1

$$\langle O_{\mathrm{p}}(x_2) O_{\mathrm{p}}(x_1)\rangle = -\ \mathrm{Tr}\ \left[D^{-1}(x_2,x_1)\gamma_5 D^{-1}(x_1,x_2)\gamma_5\right]. \tag{3.33}$$

The source and sink positions of the correlation function can be placed close to the boundaries, *i.e.* $x_{0_1} = 0, (T-2a)$. In this way, the ground state can be extracted with a cleaner signal, since the sink position can be placed sufficiently far away from the boundaries in order to reduce boundary effects and excited state contaminations. To increase the statistics, we average over equivalent correlators

whose sources are placed at the symmetric time point with respect to the middle of the lattice. In case of the pseudoscalar correlators, we average

$$\mathcal{C}^{rs}_{\rm pp}(x_0) \equiv \frac{1}{2}\left[C^{rs}_{\rm pp}(x_{0_2}, x_{0_1}) + C^{rs}_{\rm pp}((T-a-x_{0_1})-x_{0_2}, (T-a-x_{0_1}))\right], \quad (3.34)$$

where we denote $x_0 = x_{0_2} - x_{0_1}$. The sign between both terms in eq. (3.34) depends on the considered Dirac structure and it may change when other two-point functions are averaged.

The effective mass, defined in terms of the Euclidean distance, is meant to extract the ground state energy in the limit where the Euclidean time is large enough to safely neglect excited state contaminations [3]

$$aM^{\rm eff}_{\rm ps}(x_0) \equiv \log\left(\frac{\mathcal{C}_{\rm pp}(x_0)}{\mathcal{C}_{\rm pp}(x_0+a)}\right). \quad (3.35)$$

The ratio provides the advantage to cancel out the matrix elements asymptotically.

Although a rough estimation of the pseudoscalar mass is obtained for any Euclidean time x_0 far from the boundaries, averaging over the region where $M^{\rm eff}_{\rm ps}(x_0)$ reaches plateau increases the statistics

$$M_{\rm ps} = \left\langle M^{\rm eff}_{\rm ps}(x_0)\right\rangle^{\rm weig}_{x_0}. \quad (3.36)$$

The superscript above indicates that the average is weighted by its errors.

3.5.3 PCAC quark mass

The definition of the PCAC quark mass was introduced along with the Ward Identities, in Section 2.7. Considering that the light quark masses are degenerate in eq. (2.63), the PCAC mass in the Wilson formalism reads as

$$m_{rs} = \frac{\left\langle \partial_\mu \mathcal{A}^{rs}_\mu(x_2)\, O(x_1)\right\rangle}{2\left\langle \mathcal{P}^{rs}(x_2)\, O(x_1)\right\rangle}. \quad (3.37)$$

The operator $O(x_1)$, whose election leads to values of the PCAC quark mass differing only by lattice artifacts, is taken to be the pseudoscalar density $\mathcal{P}(x_1)$ because it enhances the signal of the quark mass. By construction, the subtracted quark mass, defined in eq. (2.43), must agree with the PCAC mass after renormalization up to cut-off effects. The PCAC quark mass will thus play an important role in the matching procedure in Section 3.6, because contrary to the bare quark mass,

[3] The quark flavor indices r and s will be omitted for the pseudoscalar masses. Instead we will refer the meson by its symbol on the subscript.

its use avoids the need to know a priori the additive mass renormalization. It is therefore a suitable choice for the tuning to maximal twist defined as the vanishing point of the valence PCAC quark mass.

In the notation of the PCAC quark masses m_{rs}, the indices $r, s = 1, 2, 3$, label combinations of up, down and strange quarks, respectively. Since we consider the up and down quark masses to be degenerate, the PCAC quark masses where $r \neq s$ are obtained from non-singlet two-point functions where disconnected diagrams are absent

$$m^R_{\ell,q} = m^R_{12}. \tag{3.38}$$

The strange quark mass is then determined by the combination

$$m^R_{s,q} = 2m^R_{13} - m^R_{12}. \tag{3.39}$$

As mentioned in Section 2.6, improving the lattice action does not imply an automatic $\mathcal{O}(a)$-improvement for the observables. As for the action, in order to improve the quark bilinears, we have to consider all the possible higher dimension operators with the same quantum numbers and symmetry properties as the desired operator. In particular for the axial current, defined in eq. (B.12), there are three dimension-5 operators which contribute to $\mathcal{O}(a)$ discretization effects. We will refer as improved bilinears to the operators which are free from mass-independent $\mathcal{O}(a)$ lattice artifacts. In other words, based on this denomination, labeled by the superscript "(I)", improved bilinears will be $\mathcal{O}(a)$-improved in the chiral limit, but not necessarily in the massive case. The improved axial current is thus defined by adding a single counterterm c_A proportional to the derivative of the pseudoscalar density

$$\mathcal{A}^{rs\,(I)}_{\mu} = \mathcal{A}^{rs}_{\mu} + a c_A(g_0^2)\, \widetilde{\partial}_{\mu} \mathcal{P}^{rs}. \tag{3.40}$$

The improvement coefficient c_A has been determined in a non-perturbative fashion for our lattice action [57] and its dependence on the bare coupling can be parametrized as follows,

$$c_A\left(g_0^2\right) = -0.006033 g_0^2 \left[1 + \exp\left(9.2056 - \left(\frac{13.9847}{g_0^2}\right)\right)\right], \tag{3.41}$$

in terms of the bare coupling. Among the conserved bilinears, detailed in eqs. (B.11) to (B.15), the only one which does not receive $\mathcal{O}(a)$ lattice artifacts in the chiral limit is the pseudoscalar density. The other operators get contributions from dimension five operators.

Using the improved axial current, the effective PCAC mass reads [4]

$$m^{\mathrm{eff}\,(I)}_{rs}(x_0) = \frac{\widetilde{\partial}_0 \mathcal{C}^{rs\,(I)}_{\mathrm{a0p}}(x_0)}{2\mathcal{C}^{rs}_{\mathrm{pp}}(x_0)} = \frac{\widetilde{\partial}_0 \mathcal{C}^{rs}_{\mathrm{a0p}}(x_0) + a c_A(g_0^2) \partial_0 \partial_0^* \mathcal{C}^{rs}_{\mathrm{pp}}(x_0)}{2\mathcal{C}^{rs}_{\mathrm{pp}}(x_0)}, \tag{3.42}$$

[4] The discrete second derivative is given by $\triangle_0 f(x_0) = \partial_0 \partial_0^* f(x_0) = \frac{1}{a^2}\left(f(x_0 + a) + f(x_0 - a) - 2f(x_0)\right) + \mathcal{O}(a^2)$.

where the axial-pseudoscalar correlator $C^{rs}_{\mathrm{a_0p}}(x_0)$ is computed on the lattice in a similar way to the pseudoscalar correlator in eq. (3.32)

$$C^{rs}_{\mathrm{a_0p}}(x_{0_2}, x_{0_1}) = \frac{a^6}{L^3} \sum_{\boldsymbol{x_2}, \boldsymbol{x_1}} \langle \mathcal{A}^{rs}_0(x_2) \mathcal{P}^{sr}(x_1) \rangle \,. \tag{3.43}$$

Notice that the spatial dependency is lost after the summation over $\boldsymbol{x_2}$ and $\boldsymbol{x_1}$. As in eq. (3.34), it can be symmetrized according to the time-reversal transformation, derived in eqs. (C.10) and (C.11)

$$\mathcal{C}^{rs}_{\mathrm{a_0p}}(x_0) \equiv \frac{1}{2} \left[C^{rs}_{\mathrm{a_0p}}(x_{0_2}, 0) - C^{rs}_{\mathrm{a_0p}}((T-1) - x_{0_2}, (T-1)) \right], \tag{3.44}$$

thereby increasing the statistics. The improved PCAC mass is computed through weighted averaged over x_0 values in the plateau region of the effective mass $m^{\mathrm{eff}^{(I)}}_{rs}(x_0)$.

The renormalization of the PCAC mass involves the scale dependent renormalization constant Z_P and also the scale independent one, Z_A, due to the breaking of chiral symmetry by the lattice regularization, as pointed out in Section 2.8. Considering the $\mathcal{O}(a)$ counterterms proportional to the quark masses mentioned above, a generic renormalized quark bilinear made of distinct flavors r and s reads

bilinear $\mathcal{J}^{rs}_\mu$ in the flavor basis reads

$$\mathcal{J}^{rs^R}_\mu = Z_J(\tilde{g}^2_0, a\mu) \left(1 + \bar{b}_J(g^2_0) a \mathrm{Tr}(M_q|_s) + \tilde{b}_J(g^2_0) a m_{rs}\right) \mathcal{J}^{rs^{(I)}}_\mu, \tag{3.45}$$

where concrete examples of $\mathcal{J}^{rs}_\mu$ will be the axial current $\mathcal{A}^{rs}_\mu$ and the pseudoscalar density $\mathcal{P}^{rs}$. The quantity Z_J denotes the renormalization constant while $\bar{b}_J$ and $\tilde{b}_J$ refers to the counterterms controlling mass-dependent $\mathcal{O}(a)$ effects. In particular, the axial renormalization factor Z_A does not depend on the renormalization scheme and is computed in the mass-independent renormalization scheme [58]. We can employ the bare quark mass matrix in eq. (3.45) since the difference between considering the bare or the renormalized trace quark mass matrix only leads to $\mathcal{O}(a^2)$ discrepancies.

Focusing on the PCAC quark masses with $r \neq s$, we can derive its renormalized expression from eqs. (3.37) and (3.45)

$$m^R_{rs} = \frac{Z_A(\tilde{g}^2_0) \left(1 + a\bar{b}_A \mathrm{Tr}(M_q|_s) + a\tilde{b}_A m^{(I)}_{rs}\right)}{Z_P(\tilde{g}^2_0, a\mu) \left(1 + a\bar{b}_P \mathrm{Tr}(M_q|_s) + a\tilde{b}_P m^{(I)}_{rs}\right)} m^{(I)}_{rs} + \mathcal{O}(a^2), \tag{3.46}$$

$$= \frac{Z_A(\tilde{g}^2_0)}{Z_P(\tilde{g}^2_0, a\mu)} \left[1 + a\left(\bar{b}_A - \bar{b}_P\right) \mathrm{Tr}(M_q|_s) + a\left(\tilde{b}_A - \tilde{b}_P\right) m^{(I)}_{rs}\right] m^{(I)}_{rs} + \mathcal{O}(a^2), \tag{3.47}$$

where $\left(\bar{b}_A - \bar{b}_P\right) = \mathcal{O}(g_0^4)$ and the coefficients $\left(\tilde{b}_A - \tilde{b}_P\right)$ were computed non-perturbatively in [31]. The renormalization factors Z_A/Z_P defined in a the mass-independent scheme have been determined on the chirally rotated Schrödinger functional in [32, 59].

3.5.4 Pseudoscalar meson decay constant

The decay constant is an hadronic form factor that can be related to the leptonic decay amplitude of a meson through the weak interactions. Focusing on charged pseudoscalar mesons P, the axial current can mediate the coupling of the meson to the vacuum, in order to satisfy the parity symmetry in the process. The matrix element that characterizes the process of an incoming pseudoscalar meson at rest, $\mathbf{p} = 0$, decaying weakly at position x, is given by:

$$\langle 0 | \, \mathcal{A}_0^{rs^{(I)}}(x) \, | \mathrm{P}^{rs}(\mathbf{p} = 0) \rangle = f_{\mathrm{ps}}^{rs} M_{\mathrm{ps}} \left(2 M_{\mathrm{ps}} L^3\right)^{-\frac{1}{2}}, \tag{3.48}$$

where the decay constant f_{ps}^{rs} is the factor containing the non-perturbative information in the only parametrization of the matrix element allowed by the Lorentz invariance and flavor constraints. The factor $(2M_{\mathrm{ps}}L^3)^{-\frac{1}{2}}$ is included to enforce the conventional normalization of the decay constant.

Matrix elements can be computed on the lattice through a combination of correlation functions defined in eq. (3.30). In particular, the matrix element shown in eq. (3.48) can for instance be extracted from the pseudoscalar and axial-pseudoscalar correlators,

$$R_{\mathrm{a_0p}}^{rs}(x_0) \equiv \left(\frac{\left| \mathcal{C}_{\mathrm{a_0p}}^{rs^{(I)}}(x_0) \mathcal{C}_{\mathrm{a_0p}}^{rs^{(I)}}((T-1) - x_0) \right|}{\mathcal{C}_{\mathrm{pp}}^{rs}(T-1)} \right)^{\frac{1}{2}} = \left| \langle 0 | \, \mathcal{A}_0^{rs^{(I)}} \, | \mathrm{P}^{rs} \rangle \right|, \tag{3.49}$$

in the limit of large Euclidean times, where the low-lying exponential factors cancel. The pseudoscalar meson decay constant f_{ps} renormalizes as the axial current in Subsection 3.5.3, leading to the following expression

$$f_{\mathrm{ps}}^{rs^R} = Z_A\left(g_0^2\right)\left(1 + a b_A m_{rs}^{(I)}\right) \sqrt{\frac{2}{M_{\mathrm{ps}}}} \left\langle R_{\mathrm{a_0p}}^{rs}(x_0) \right\rangle_{x_0}^{\mathrm{weig}}, \tag{3.50}$$

neglecting $\mathcal{O}(a^2)$ terms. The term m_{rs} refers the PCAC mass whose quark flavors, r and s, compose the valence quarks of the meson P. The improvement coefficient b_A employed was estimated at one-loop in perturbation theory for our gauge action [60].

The decay constant can also be determined from the pseudoscalar correlator only, by substituting the axial-pseudoscalar correlator according to the PCAC

relation. Although this alternative holds for the Wilson action, it was shown to suffer from larger boundary effects on the lightest ensembles [61]. This implies that the previous definition of the ratio $R^{rs}_{\mathrm{a_0p}}$ leads to larger plateaus, reducing thus the systematic uncertainty introduced by the average over the Euclidean time.

As mentioned in Subsection 2.5.3, the axial current in the physical basis transforms into the vector current in the twisted basis at maximal twist. This implies that the pseudoscalar decay constant in the twisted basis is proportional to the vector matrix element in a similar way to eq. (3.48) in the physical basis. Setting the generic operator O to the identity in the Wtm PCVC relation. (2.64), the vector matrix element can be related to the pseudoscalar matrix element by taking the time derivative [5]

$$\langle 0|\, V_0^{rs}(x)\, |\mathrm{P}^{rs}(\mathbf{p}=0)\rangle = \frac{2\mu_{rs}}{M_{\mathrm{ps}}}\, \langle 0|\, P^{rs}(x)\, |\mathrm{P}^{rs}(\mathbf{p}=0)\rangle\,, \qquad r \neq s. \tag{3.51}$$

We define the quantity R^{rs}_{pp} as an analogous ratio to the one defined in eq. (3.52) formed by a product of pseudoscalar correlators instead

$$R^{rs}_{\mathrm{pp}}(x_0) \equiv \left(\frac{\left| \mathcal{C}^{rs^{(I)}}_{\mathrm{pp}}(x_0) \mathcal{C}^{rs^{(I)}}_{\mathrm{pp}}((T-1)-x_0) \right|}{\mathcal{C}^{rs}_{\mathrm{pp}}(T-1)} \right)^{\frac{1}{2}}. \tag{3.52}$$

The renormalized pseudoscalar decay constant for the Wtm regularization is obtained from the following equation

$$f^R_{\mathrm{ps}} = \mu_{rs} \sqrt{\frac{8}{M^3_{\mathrm{ps}}}}\, \langle R_{\mathrm{pp}}(x_0)\rangle^{\mathrm{weig}}_{x_0}\,, \tag{3.53}$$

avoiding, in this case, the need of a renormalization factor.

3.6 Matching procedure

The subtracted quark mass of the valence sector must be tuned to zero in order to reach maximal twist. Considering that both the subtracted and the PCAC mass renormalize multiplicatively, the previous condition can be satisfied by tuning the bare PCAC mass to the vanishing point. This process is strongly simplified due to the fact that it only has to be carried out in the valence sector. In practice, the tuning is performed by simulating different values of the hopping parameter $am_{0,\ell}\big|_v = 1/(2\,\kappa_\ell\big|_v)$ around the vanishing point, in a way that $m^{(I)}_{12}\Big|_v = 0$ can be reached by a simple interpolation.

[5] The flavor notation for m_{rs} holds analogously for the twisted mass $\mu_{rs} = \frac{1}{2}(\mu_r + \mu_s)$.

The actions implemented for the sea and the valence sector only differ by the mass term, leading to a partially quenched mixed action. As stated in Section 3.3, unitarity can be recovered by matching the renormalized sea quark masses to the twisted masses [6],

$$\mu_\ell^R\Big|_v \equiv m_{12}^R\Big|_v\,, \qquad \mu_s^R\Big|_v \equiv m_{34}^R\Big|_v\,. \tag{3.54}$$

Enforcing both conditions ensemble by ensemble is sufficient to recover unitarity in the continuum limit.

The matching conditions can be imposed by taking two different approaches. The first method imposes directly the equality of the renormalized quark masses [62], which reads

$$1) \quad \frac{1}{Z_P}\mu_{\ell(s)} \equiv \frac{Z_A}{Z_P}\left[1 + a\left(\tilde{b}_A - \tilde{b}_P\right) m_{12(34)}^{(I)}\right] m_{12(34)}^{(I)}. \tag{3.55}$$

The appearance of Z_P in both side of the relation avoid to include its error contribution in the matching process. The matching above does not include on both sides of the equation the $\mathcal{O}(a)$ improvement terms related to the trace of the sea quark mass matrix, since the improvement coefficients are of $\mathcal{O}(ag_0^4)$ and are therefore expected to induce a small correction. This condition provides a way to match both regularizations through a limited number of simulations around the vanishing PCAC mass.

The alternative approach relies in the relation between the squared pseudoscalar masses and the quark valence masses, so that matching $m_{\pi(K)}^2\Big|_v \equiv m_{\pi(K)}^2\Big|_s$ [63] implies the matching condition in eq. (3.54). In the light sector, this method requires to perform simulations on a set of points in the plane $(\kappa_\ell|_v\,, \mu_\ell)$, referred as a *grid* henceforth. The target values for which the matching and the maximal twist conditions are both guaranteed, is obtained through interpolations among the various data points of the grid. To carry out the interpolations, the valence PCAC mass and the pseudoscalar squared mass, or ϕ_2 equivalently, are parametrized linearly in terms of the twisted mass, and quadratically on the light hopping parameter

$$2) \quad m_{12}|_v\,(\kappa_\ell|_v\,, \mu_\ell) = \frac{p_{11}}{2\,\kappa_\ell|_v} + p_{12}\mu_\ell + p_{13} \equiv 0, \tag{3.56}$$

$$\phi_2|_v\,(\kappa_\ell|_v\,, \mu_\ell) \;= \frac{p_{21}}{(2\,\kappa_\ell|_v)^2} + \frac{p_{22}}{2\,\kappa_\ell|_v} + p_{23}\mu_\ell + p_{24} \equiv \phi_2|_s\,, \tag{3.57}$$

which hold accurately in the neighborhood of the target values.

To match the strange sector as well, we need to consider an hyperplane $(\kappa_\ell|_v\,, \mu_\ell, \mu_s)$ and add the equivalent constraint over the kaon mass or ϕ_4. As in the light sector,

[6] The connected strange quark mass is referred as m_{34}.

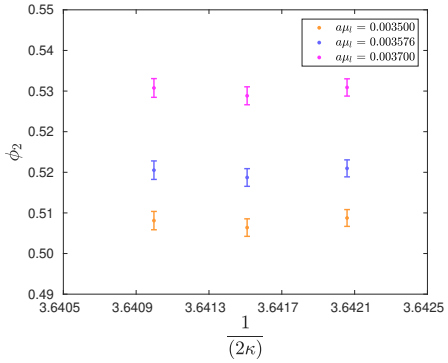

(a) ϕ_2 in terms of the inverse of the hopping parameter for various values of the twisted light quark mass.

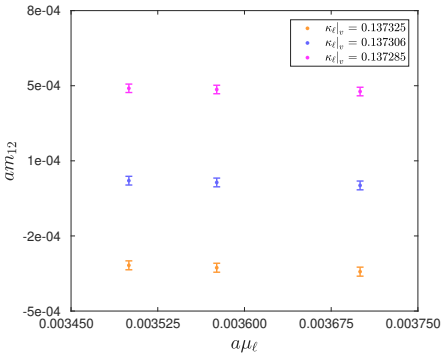

(b) Valence PCAC light quark mass in terms of the twisted light quark mass for various values of the hopping parameter. Data shows a linear behavior for an small interval around the matching point.

Figure 3.1: Illustration of the data used in the tuning procedure to maximal twist. Data points refer to the different simulations employed in the matching of the valence and sea quark masses and in the tuning to maximal twist for the ensemble N203 when using pseudoscalar meson masses in the matching procedure.

ϕ_4 behaves linearly in terms of the twisted quark masses around the matching point

$$2) \quad \phi_4|_v \left(\kappa_\ell|_v, \mu_\ell, \mu_s\right) = \frac{p_{31}}{\left(2\,\kappa_\ell|_v\right)^2} + \frac{p_{32}}{2\,\kappa_\ell|_v} + p_{33}\mu_\ell + p_{34}\mu_s + p_{35} \equiv \phi_4|_s \,. \tag{3.58}$$

Notice that the validity of the parametrizations above relies on the range considered to explore the parameters $\kappa_\ell|_v$, μ_ℓ and μ_s. To ensure a range close enough to the target values, and therefore to reduce the systematic uncertainties in the matching, an initial matching was performed, ensemble by ensemble, according to the first approach in eq. (3.55).

The large amount of simulations needed with respect to the first matching to explore the space of parameters $(\kappa_\ell|_v, \mu_\ell, \mu_s)$ is justified by taking into account that the meson masses are already $\mathcal{O}(a)$-improved. Furthermore, the availability of a grid of points allows to incorporate a refined analysis of the mass-shifts towards a renormalised chiral trajectory (Section 3.4).

Chapter 4

Numerical methods

In this chapter, we will briefly review some of the algorithms involved in the dynamical simulations of QCD on the lattice, pointing out the specific features used in the generation of CLS. Sections 4.2 and 4.3 describes the techniques employed to improve the extraction of the ground state of fermionic observables which are particularly relevant in the heavy quark sector. In the last Section 4.4, we also present the error analysis strategy followed along this work. We will describe an error propagation method constructed to estimate the MC autocorrelation times directly from the derived observables, which allows to simplify the error analysis compared to more standard techniques.

4.1 Algorithms for dynamical simulations

A large fraction of the computational resources devoted to a lattice QCD computation goes into the generation of gauge field configurations through dynamical simulations. However, for some type of observables or when targeting very high precision, the cost of the measurements can become similar or even larger than the one of the generation of the configurations. Measurements which involve the computation of a large number of diagrams or that receive contributions from disconected diagrams are examples of computationally intensive observables.

Algorithmic developments play a decisive role in the advance of lattice QCD simulations. In this section we review some of the basic methodology used in these simulations.

4.1.1 Monte Carlo integration of the path integral

Lattice QCD computations are based on the calculation of expectation values through the path integral formalism, as detailed in Section 2.2. In general, such

functional integrals are not prone for an analytical treatment and they are therefore evaluated numerically through sampling techniques such as the Monte Carlo integration. The MC integration is a stochastic approach which employs random chosen samples to approximate an integral. This procedure tends to outperform the deterministic methods as the dimension of the integral grows.

As described in Appendix D, an integral can be estimated by evaluating $f(x)$ in a set of points drawn from a random probability density $dP(x) = \omega(x)$

$$\int_{\mathcal{D}} f(x)\omega(x)dx = \frac{1}{N}\sum_{i=1}^{N} f(X_i) + \mathcal{O}\left(\frac{1}{\sqrt{N}}\right), \tag{4.1}$$

where $\mathcal{D}$ is the integration domain and $dP(X)$. Instead of estimating the integral of $f(x)$ with a uniform random sampling, *i.e.* $\omega(x) = 1$, the function $f(x)$ can be redefined by reabsorbing any factor on the probability density function $\omega(x)$.

As stated in Section 2.2, the path integral shown in eq. (2.14) can be written in terms of an integral over the gauge fields by applying the Matthews-Salam eq. (2.16) to the fermionic determinant

$$\langle O \rangle = \frac{1}{Z}\int \mathcal{D}\left[U\right] e^{-S_G[U]} \prod_f \mathrm{Det}\left(D^f\right) O. \tag{4.2}$$

This integral can be approximated by a sampling according to the exponential of the action, since once it is normalized it can be interpreted as a probability density function. In practice, the exponential acts as a weight factor, suppressing the regions where the contribution of the action is highly suppressed.

A direct computation of the determinant of a Dirac operator turns out to be prohibitively expensive for large lattices, since the dimension of the fermionic matrix is $12 \times T \times L^3$. Therefore, evaluating the fermionic determinant as a part of the integrand is not feasible for realistic lattice simulations.

An alternative approach is to consider the product of the determinants as part of the weight function $\omega(x)$, which implies that the determinant of the Dirac operator is required to be real and positive. In this approach, the determinant is reexpressed in the following way

$$\mathrm{Det}\left(D\right) = e^{\mathrm{Tr}(\mathrm{Ln}(D))} = e^{-S_F^{\mathrm{eff}}}, \tag{4.3}$$

where the effective action S_F^{eff} receives non local contributions. While for most lattice regularizations the determinant of the Dirac operator is real, positivity is not in general guaranteed and requires further constraints. Considering a pair of degenerate quark masses allows to rewrite the fermionic determinant in terms of a single positive-definite Hermitian operator

$$\mathrm{Det}\left(D^\ell\right)^2 = \mathrm{Det}\left(D^\ell\right)\mathrm{Det}\left(\gamma_5 D^\ell \gamma_5\right) = \mathrm{Det}\left(D^\ell D^{\ell\dagger}\right), \tag{4.4}$$

where γ_5-hermiticity was used.

The approach followed for the light quark masses in eq. (4.4) does not apply to the strange quark, for which the sign of the determinant is not, in general, protected. This issue can be circumvented by estimating the determinant of the positive square root of $R^{-1} = D^{s\dagger}D^s$ through a rational approximation. In this way, the determinant of the strange quark Dirac operator can be written as follows

$$\mathrm{Det}\left(D^{s^{\mathrm{eff}}}\right) \equiv W_s \mathrm{Det}\left(R^{-1}\right), \tag{4.5}$$

where the reweighting factor $W_s = \mathrm{Det}\left(D^s R\right)$ is included to eliminate residual effects due to the use of a rational approximation. Subsequently, once positivity is satisfied, the determinant can be computed by applying an analogous relation to eq. (2.15) for commuting fields in such a way that the original Grassmann integration turns into a standard Gaussian integral in terms of bosonic fields.

The dynamical simulations used to generated the CLS ensembles introduce a factorization of the light quark fermionic determinant in order to reduce instabilities. A twisted mass parameter μ_0 is added to the fermionic determinant in order to protect the spectrum from the presence of unphysical states that would otherwise introduce numerical instabilities

$$\mathrm{Det}\left(Q^{\ell}\right)^2 = \mathrm{Det}Q_{oo}\mathrm{Det}\left(\frac{\hat{Q}^2+\mu_0^2}{\hat{Q}^2+2\mu_0^2}\right)\mathrm{Det}\left(\hat{Q}^2+\mu_0^2\right), \tag{4.6}$$

where $\hat{Q}$ and Q_{oo} are elements of the even-odd precondition decomposition of $Q = \gamma_5 D$ [64]. In order to eliminate the effect of the twisted mass μ_0, a reweighting procedure is applied. The reweighting factor W [35] has to be averaged together with primary observables as follows

$$\langle p^{\alpha}\rangle_c^{\mathrm{rew}} = \frac{\langle p^{\alpha} W\rangle_c}{\langle W\rangle_c}. \tag{4.7}$$

In addition, the Wilson Dirac determinant is factorized according to the Hasenbusch's factorization [65] involving a chain of twisted mass operators in order to improve the efficiency of the dynamical simulations. An analogous procedure is also applied in the computation of the strange quark fermionic determinant [34].

After fermionic integration, the MC approach can be applied to estimate the path integral over the link variables

$$\langle O\rangle = \frac{1}{Z}\int \mathcal{D}\left[U\right] e^{-S^{\mathrm{eff}}[U]} O\left[U\right], \tag{4.8}$$

$$= \frac{1}{N}\sum_{i=1}^{N} O\left[U_i\right], \qquad dP(U) = \frac{e^{-S^{\mathrm{eff}}}}{\int \mathcal{D}\left[U\right] e^{-S^{\mathrm{eff}}}}, \tag{4.9}$$

according to probability density function $dP(U)$ given by the effective action. Notice that $dP(U)$ is normalized in the equation above.

4.1.2 Markov Chain

Estimating random field configurations U_i through the probability distribution function defined in eq. (4.9) would require to compute several high dimensional integrations, which is impractical for realistic lattice data. Instead, the gauge configurations U_i are generated through a stochastic process following an equilibrium distribution. The $\{U_i\}_{i=0}^{N}$ sequence is initiated by a random configuration U_0. In this context, i is understood as labeling the MC time. The price to pay for generating the configurations efficiently is that they are not completely independent among each other, leading to correlations between subsequent configurations. A correct treatment of correlated data will be discussed in Section (4.4).

The Markov chain is described by a transition probability between two successive configuration states U_i and U_{i+1}, that is independent of the initial time i and of the rest of the elements of the chain, meaning that the Markov process is a one–time–step procedure

$$\mathbb{P}_{U_{i+1},U_i} \equiv P\left(U_{i+1} \leftarrow U_i\right). \tag{4.10}$$

The transition matrix $\mathbb{P}$ is a square matrix that controls the probability of all possible transitions in configuration space.

The successive application of the transition probability matrix generates a Markov chain if it fulfills three conditions: *ergodicity*, normalization and stationarity. Ergodicity is represented by a matrix whose elements are greater than zero, which ensures that all transitions are plausible. In fact, to guarantee convergence [1], a slightly stronger condition is required by imposing that for every gauge field there exists an open space $\mathcal{V}$, such that $\mathbb{P}_{U_{i+1},U_i} \geq |\epsilon|$ for all the fields inside the configuration space. A large enough value of ϵ may simplify the communication between topological sectors on the lattice. Besides, the sum of all the elements of a row/column must be normalized $\sum_n \mathbb{P}_{U_i,U_n} = 1$. Stationarity imposes the absence of sinks and sources in the state space, meaning that the probability of the system to be in the configuration U_i, after N steps, is equivalent to the probability of hopping out from U_i after the same number of steps

$$\sum_n \mathbb{P}_{U_i,U_n} P^{(N)}\left(U_n\right) \equiv \sum_n \mathbb{P}_{U_n,U_i} P^{(N)}\left(U_i\right), \tag{4.11}$$

where $P^{(N)}(U_n)$ denotes the probability to end up in the configuration U_n after N steps.

After the *thermalization* period [2], a state of equilibrium is achieved asymptotically. At this stage, importance sampling helps to sample more frequently the

[1] In the context of a Markov chain, convergence implies that the chain tends to a unique stationary distribution regardless of the initial state.

[2] All configurations generated in the thermalization period must be discarded.

most relevant region in the state space given by the weight factor $e^{-S^{\text{eff}}}$. The range of MC steps after which the distribution can be safely considered in equilibrium depends on how every observable couples to the slowest modes of the transition matrix. The natural MC time scale that characterizes the slowest modes of the transition matrix is the exponential auto-correlation time, τ_{exp}. The parameter τ_{exp} is uniquely defined for a given Markov chain and it is this thus observable independent.

In order to secure that the equilibrium distribution has been reached, it is possible to generate various Markov chains differing only by the choice of the initial configuration and monitor the stability of the fluctuations among statistically compatible mean values.

4.1.3 Metropolis algorithm

The implementation of the transition probability matrix $\mathbb{P}$ is not unique but most common algorithms stick to a particular solution of the equilibrium equation (see eq. (4.11)), which considers its equality for every term of the sum

$$\mathbb{P}_{U_{i+1},U_i} P^{(N)}(U_i) = \mathbb{P}_{U_i,U_{i+1}} P^{(N)}(U_{i+1}) \,. \tag{4.12}$$

The Metropolis algorithm is the most common implementation of a Markov chains. It considers the solution proposed in eq. (4.12) and provides a way to generate a new configuration U_{i+1} according to a probability density function, used in eq. (4.9)

$$dP(U) = \frac{e^{-S^{\text{eff}}}}{\int \mathcal{D}[U]\, e^{-S^{\text{eff}}}} \mathcal{D}[U] \,. \tag{4.13}$$

Starting from an arbitrary configuration U_0, [3] the following procedure is performed iteratively to generate U_{i+1}:

1. Define a set of small random perturbations of any given configuration $\xi^\alpha U_i$, under the condition that ξ^α is a random element of $SU(3)$ close to $\mathbb{1}$.

2. Propose an a priori transition matrix $\mathbb{P}^{(0)}_{U_{i+1},U_i}$ from the initial configuration and select the following configuration according to it. Any transformation ξ^α and its inverse must be equally probable leading to a symmetric transition matrix $\mathbb{P}^{(0)}$.

3. $U_{i+1} = \xi^i U_i$ is accepted as a new element according to

$$\mathbb{P}^{(A)}_{U_{i+1},U_i} = \min\left(1, \frac{P(U_{i+1})}{P(U_i)}\right), \tag{4.14}$$

[3] After reaching equilibrium, the chain becomes independent of the initial choice.

or it is rejected and therefore $U_{i+1} = U_i$. The probability shown in eq. (4.14) allows to accept a configuration whose value for the action increases. In this way, the algorithm can explore quantum fluctuations that are forbidden in the classical theory.

4. The transition matrix is constructed according to the above steps

$$\mathbb{P}_{U_{i+1},U_i} = \mathbb{P}^{(A)}_{U_{i+1},U_i}\mathbb{P}^{(0)}_{U_{i+1},U_i} + \delta_{U_{i+1},U_i}\sum_n \mathbb{P}^{(0)}_{U_n,U_i}\left(1 - \mathbb{P}^{(A)}_{U_n,U_i}\right), \tag{4.15}$$

where it is straightforward to check that the equilibrium condition above (4.12) is satisfied. As pointed out in Subsection 4.1.2, the partition function does not need to be explicitly computed since it cancels in the computation of $\mathbb{P}^{(A)}$.

Notice that the above procedure can be performed link by link according to following equation

$$\mathbb{P}_{U_{i+1},U_i} = \sum_n \mathbb{P}_{U_{i+1},U_n}\mathbb{P}_{U_n,U_i}, \tag{4.16}$$

allowing the generation of fields by elementary transitions. This algorithm, in its naive formulation, provides implementation for pure gauge theories where the gauge action involves link variables that connect only the neighboring points. In this case one can benefit from the element-wise updating character of the Metropolis algorithm. Methods as *heat bath* [66] or *overrelaxation* [67, 68] improve significantly the performance. In order to include dynamical fermions, different techniques were proposed to improve the algorithm.

4.1.4 Hybrid Monte Carlo

Dealing with dynamical fermions on the lattice implies a high level of non-locality, as mentioned in Subsection 4.1.1 The Hybrid Monte Carlo (HMC) method [69, 70], which takes over some of the features of the Metropolis algorithm 4.1.3, allows to update the gauge configuration globally, while keeping the acceptance rate to an acceptable level.

Unlike the Metropolis algorithm, the proposal for the subsequent gauge configuration is not a product of random variations but an update according to the classical equations of motion (EOM). It is based on *molecular dynamics* (MD) evolution, where the action becomes an effective potential and the links act as generalized position coordinates. In analogy to the classical theory, the field space is completed by defining the conjugate momenta to the link variables in eq. (2.8)

$$\Pi_\mu(x) = a\sum_{c=1}^{8}\lambda_c\pi_{\mu,c}(x), \tag{4.17}$$

where λ_c are the Gell-Mann matrices and $\pi_{\mu,c}(x)$ are the conjugate momentum of $U_{\mu,c}(x)$. The Hamiltonian governing the MD evolution can thus be written as follows,

$$H\left[\Pi, U\right] = \sum_{\mu,x} \mathrm{Tr}\left[\Pi_\mu^2(x)\right] + S_G\left[U\right] + S_F^{\mathrm{eff}}\left[U\right], \tag{4.18}$$

where, as previously discussed, the fermionic determinant has been expressed in terms of an effective action.

The evolution of the classical system can be computed in terms of a MC time through the equations for $\dot{\Pi}(\Pi, U)$ and $\dot{U}(\Pi, U)$ [71]. [4] Those equations, if exactly solved, would guarantee that the Hamiltonian would be exactly conserved over time. This implies that they would provide, in a deterministic way, a sequence of gauge configurations generated flawlessly according to the generalization of the probability distribution function in eq. (4.13)

$$P\left(\Pi, U\right) = \frac{e^{-H}}{\int \mathcal{D}\left[\Pi, U\right] e^{-H}} \mathcal{D}\left[\Pi, U\right], \tag{4.19}$$

in terms of the Hamiltonian. The numerical integration of the EOM introduces a systematic error that requires an acceptance/rejection step analogous to eq. (4.14) in order to discard large fluctuations in the Hamiltonian along the MD trajectory.

To sum up, the HMC algorithm provides consecutive gauge configurations U_{i+1} following a set of iterative steps:

1. Taking advantage of the fact that the joint probability distribution function in eq. (4.19) factorizes, the momenta Π_{i+1} value can be sampled randomly according to the Gaussian distribution

$$P(\Pi) = \exp(-\frac{1}{2}\Pi^2). \tag{4.20}$$

2. The MD evolution provides the EOM required to produce a new configuration U_{i+1}.

3. U_{i+1} is accepted according to

$$\mathbb{P}^{(A)}_{U_{i+1},U_i} = \min\left(1, \frac{\exp\left(-H\left[\Pi_{i+1}, U_{i+1}\right]\right)}{\exp\left(-H\left[\Pi_i, U_i\right]\right)}\right). \tag{4.21}$$

The procedure aims to generate new gauge configurations that can change significantly in configuration space while keeping the Hamiltonian invariant. In practice, reversibility is imposed by eq. (4.12) and redoing the above steps with

[4] The dot notation is employed to refer to the time derivative of an operator.

$-\Pi_{i+1}$, *i.e.* with the final momentum in the opposite direction, allows to monitor the smallness of the size of the reversibility violations along a given trajectory.

To improve the computational efficiency, the action of the CLS ensembles was integrated in different hierarchical stages, splitting the gauge action from the computation of the light and strange determinants [49].

In the next sections, two different techniques aimed to improve the control in the process of isolating the ground state from fermionic correlation functions will be described.

4.2 Distance Preconditioning

The Dirac operator is a high dimensional matrix which is inverted through iterative numerical procedures minimizing progressively the residue

$$\frac{\left|\sum_{x_2}\left(D\left(x_1,x_2\right)\xi^{(n)}(x_2)-\eta(x_1)\right)\right|}{\left|\sum_{\boldsymbol{x_2}}\xi^{(n)}(x_2)\right|}<r, \tag{4.22}$$

until it reaches the stopping criterion r. The norm in eq. (4.22) is the sum of contributions from all distances on the lattice. The quantity $\eta(x_1)$ refers to a source placed in a particular position x_1. $\xi^{(n)}(x_2)$ denotes the solution at a given iteration n, *i.e.* an approximation of the quark propagator, while the residue measures the relative numerical accuracy achieved in its computation.

According to eq. (3.30), the two-point correlation function signal decays asymptotically as $e^{-\Delta x_0 m_H}$, where m_H denotes the ground state hadron. The fact that the propagator rapidly decreases at large separations between the source and sink positions may imply negligible contributions to the norms in eq. (4.22). The solver is therefore not sensitive to these long distance effects, leading to an inaccurate calculation of the solution when the stopping criterion is not sufficiently small. This issue is easily evidenced for heavy hadrons, and although it can be solved naively by increasing the precision of the calculation, arbitrary precision algorithms become quickly extremely costly.

Distance Preconditioning [72, 73] is an alternative method aimed to avoid the appearance of noise originated by this issue without reducing the stopping criteria r or working with arbitrary precision. It is based on multiplying the Dirac operator by a diagonal matrix in Euclidean time

$$Q_{N_t\times N_t}=\mathrm{diag}\left(q_1,q_2,...,q_{N_t}\right), \qquad q_i=e^{\alpha_0|x^{(i)}_{0_2}-x_{0_1}|}, \tag{4.23}$$

in order to compensate the decrease of the quark propagator in the time direction by the effect of an exponential enhancement depending on a parameter α_0. In

order the keep eq. (4.22) unchanged, the various terms are transformed as follows

$$D \to QDQ^{-1}, \qquad \xi \to Q\xi, \qquad \eta \to Q\eta, \tag{4.24}$$

requiring thus to unfold the transformation over the propagator ξ.

For every correlator and lattice size, there is a large enough value of α_0 for which the accuracy of the various contributions to the norm is not compromised. Larger values of α_0 can lead to reliable computations but they tend to increase the computational cost. In practice, the parameter is tuned according to a few simulations carried out with low statistics at different values of α_0. The minimum value that does not introduce numerical inaccuracies at large distances will be considered for the simulations.

4.3 Smearing

The signal of lattice quantities is subject to an exponential degradation in terms of the Euclidean time that is evaluated by the signal-to-noise ratio. The effect is not perceptible for the pion meson, but it arises for heavier masses. The signal-to-noise ratio R_{SN} is defined as the quotient between the expectation value of a correlator, whose leading term is given by the ground state mass (see eq. (3.30)), and its variance. Considering that the interpolators $O_{H}(x_2)\overline{O}_{H}(x_1)$ generate from the vacuum a meson with mass M_{H}, the variance reads

$$\sigma_{H}^{2} = \sum_{\boldsymbol{x}_2,\boldsymbol{x}_1} \left[\left\langle \left(O_{H}(x_2)\overline{O}_{H}(x_1) \right)^{2} \right\rangle - \left\langle O_{H}(x_2)\overline{O}_{H}(x_1) \right\rangle^{2} \right], \tag{4.25}$$

which receives contributions from four-point correlation functions.

In the limit of large separations Δx_0, [5] the signal-to-noise ratio decreases exponentially fast when the desired ground state mass is heavier than the pion mass,

$$R_{\mathrm{SN}} \equiv \frac{\mathcal{C}_{H}}{\sigma_{H}} \propto e^{-\left(M_{H}-M_{\pi}\right)\Delta x_0}. \tag{4.26}$$

A way to mitigate the problem is to use smeared interpolating operators as previously mentioned in Subsection 2.3.2. Fermion smearing consists in employing non-local interpolating fields, whose overlap with the ground state is enhanced with respect to the local fields. Although the smeared fermions do not improve the signal-to-noise ratio, the exponentials of the higher energy states can be suppressed at short distances, so that the plateau regime of the effective mass is reached before the noise dominates over the signal. In order to suppress the boundary effects due

[5] Normalization factors are here omitted.

to the use of OBC in the time direction, when the signal-to-noise effect emerges very soon in time, the source position can be located in the middle of the lattice.

We employ Wuppertal or Gaussian smearing [74] for the functions S in eqs. (2.26) and (2.27). Wuppertal smearing consists in an update of the fermion fields by the average over their neighboring fields placed within a radius n_s and weighted by the distance. The smeared fields are built iteratively through

$$\psi^{(i+1)}(x) = \frac{1}{6\alpha}\left[\psi^{(i)}(x) + \alpha \sum_{\mu=\pm 1}^{\pm 3} U_\mu(x)\psi^{(i)}(x+\hat{\mu})\right], \tag{4.27}$$

where α is a smearing parameter and i denotes the iteration from 1 to n_s. The smearing procedure can be suitably applied to both source and sink operators.

In the next section, we will describe the methodology developed for the error propagation analysis of primary and derived observables.

4.4 Error analysis

LQCD demands expensive numerical simulations that exploit the limits of the current computational resources. The analysis of lattice data requires a proper assessment of statistical and systematic uncertainties. In this Chapter we present the error analysis developed in this work, based mainly in the methodology developed over the recent years by the ALPHA collaboration [61, 75–77]. As the complexity of an observable derived from MC data increases, the error propagation procedure needed to keep track of the original correlations can become a daunting task. The methodology described in this chapter intends to simplify the process by keeping in memory the correlations at the various stages of the computation.

4.4.1 Notation

To avoid ambiguities, the introduced notation will explicitly show the dependencies of an observable in terms of superscripts and subscripts. Primary observables are usually defined as p whereas derived observable are denoted as $F = f(p)$. The following indices α, r, and c denote an observable, a replica [6] and a configuration of the MC chain, respectively. Furthermore, it is useful to imagine that the same experiment can be repeated an infinite number of times as a way of relating the measured observable or estimate, $\langle p \rangle$, with its true value, P. The index of such experiment can be understood as playing an analogous to the replica index when the number of replicas tend to infinity, but for definiteness it will be called e.

[6] Replicas refer to Markov chains with identical parameters but starting from different seeds of the random number generator.

Expectation values are expressed by $\langle p^a \rangle_b$ where the label in superscripts characterizes a given observable and the subscript outside the bracket denotes a generic quantity over which the average has being applied. The list of dependencies of p are denoted through superscripts. The initial α index will always refer to the observable and will be separated from the other indices by a comma. If two or more subscripts appear, they are sorted according to the order in which the average is carried out, where the average over the rightmost index is applied first.

For simplicity, we define the fluctuations $\delta p_c^{\alpha,b}$ in terms of generic indices b and c such that

$$\delta p_c^{\alpha,b} = \left\langle p^{\alpha,b} \right\rangle_c - P^\alpha, \tag{4.28}$$

which cannot be computed in practice since the true value is unknown. Instead, we approximate P by the average over the whole set of data

$$\hat{\delta} p_c^{\alpha,b} = \left\langle p^{\alpha,b} \right\rangle_c - \langle p^\alpha \rangle_{bc} \,. \tag{4.29}$$

We designate as derived observable F to a quantity which is a function of the primary observables P^α. The partial derivative over one of its arguments is denoted by

$$\partial_\alpha F = \frac{\partial F}{\partial P^\alpha}. \tag{4.30}$$

4.4.2 Primary observable

Since the configurations, Φ^c, are generated through a Markov chain, an observable computed in those configurations $p^{\alpha,c} = p^\alpha(\Phi^c)$ is expected to be carry information about the correlations in Monte Carlo time. The statistical accuracy at which an observable can be determined is thus dependent of the level of correlation among successive measurement within the Markov chain.

Let us define a primary observable, p^α, computed for a set of configurations $\{\Phi\}_1^{N_c}$ which are assumed to be thermalized, $p^{\alpha,c} = p^\alpha(\Phi^c)$. The true value P^α is unknown, but the standard estimator on a single sample of data is given by the mean:

$$\langle p^\alpha \rangle_c = \frac{1}{N_c} \sum_{i=1}^{N_c} p^{\alpha,c}. \tag{4.31}$$

In general, the deviation of $\langle p^\alpha \rangle_c$ from P^α depends on the length of the ensemble, N_c. To analyze the statistical properties of this deviation, one can consider a hypothetical situation in which the experiment is repeated N_e times, where N_e tends to infinity. Consequently, we consider an additional index e, $p^{\alpha,ec}$, to point out each single experiment. The configuration index c would range between 1 and

$N_c(e)$, but we will keep N_c constant for simplicity. According to the law of large numbers

$$\langle p^\alpha \rangle_{ec} = \lim_{N_e \to \infty} \frac{1}{N_e} \sum_{e=1}^{N_e} \langle p^{\alpha,e} \rangle_c = P^\alpha, \tag{4.32}$$

one can determine the statistical uncertainty of the estimator $\langle p^\alpha \rangle_c$, as well as its unbiased character

$$B\left[\langle p^\alpha \rangle_c\right] = E\left[\langle p^\alpha \rangle_c - P^\alpha\right] = \left\langle \langle p^{\alpha,e} \rangle_c - \langle p^\alpha \rangle_{ec} \right\rangle_e = 0, \tag{4.33}$$

where E and B refer to the expectation value or average and to the bias, respectively.

Independently of the distribution that generates the samples $p^{\alpha,c}$, the Central Limit Theorem (CLT) ensures that $\langle p^{\alpha,e} \rangle_c$ behaves as a Gaussian distribution in e. This implies that the statistical uncertainty for any estimand $\langle p^\alpha \rangle_c$ is uniquely defined by the width σ_c^α

$$P^\alpha \sim \langle p^\alpha \rangle_c + \sigma_c^\alpha, \tag{4.34}$$

which is commonly rewritten in terms of the autocorrelation function Γ

$$\sigma_c^{\alpha^2} = \left\langle \left(\langle p^{\alpha,e} \rangle_c - P^\alpha \right)^2 \right\rangle_e, \tag{4.35}$$

$$= \frac{1}{N_c^2} \sum_{c,c'=1}^{N_c} \left\langle \left(p^{\alpha,ec} - P^\alpha \right) \left(p^{\alpha,ec'} - P^\alpha \right) \right\rangle_e, \tag{4.36}$$

$$\equiv \frac{1}{N_c^2} \sum_{c,c'=1}^{N_c} \Gamma_c^{\alpha\alpha}(c,c'). \tag{4.37}$$

The autocorrelation function provides a generalization of the variance, which is reached at $\Gamma_c^{\alpha\alpha}(c=c')$, that considers the correlations between the measurements of a MC chain. Notice that, after thermalization, MC samples ensure translational invariance in configuration space, leading thus to an autocorrelation function which depends only on relative MC times, $\Gamma_c^{\alpha\alpha}(c,c') = \Gamma_c^{\alpha\alpha}(c-c')$.

Although, the index e allows to formally define the autocorrelation time, we need to extract its value from the actual data. The derivation relies on the translation invariance property and on the fact that Γ vanishes asymptotically for long MC distances

$$\Gamma_c^{\alpha\alpha}(c,c') \propto e^{-\frac{|c-c'|}{\tau_{\exp}}}, \qquad |c-c'| \gg 1, \tag{4.38}$$

due to the ergodicity property of the Markov chains. By counting the number of times that the argument $c-c'$ is repeated in the double sum in eq. (4.37), the

statistical error can be rewritten into a single sum

$$\sigma_c^{\alpha^2} = \frac{1}{N_c^2} \sum_{t=1-N_c}^{N_c-1} \Gamma(t) \left(N_c - |t|\right), \tag{4.39}$$

$$= \frac{1}{N_c} \sum_{t=-\infty}^{\infty} \left(\Gamma(t) + \mathcal{O}\left(\frac{t_{\text{exp}}}{N_c}\right)\right). \tag{4.40}$$

In this way, the average over the index e can be substituted by a sum over the larger range available on our MC chain, given by N_c

$$\Gamma_c^{\alpha\alpha}(t) = \left\langle \delta p^{\alpha,e(t+t')} \delta p^{\alpha,et'} \right\rangle_e, \tag{4.41}$$

$$\simeq \frac{1}{N_c - |t|} \sum_{t'=1}^{N_c-t} \left(\hat{\delta} p^{\alpha,(t+t')} \hat{\delta} p^{\alpha,t'}\right). \tag{4.42}$$

We consider various replicas for some ensembles in order to improve the statistics. We determine $N_c(r)$ as the number of configurations for a given replica r, among a total of N_r replicas, the mean estimator reads

$$\langle p^\alpha \rangle_{rc} = \frac{1}{N_C} \sum_{r=1}^{N_r} \sum_{c=1}^{N_c(r)} p^{\alpha,rc} = \frac{1}{N_C} \sum_{r=1}^{N_r} N_c(r) \langle p^{\alpha,r} \rangle_c, \qquad N_C = \sum_{r=1}^{N_r} N_c(r). \tag{4.43}$$

The contributions from all replicas can be included in the estimation of the uncertainty as follows

$$\sigma_{rc}^{\alpha^2} = \langle \delta p_{rc}^{\alpha,e} \delta p_{r'c'}^{\alpha,e} \rangle_e, \tag{4.44}$$

$$= \frac{1}{N_C^2} \sum_{r,r'=1}^{N_r} \sum_{c,c'=1}^{N_c(r)} \delta_{rr'} \left\langle \delta p^{\alpha,erc} \delta p^{\alpha,er'c'} \right\rangle_e, \tag{4.45}$$

where after applying the same reasoning than as eqs. (4.36) and (4.41), one can derive the expression of $\Gamma(t)$ for several replicas

$$\sigma_{rc}^{\alpha^2} \simeq \frac{1}{N_C} \sum_{t=-\infty}^{\infty} \Gamma_{rc}^{\alpha\alpha}(t), \tag{4.46}$$

$$\Gamma_{rc}^{\alpha\alpha}(t) = \frac{1}{N_C} \sum_{r=1}^{N_r} \frac{N_c(r)}{N_c(r) - |t|} \sum_{t'=1}^{N_c(r)-|t|} \left(\hat{\delta} p^{\alpha,r(t+t')} \hat{\delta} p^{\alpha,rt'}\right). \tag{4.47}$$

4.4.3 Derived observable

Derived quantities are defined as a function which ultimately depends, directly or indirectly, on primary observables generated through a MC sampling process. The

following error propagation approach relies on an expansion of the derived observable F in a way that the fluctuations of the primary observables can be transferred to any function of them. In this way, the full error of a derived observable with the correlations properly taken into account can be estimated through its own stored fluctuations, avoiding the need to keep track of those arising from the original primary MC simulations. This procedure can be generalized to derived observables which are defined as through function composition, *e.g.*, functions of functions of primary observables.

The true value of the function for a set of parameters $\{P^\alpha\}_{\alpha=1}^{N_\alpha}$ is defined by

$$F \equiv f\left(\{P^\alpha\}_{\alpha=1}^{N_\alpha}\right) = f\left(P\right), \tag{4.48}$$

where the vector character of the dependency will be assumed from now on. Similarly to the case of primary observables discussed in the previous Subsection 4.4.2, different replicas are combined in the computation of the autocorrelation time in order to reduce the bias of the derived observables. The autocorrelation function $\Gamma^{\alpha\beta}(t)$ defined in terms of two primary observables, P^α and P^β, measures the correlation between these observables at different MC separations t

$$\Gamma_{rc}^{\alpha\beta}(t) = \frac{1}{N_C}\sum_{r=1}^{N_r}\frac{N_c(r)}{N_c(r)-|t|}\sum_{t'=1}^{N_c(r)-|t|}\left(\hat{\delta}p^{\alpha,r(t+t')}\hat{\delta}p^{\beta,rt'}\right). \tag{4.49}$$

At $t=0$, eq. (4.49) leads to the covariance estimator.

Conversely to the case of the primary observables, two different estimators of the true value F appear naturally for any derived observable, depending on the order in which the mean over the replicas is applied

$$F_{(rc)} = f\left(\langle p^\alpha\rangle_{rc}\right), \tag{4.50}$$

$$F_{r(c)} = \frac{1}{N_C}\sum_{r=1}^{N_r} N_c(r)F_{(c)}^r, \qquad F_{(c)}^r = f\left(\langle p^{\alpha,r}\rangle_c\right). \tag{4.51}$$

Notice that the index convention introduced for primary observables holds for derived observables. The superindices indicate the arguments of the observable. Subindices between parenthesis indicate that the respective average was carried out before the function application. Both estimators turn out to be biased but consistents [7]. The bias is derived by Taylor expanding the estimates around the estimand F up to second order

$$F_{(rc)} \simeq F + \sum_\alpha \partial_\alpha f|_{\{P\}}\,\delta p_{rc}^\alpha + \frac{1}{2}\sum_{\alpha\beta}\partial_\alpha\partial_\beta f|_{\{P\}}\,\delta p_{rc}^\alpha \delta p_{rc'}^\beta, \tag{4.52}$$

[7] Consistent estimators generate estimates that converge faster to their true values as the number of data point considered increases.

assuming differentiability of the function f in the neighborhood of $\{P^\alpha\}$. The first estimator bias is related to the autocorrelation function through eqs. (4.44) and (4.46)

$$B\left[F_{(rc)}\right] = \left\langle F_{(rc)} - F \right\rangle_e , \tag{4.53}$$

$$\simeq \sum_\alpha \partial_\alpha f|_{\{P\}} \cancel{\langle \delta p_{rc}^{\alpha,e} \rangle_e} + \frac{1}{2} \sum_{\alpha\beta} \partial_\alpha \partial_\beta f|_{\{P\}} \langle \delta p_{rc}^{\alpha,e} \delta p_{rc'}^{\alpha,e} \rangle_e , \tag{4.54}$$

$$\simeq \frac{1}{2} \sum_{\alpha\beta} \partial_\alpha \partial_\beta f|_{\{\langle p \rangle_{rc}\}} \frac{1}{N_C} \sum_{t=-\infty}^{\infty} \Gamma_{rc}^{\alpha\beta}(t). \tag{4.55}$$

Following the same reasoning for the second estimator, defined in eq. (4.51), the bias of $F_{(rc)}$ is proved to be reduced with respect to the bias of $F_{r(c)}$ as the number of replicas grow

$$B\left[F_{(rc)}\right] = \frac{1}{N_r} B\left[F_{r(c)}\right]. \tag{4.56}$$

This implies that the systematic error introduced by the bias of $F_{(rc)}$ is reduced with respect to $F_{r(c)}$.

Considering thus $F_{(rc)}$, the error with respect to the true value F is calculated by considering an average over an infinite number of experiments e, in a similar way to eq. (4.35), combined with a Taylor expansion

$$\sigma_{rc}^{F^2} = \left\langle \left(F_{(rc)} - F\right)^2 \right\rangle_e = \sum_{\alpha\beta} \partial_\alpha f|_{\{P\}} \partial_\beta f|_{\{P\}} \left\langle \delta p_{rc}^{\alpha,e} \delta p_{rc'}^{\beta,e} \right\rangle_e , \tag{4.57}$$

$$\approx \frac{1}{N_C} \sum_{\alpha\beta} \partial_\alpha f|_{\{\langle p \rangle_{rc}\}} \partial_\beta f|_{\{\langle p \rangle_{rc}\}} \sum_{t=-\infty}^{\infty} \Gamma_{rc}^{\alpha\beta}(t), \tag{4.58}$$

where contrary to the case of the bias, the expansion is carried out up to first order.

At this point, the error of a derived observable can be computed by estimating the derivatives of the observable with respect to the complete set of primary observables that it depends on. However, the equation (4.57) requires the computation of the fluctuations of all the primary observables, which may become a computationally demanding task. This is the case, in particular, when we aim to shift the final observable towards the renormalized chiral trajectory, introduced in Section 3.4.

For that purpose, we define the derived observable F for every replica and configuration as F^{rc}. For the sake of generalization, it can furthermore be characterized as the image of an N_F dimensional vectorial function

$$\boldsymbol{f} : \mathbb{R}^{N_\alpha} \to \mathbb{R}^{N_F}. \tag{4.59}$$

In order to identify the components of the function, the superscript n is added to both the name of the function f^n and to the true value $F^{n,rc}$.

We combine eqs. (4.44) and (4.57) to express the statistical uncertainty in terms of the fluctuations of the primary observable

$$\sigma_{rc}^{F^n 2} = \frac{1}{N_C^2} \sum_{\alpha\beta} \partial_\alpha f^n \partial_\beta f^n \sum_{r=1}^{N_r} \sum_{cc'=1}^{N_c(r)} \left\langle \delta p^{\alpha,erc} \delta p^{\alpha,erc'} \right\rangle_e , \tag{4.60}$$

$$= \frac{1}{N_C^2} \sum_{r=1}^{N_r} \sum_{cc'=1}^{N_c(r)} \left\langle \left(\sum_\alpha \partial_\alpha f^n \delta p^{\alpha,erc} \right) \left(\sum_\beta \partial_\beta f^n \delta p^{\beta,erc'} \right) \right\rangle_e . \tag{4.61}$$

The equation above is the generalization of eq. (4.45) to the case of derived observables, where the fluctuations are given by

$$F^{n,rc} \equiv F + \delta F^{n,rc} = F + \frac{1}{N_c} \sum_\alpha \partial_\alpha f^n \delta p^{\alpha,rc}. \tag{4.62}$$

These new fluctuations δF contain all the relevant information about the correlations so that the error propagation over a function of F can be directly derived from them. Considering a generic composed function $g(P) = \tilde{g}(\boldsymbol{f}(P))$, the chain rule allows to express the derivative of the outer function in terms of the inner function

$$\partial_\alpha g(P) = \sum_{n=1}^{N_F} \left. \frac{\partial \tilde{g}}{\partial f^n} \right|_{f^n(P)} \partial_\alpha f^n|_{\{P\}} . \tag{4.63}$$

Taking into consideration that eq. (4.60) holds for any function of the primary observables, the chain rule can be used to relate the uncertainties of composed functions

$$\sigma_{rc}^{G^2} = \frac{1}{N_C^2} \sum_{r=1}^{N_r} \sum_{cc'=1}^{N_c(r)} \left\langle \delta G^{erc} \delta G^{erc'} \right\rangle_e , \tag{4.64}$$

$$\delta G^{rc} = \sum_\alpha \partial_\alpha g \delta p^{\alpha,rc} = \sum_{n=1}^{N_F} \frac{\partial \tilde{g}}{\partial f^n} \underbrace{\sum_\alpha \partial_\alpha f^n \delta p^{\alpha,rc}}_{\delta F^{n,rc}} . \tag{4.65}$$

This result facilitates the error propagation in any lattice computation, since the autocorrelation function can be approximated by a similar expression as the one in eq. (4.47) in terms of the MC fluctuations of the derived observables.

4.4.4 Autocorrelation

The integrated autocorrelation time τ_{int} measures the effective number of independent samples in a MC chain. Contrary to the exponential autocorrelation time

τ_{exp}, this quantity is observable dependent. The integrated autocorrelation time is defined through the ratio between the correlated and uncorrelated squared error, denoted by σ^2 and σ_0^2 respectively [8]

$$\tau_{\text{int}}\left(X^\alpha\right) \equiv \frac{1}{2}\frac{\sigma^{\alpha^2}}{\sigma_0^{\alpha^2}} = \frac{1}{2} + \sum_{t=1}^{\infty}\frac{\Gamma^{\alpha\alpha}(t)}{\Gamma^{\alpha\alpha}(0)}, \tag{4.66}$$

where the infinite series is truncated, in practice, up to W. Then, the effective number of independent samples for a given observable reads

$$N_C^{\text{eff}}\left(X^\alpha\right) = \frac{N_C}{2\tau_{\text{int}}\left(X^\alpha\right)}. \tag{4.67}$$

The essential point at this stage consists to truncate the infinite sum over the autocorrelation function at different MC lengths in eq. (4.47). The nature of a Markov chain implies that configurations become uncorrelated as the distance t increases, meaning that the function $\Gamma(t)$ tends to vanish asymptotically. The maximum value for t considered, denoted as W, must be sufficiently large to avoid omitting relevant contributions, but not large enough to avoid introducing the noise coming from fluctuations around zero. The procedure implemented is based on [76], with the difference that our implementation is carried out directly on derived observables.

In practice, W is chosen such that the statistical and the systematic error, expressed below, are minimized at the same time according to a proportionality relation. The statistical error was derived in [78] by neglecting the connected parts of the variance's uncertainty

$$\frac{\delta_{\text{stat}}\sigma^{\alpha^2}}{\sigma^{\alpha^2}} \approx \sqrt{\frac{4W+2}{N_C}}. \tag{4.68}$$

The relative systematic error is approximated by the bias of the truncated variance estimator with respect to the complete estimator

$$\frac{\delta_{\text{syst}}\sigma^{\alpha^2}}{\sigma^{\alpha^2}} = \frac{2}{N_C}\frac{\sum_{t=W+1}^{\infty}\Gamma^{\alpha\alpha}(t)}{\sigma^{\alpha^2}} \propto e^{-\frac{W}{\tau_{\text{ext}}}}, \tag{4.69}$$

where the asymptotic behavior, shown in eq. (4.38), holds for large values of W. The minimization of the sum of the statistical and systematic relative errors

$$W_{\text{opt}} = \min_W\left(\sqrt{\frac{4W+2}{N_C}} + e^{-\frac{W}{S\tau_{\text{int}}}}\right), \tag{4.70}$$

[8] The quantity X^α refers to a generic observable, either primary or derived.

provides a way to set the value of W. The parameter S relates the integrated and the exponential autocorrelation time. Since τ_{ext} is often unknown, an a prior study of the autocorrelation function is required to set the value of S.

The autocorrelation functions of observables generated through a Markov chain fulfilling the detailed balance condition in eq. (4.12), can be expressed as a sum of several decaying exponentials. The coefficient associated to each of the exponential factors can be interpreted as the coupling of a given observable to the eigenmodes of the transition matrix of the algorithm. The mode contributing in the limit of large MC time separations is controlled by the exponential autocorrelation time, as shown in eq. (4.38). We follow the methodology detailed in [75] to include this contribution. Although the exact value for τ_{exp} is difficult to compute on from realistic MC simulations, we consider the conservative estimation given in [34] for the CLS ensembles

$$\tau_{\text{exp}} = 14(3)\frac{t_0}{a^2}. \tag{4.71}$$

4.4.5 Error propagation of non-stochastic observables

In multiple occasions a lattice computation may depend on several observables which are not obtained by a MC process or whose fluctuations are not available. Observables derived by perturbative computations, or by non-perturbative estimations carried out in a different set of ensembles, belong to this type of quantities, whose errors and correlations have to be treated differently. This could for instance be the case of the inclusion of a renormalization factors Z or of an improvement coefficient in a lattice. Besides their mean values and errors, when available, we can take into account their correlations. We refer by c_k to the mean of the observable k while $\sigma^{c^2}_{kj}$ denotes the covariance between the elements.

Considering a derived function depending on a set of primary observables P^α and, furthermore, a set of additional observables $\{c\}$ through an intermediate function $\tilde{g}\left(\boldsymbol{f}\left(P, c\right)\right)$ (in a similar way to Subsection 4.4.3), the contribution of $\sigma^{c^2}_{kj}$ to the outer function is determined through

$$\sigma^{G^2} = \sigma^{G^2}_{rc} + \sum_{k,l} \frac{\partial \tilde{g}}{\partial c_k}\frac{\partial \tilde{g}}{\partial c_l}\sigma^{c^2}_{kj}, \tag{4.72}$$

where the expression of $\sigma^{G^2}_{rc}$ is given in eq. (4.64), which contains the autocorrelations of a given ensemble.

By saving the gradient of the intermediate function $\vec{\nabla}_c f^n$ with respect to the additional parameters c_k, in a similar way to the uncertainties $\delta F^{n,rc}$, the last term in the above equation can be estimated by applying the chain rule

$$\left(\vec{\nabla}_c \tilde{g}\right)_k = \frac{\partial \tilde{g}}{\partial c_k} = \sum_{n=1}^{N_F} \frac{\partial \tilde{g}}{\partial f^n}\frac{\partial f^n}{\partial c_k}. \tag{4.73}$$

4.4.6 Derived observables from different ensembles

Different ensembles are uncorrelated as long as the physical or algorithmic parameters differ from each other. Therefore, the autocorrelation of the observables measured in different ensembles can be treated independently. The only source of correlation between two observables f^n and f^m analyzed in different ensembles may come from shared additional parameters c_k, which play a role in the derivation of the function, but are not estimated through any of these ensembles. The procedure followed in Subsection 4.4.5 allows us to decouple the contributions of these parameters c_k from the MC measurements, ensuring a solid uncorrelated analysis of the data from different ensembles.

Following the reasoning of the previous Section 4.4.3, the error of a function $\tilde{g}\left(\boldsymbol{f}\left(P,c\right)\right)$ is given by a double sum over the complete set of functions f^n, where the sole difference with respect to equation (4.65) is the cancellation between of the crossed terms f^n which belong to different ensembles

$$\sigma^{G^2} = \sum_{E=1}^{N_E} \frac{1}{N_C(E)} \sum_{n,m\in E} \frac{\partial \tilde{g}}{\partial f^n} \frac{\partial \tilde{g}}{\partial f^m} \sum_{t=-\infty}^{\infty} \Gamma_{rc}^{nm}(t) + \sum_{kl} \frac{\partial \tilde{g}}{\partial c_k} \frac{\partial \tilde{g}}{\partial c_l} \sigma_{kl}^{c^2}, \tag{4.74}$$

where the index E denotes the ensemble and the last term was previously defined in eq. (4.72).

Chapter 5

Scale setting and determination of quark masses

In this chapter we present the physical results obtained within our mixed action approach. A comparison and a combination with the results achieved with the unitary Wilson formalism will be also considered. In Section 5.1, we compare the continuum limit scaling of both regularizations and analyze the convergence towards a common value as the lattice spacing is reduced. In Section 5.2 we describe a scale setting procedure using physical values of the pion and kaon masses and decay constants. The gradient flow scale t_0 is used as an intermediate quantity and an iterative procedure involving the extrapolation of t_0 to the physical point is presented. Various approaches are considered in order to estimate the systematic effects in the extrapolation to the physical point. In Section 5.3, we apply the previously obtained results for the scale setting to the determination of the light and strange quark masses. The physical values are converted into the RGI scheme thanks to the renormalization and running of the quark mass computed in [32]. We extract the RGI quark masses through appropriate combinations of quark and meson masses aiming to reduce the contributions of the unknown ChPT low-energy couplings (LECs) while also taming the leading dependence on the light pseudoscalar meson mass [79].

5.1 Continuum limit scaling of symmetric point ensembles

We carry out a continuum-limit scaling analysis of the renormalized PCAC quark masses and of the pseudoscalar meson decay constants for the symmetric point ensembles. This study aims at testing the universality of our mixed action approach by comparing the continuum results to those obtained when using Wilson

fermions in both the sea and valence sectors. This study also provides some information about the relevance of the residual $\mathcal{O}(a)$ cut-off effects proportional to the sea quark masses.

In Figure 5.1, we illustrate the continuum-limit scaling of the pseudoscalar meson masses in units of t_0. It shows a comparison between the Wilson and the Wilson twisted mass regularizations, when the twisted mass is matched through the PCAC quark masses. The difference is expected to arise from the relative cut-off effects of $\mathcal{O}(a^2)$ between the pseudoscalar meson masses of the sea and the valence sectors. The figure confirms that relative lattice artifacts are reduced as the lattice spacing decreases.

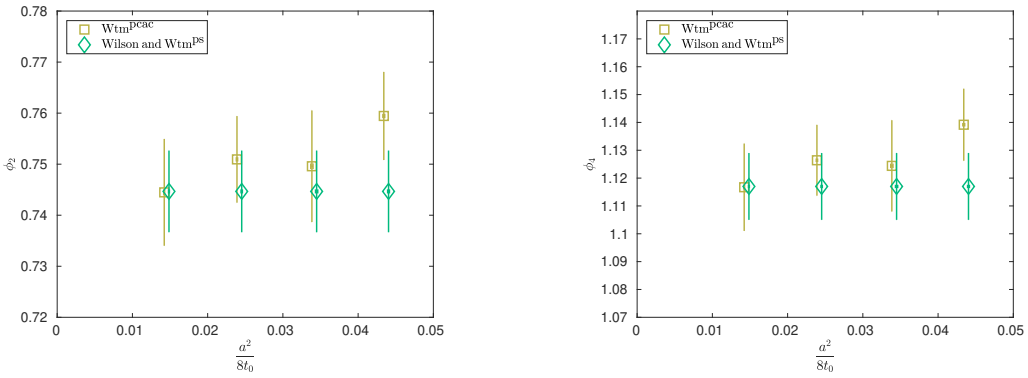

Figure 5.1: Continuum limit scaling of ϕ_2 and ϕ_4, defined in eqs. (3.18) and (3.17), for symmetric point ensembles. Green diamond data points refer to the case of the Wilson and the fully twisted tmQCD mixed action matched through the pseudoscalar masses to $\phi_4 = 1.117$. The yellow squares refer to a similar case but now using a matching of the sea and valence by means of the renormalized PCAC quark masses.

In the two panels of Figure 5.2, we show the continuum limit scaling of the PCAC quark mass m_{12}^R and of a linear combination of the pion and kaon decay constants

$$f_{\pi K} = \frac{2}{3}\left(\frac{1}{2}f_\pi + f_K\right), \tag{5.1}$$

that will be used to perform the scale setting in Section 5.2. As expected, the results for these quantities coming from the two regularizations agree in the continuum limit and the behavior is consistent with $\mathcal{O}(a)$ improvement for both the sea and valence sectors.

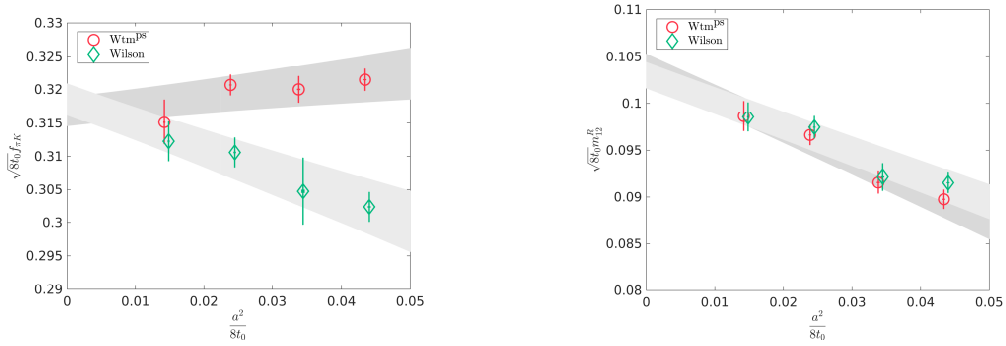

Figure 5.2: Continuum limit scaling of $f_{\pi K}$ defined in eq. (5.1) and of the renormalized PCAC light quark mass m_{12}^R in units of t_0 using symmetric point ensembles. Green diamond points refer to the Wilson case while red circular symbols indicate the fully twisted tmQCD mixed action matched through pseudoscalar masses to $\phi_4 = 1.117$.

5.2 Extrapolation to the physical point and scale setting

The scale setting of the CLS $N_f = 2 + 1$ ensembles listed in Table 3.1 is carried out by two dimensionful quantities: the gradient flow scale t_0 and a combination of the pion and kaon decay constants, as proposed in [54]. The high accuracy with which t_0 can be determined makes it a useful intermediate quantity in the scale setting procedure. As mentioned in Subsection 3.5.1, t_0^{ph} cannot be extracted from experiment but it has a field theoretical definition with a proper continuum limit which allows its determination through an extrapolation to the physical point.

The strategy adopted for the determination of t_0^{ph} follows an iterative procedure where an educated guess is used as an initial value [1], called $t_0^{\text{ph}(0)}$, to determine $\phi_4^{\text{ph}(1)}$ from a continuum and physical point extrapolations. In this way a new value of $t_0^{\text{ph}(i)}$ can be obtained and the process is iterated until the latest value of $t_0^{\text{ph}(i+1)}$ is consistent with the previous one. The updated value of t_0^{ph} can then be used to fix the renormalized chiral trajectory – see Section 3.4 – that extrapolates to the physical point

$$\phi_4^{\text{ph}(i)} = 8t_0^{\text{ph}(i)} \left(\frac{1}{2} M_\pi^{\text{ph}\,2} + M_K^{\text{ph}\,2} \right) \equiv \phi_4^{(i)}. \tag{5.2}$$

At every iteration, the physical point is reached by fixing the value of $\phi_4^{\text{ph}(i)}$ and by the chiral extrapolation of an observable f to $\phi_2^{\text{ph}(i)}$. In practice, $f(\phi_2)$ can be

[1] In practice, the first value for $\phi_4^{\text{ph}(0)} = 1.11$ was taken from [54] .

chosen to be the decay constant of the pion f_π or of the kaon f_K, as well as the linear combination defined in eq. (5.1). The physical value of t_0 is finally extracted by imposing

$$\sqrt{8\frac{t_0}{a^2}}af(\phi_2) \equiv \sqrt{8t_0^{\mathrm{ph}(i)}}f^{\mathrm{ph}}, \tag{5.3}$$

where the physical value of f, denoted by f^{ph} is required as an external input. In the matching procedure, the physical meson masses involved are corrected for strong and electromagnetic isospin breaking effects [80]

$$M_\pi^{\mathrm{ph}} = 134.8(3)\ \mathrm{MeV}, \quad M_K^{\mathrm{ph}} = 494.2(3)\ \mathrm{MeV}. \tag{5.4}$$

The physical values for the pion and the kaon decay constants are taken from the PDG [81]

$$f_\pi^{\mathrm{ph}} = 130.4(2)\ \mathrm{MeV}, \quad f_K^{\mathrm{ph}} = 156.2(7)\ \mathrm{MeV}. \tag{5.5}$$

Different approaches were considered in order to bound the systematic errors induced by the choice of the decay constant parametrization in terms of the meson masses and of the lattice spacing. The functional forms considered are either derived from next-to-leading order (NLO) ChPT [82] expressions or from Taylor expansions around the symmetric point. In order to incorporate discretization effects into these functional forms, they could be supplemented by terms which include mass independent and mass dependent $\mathcal{O}(a^2)$ lattice artifacts [79]

$$\sqrt{8\frac{t_0}{a^2}}af = \left(\sqrt{8\frac{t_0}{a^2}}af\right)^{\mathrm{cont}} + \frac{a^2}{8t_0}\left(A_0 + A_1\phi_2 + A_2\phi_4\right). \tag{5.6}$$

Note, however, that standard power-counting schemes in ChPT indicate that $\mathcal{O}(a^2)$ terms appear at the same order as the squared meson mass [83, 84], meaning that A_1 and A_2 can be consistently neglected when working at NLO.

As pointed out in Section 3.4, the chiral trajectory evolves from the symmetric point to the physical point through a line where the light quark mass decreases as the strange quark mass increases. $SU(3)$ ChPT is then the proper effective theory to consider the change of both masses along the chiral trajectory. We thus consider the following parametrizations for the continuum and physical extrapolations

$$\sqrt{8\frac{t_0}{a^2}}af_\pi = p_1 + p_2\phi_2 + p_3K\left(2\mathcal{L}_2 + \mathcal{L}_K\right) + c_1\frac{a^2}{8t_0}, \tag{5.7}$$

$$\sqrt{8\frac{t_0}{a^2}}af_K = p_1 + p_2\left(\phi_4 - \frac{1}{2}\phi_2\right) + \frac{3}{4}p_3K\left(\mathcal{L}_2 + 2\mathcal{L}_K + \mathcal{L}_\eta\right) + c_2\frac{a^2}{8t_0}, \tag{5.8}$$

where K and the chiral logarithms $\mathcal{L}_i$ are defined in Appendix F, together with the fitting parameters p_i.

It is interesting to monitor the light quark mass dependence through quantities normalized to their symmetric point values. In Figure 5.3 we illustrate the dependence of $\frac{f_{\pi K}}{f_{\pi K}^{\rm sym}}$ as a function of ϕ_2 for the mixed action and for the unitary Wilson case.

We construct the trace of the mass matrix through PCAC quark masses,

$$\mathrm{Tr}\left(M_q^R\right) = m_{12}^R + 2m_{13}^R. \tag{5.9}$$

This is used in Figure 5.4 to build its ratio with respect to the symmetric point

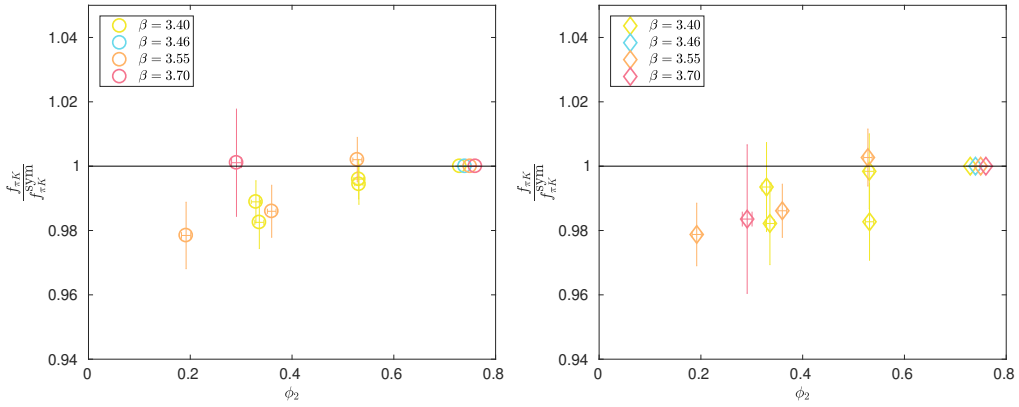

Figure 5.3: Light quark mass dependence of $f_{\pi K}$ normalized by its symmetric point value. The left panel corresponds to the mixed action, while right panel illustrates the unitary Wilson results.

In addition to the expressions of f_π (5.7) and f_K (5.8), we also consider the combination $f_{\pi K}$ defined in eq. (5.1). This quantity is chosen since, up to logarithmic corrections in $SU(3)$ ChPT, it remains constant along the chiral trajectory defined by a constant value of ϕ_4

$$\sqrt{8\frac{t_0}{a^2}}af_{\pi K} = p_1 + \frac{2}{3}p_2\phi_4 + \frac{1}{6}p_3K\left(7\mathcal{L}_2 + 8\mathcal{L}_K + 3\mathcal{L}_\eta\right) + c_3\frac{a^2}{8t_0}. \tag{5.10}$$

Furthermore, we consider the ratio of f_K and f_π in eqs. (5.8) and (5.7), respectively,

$$\frac{f_K}{f_\pi} = \frac{p_1 + p_2\left(\phi_4 - \frac{1}{2}\phi_2\right) + \frac{3}{4}p_3K\left(\mathcal{L}_2 + 2\mathcal{L}_K + \mathcal{L}_\eta\right)}{p_1 + p_2\phi_2 + p_3K\left(2\mathcal{L}_2 + \mathcal{L}_K\right)} + c_4\left(1 - \frac{\phi_2}{\phi_4 - \frac{1}{2}\phi_2}\right)\frac{a^2}{8t_0}, \tag{5.11}$$

in a global fit together with eq. (5.10) in order to further constraint the fit parameters. Notice that the ratio is equal to 1 at the symmetric point. As an alternative

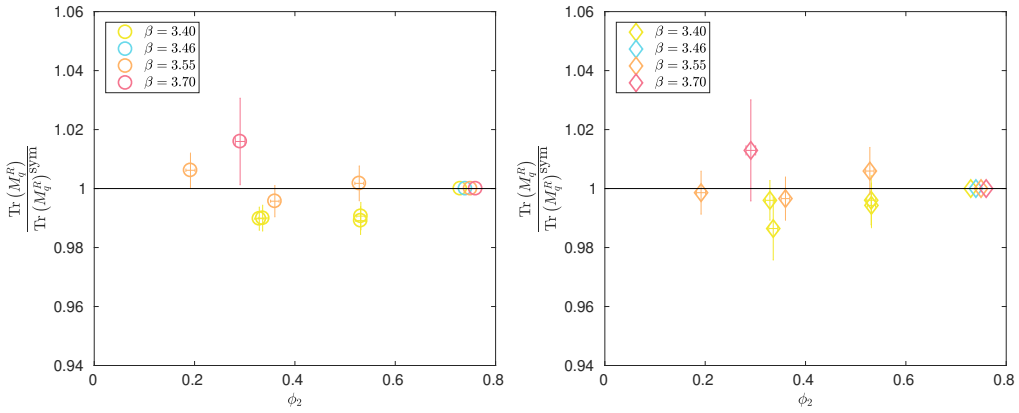

Figure 5.4: Light quark mass dependence of the trace of the mass matrix normalized by its symmetric point value. In the left panel, we use the light and strange twisted masses to construct the trace. The right panel illustrates the unitary Wilson results based on eq. (5.9).

to ChPT, we also consider a Taylor expansion around the symmetric point ϕ_2^{sym}

$$\sqrt{8\frac{t_0}{a^2}}af_{\pi K} = p_1' + p_2'\left(\phi_2 - \phi_2^{\mathrm{sym}}\right)^2 + c_1'\frac{a^2}{8t_0}, \tag{5.12}$$

where the linear term in $\phi_2 - \phi_2^{\mathrm{sym}}$ does not contribute [85].

We wish to consider various well motivated parametrizations in order to study the stability of the results. Among the proposed functional forms, we identify those whose results can be considered stable according to following criteria: reasonable chi-squared, stability when heavier ensembles are removed and compatibility of the results with respect to the other parametrizations. After an exploratory stability study, we restrict ourselves to the following three strategies in the determination of t_0^{ph}

1. Combined fit of $f_{\pi K}$ and $\frac{f_K}{f_\pi}$ using ChPT eqs. (5.10) and (5.11).

2. Single fit of $f_{\pi K}$ using the ChPT eq. (5.10).

3. Single fit of $f_{\pi K}$ using a Taylor expansion in eq. (5.12).

We employ the combined fit of $f_{\pi K}$ and $\frac{f_K}{f_\pi}$ to determine the mean value and the statistical error, while the other two parametrizations are employed to estimate the systematic uncertainties.

Both ChPT functional forms for f_π in eq. (5.7) and f_K in eq. (5.8), fitted individually, show significant deviations when heavier ensembles are discarded.

Although a combined fit of the ChPT parametrizations for f_π and f_K improves the stability, the obtained results differ with respect to the most stable fits. As a consequence, the results of these fit forms will be discarded.

In Table 5.1, the results for both $t_0^{\rm ph}$ and $\phi_4^{\rm ph}$ are shown when using three different approaches: the unitary Wilson case, the Wtm mixed action matched with pseudoscalar mesons ($\text{Wtm}^{\rm ps}$) and the Wtm mixed action matched with PCAC quark masses ($\text{Wtm}^{\rm pcac}$). We also present the physical values for t_0 and ϕ_4 obtained by a combined correlated analysis of the Wilson and $\text{Wtm}^{\rm ps}$ setups

	Wilson	$\text{Wtm}^{\rm ps}$	$\text{Wtm}^{\rm pcac}$	Combined
$t_0^{\rm ph}\left[\text{fm}^2\right]$	0.02146(31)(33)	0.02136(31)(26)	0.02140(32)(37)	0.02141(26)(29)
$\phi_4^{\rm ph}$	1.117(16)(18)	1.112(16)(7)	1.114(17)(20)	1.114(14)(10)

Table 5.1: Determination of the physical values of t_0 and ϕ_4 computed in the three different formalism. Final column shows the combined result of the Wilson and $\text{Wtm}^{\rm ps}$ regularizations. The first value in parentheses corresponds to the statistical error, while the second is the systematic uncertainty estimated by the largest difference among the variations associated to the choice of the parametrizations and of the ensembles included in the analysis.

The knowledge of the physical value of t_0 and ϕ_4 allows to set the scale by extrapolating $\frac{t_0}{a^2}$ at fixed values of β. We follow the procedure proposed in [54] and fix the scale by using t_0 at the symmetric point in order to avoid additional chiral extrapolations. Although the ChPT parametrizations may not hold at the symmetric point, the fact that there are ensembles directly simulated at this point simplifies the approach to $t_0^{\rm sym}$

$$\sqrt{8\frac{t_0^{\rm sym}}{a^2}}af(\phi_2) \equiv \sqrt{8t_0^{\rm sym}}f^{\rm ph}. \tag{5.13}$$

By dividing $t_0^{\rm sym}$ by its value in lattice units for every symmetric point ensemble, H101, H400, N202 and N300, one can extract the lattice spacing at every value of β. As before, the scale setting is carried out for the Wilson unitary setup and for both matching procedures of the Wtm mixed action. The analysis is also replicated for the three parametrizations described above in order to estimate the systematic uncertainties shown in Table 5.2.

	β	Wilson	Wtm$^{\text{ps}}$	Wtm$^{\text{pcac}}$	Combined
$t_0^{\text{sym}}\left[\text{fm}^2\right]$		0.02156(34)(22)	0.02132(34)(43)	0.02134(35)(44)	0.02144(30)(21)
a [fm]	3.40	0.08686(72)(44)	0.08637(72)(87)	0.08641(74)(89)	0.08661(64)(42)
	3.46	0.07678(64)(39)	0.07635(63)(77)	0.07638(65)(79)	0.07656(57)(38)
	3.55	0.06463(49)(33)	0.06427(49)(64)	0.06430(51)(66)	0.06445(43)(31)
	3.70	0.05009(41)(26)	0.04981(40)(50)	0.04983(41)(52)	0.04995(36)(25)

Table 5.2: Determination of the lattice spacing for the β values considered in this work and of t_0^{sym} – the value of t_0 at the symmetric point – for the three considered approaches. The last column shows the combined result of Wilson and Wtm$^{\text{ps}}$. The first value in parentheses corresponds to the statistical error, while the second gives an approximation of the systematic uncertainty estimated by the largest difference among the variations associated to the choice of the parametrizations and of the ensembles included in the analysis.

5.3 RGI quark masses

In this section, we make use of the scale setting procedure described in the previous section in order to estimate the degenerate light quark masses and the strange quark mass. In this computation with $N_f = 2 + 1$ dynamical quarks, we have not included the effects of strong and electromagnetic isospin breaking corrections and the effects of heavier dynamical quarks.

The improved and renormalized quark masses at a low-energy scale, $\mu_{\text{had}} = 233(8)\text{MeV}$, – see Subsection 3.5.3 – are multiplied with the total running factor [32] allowing the conversion to the Renormalization Group Invariant (RGI) quark masses [86]

$$m_{rs}^{RGI} = \frac{m^{RGI}}{m^R\left(\mu_{\text{had}}\right)} m_{rs}^R\left(\mu_{\text{had}}\right), \qquad \frac{m^{RGI}}{m^R\left(\mu_{\text{had}}\right)} = 0.9148(88). \tag{5.14}$$

The RGI quark masses are independent of the scheme and of the scale used in the renormalization. Note that the contribution to the error coming from the running factor must be applied after the continuum extrapolation to avoid double counting.

Starting from the renormalized PCAC quark masses, listed in Appendix G, the determination of the physical quark masses is carried out by a simultaneous physical and continuum extrapolation, in a similar fashion to the decay constant in the scale setting procedure, see Section 5.2. Different combinations of ChPT and Taylor expansions in terms of ϕ_2 around the symmetric point are considered for $\sqrt{8t_0}m_{12}^R$ and $\sqrt{8t_0}m_{13}^R$ to control the systematic effects. The ChPT expressions for the quark masses are derived from [79, 87] in Appendix F, whereas the same

function proposed in eq. (5.6) for the discretization effects can be used for the quark masses

$$\sqrt{8\frac{t_0}{a^2}}am_{12}^R = \phi_2\left[q_1 + q_2\phi_2 + q_3K\left(\mathcal{L}_2 - \frac{1}{3}\mathcal{L}_\eta\right)\right] + \frac{a^2}{8t_0}d_1, \tag{5.15}$$

$$\sqrt{8\frac{t_0}{a^2}}am_{13}^R = \phi_K\left[q_1 + q_2\phi_K + \frac{2}{3}q_3K\mathcal{L}_\eta\right] + \frac{a^2}{8t_0}d_2, \tag{5.16}$$

where ϕ_K is defined as

$$\phi_K = 8t_0M_k^2 = \phi_4 - \frac{1}{2}\phi_2. \tag{5.17}$$

Similarly to the previous analysis, we discard the results coming from the independent and combined fits based on the ChPT expressions above, since they show large deviations when heavier masses are removed in decreasing order. The Taylor expansion around the symmetric point, defined in an analogous way to equation (5.12) but considering linear terms, is also discarded for the same reason.

Alternatively, we seek for combinations of the previous equations which partially cancel cut-off effects through ratios. By neglecting higher order terms in the continuum ChPT expressions, the ratio between m_{12}^R and m_{13}^R reads

$$\frac{m_{12}^R}{m_{13}^R} = \frac{\phi_2}{\phi_K}\left[1 + \frac{q_2}{q_1}\left(\frac{3}{2}\phi_2 - \phi_4\right) - K\left(\mathcal{L}_2 - \mathcal{L}_\eta\right)\right] + \frac{a^2}{8t_0}\left(1 - \frac{\phi_2}{\phi_K}\right)d_3, \tag{5.18}$$

which is constrained to be one at the symmetric point. The term characterizing discretization effects proportional to a^2 needs to be slightly modified to fulfill this condition. Another useful expression is obtained by a linear combination of ratios between quark masses and pseudoscalar meson masses. In particular the following functional form, proposed in [79], allows to cancel the dependence of ϕ_2

$$\sqrt{8\frac{t_0}{a^2}}\left(2\frac{m_{13}^R}{\phi_K} + \frac{m_{12}^R}{\phi_2}\right) = 3q_1 + 2q_2\phi_4 + q_3K\left(\mathcal{L}_2 + \mathcal{L}_\eta\right) + \frac{a^2}{8t_0}d_4. \tag{5.19}$$

Combining these ratios and the ChPT equations for the renormalized quark masses, we notice that the fits involving eq. (5.15) present instabilities when removing the heaviest ensembles in decreasing order. Therefore, we focus on the following two functional forms to compute the RGI quark masses:

1. Combined fit of $\frac{m_{12}^R}{m_{13}^R}$ and $\sqrt{8t_0}\left(2\frac{m_{13}^R}{\phi_K} + \frac{m_{12}^R}{\phi_2}\right)$ using ChPT eqs. (5.18) and (5.19).

2. Combined fit of $\frac{m_{12}^R}{m_{13}^R}$ and $\sqrt{8\frac{t_0}{a^2}}am_{13}^R$ using ChPT eqs. (5.18) and (5.16).

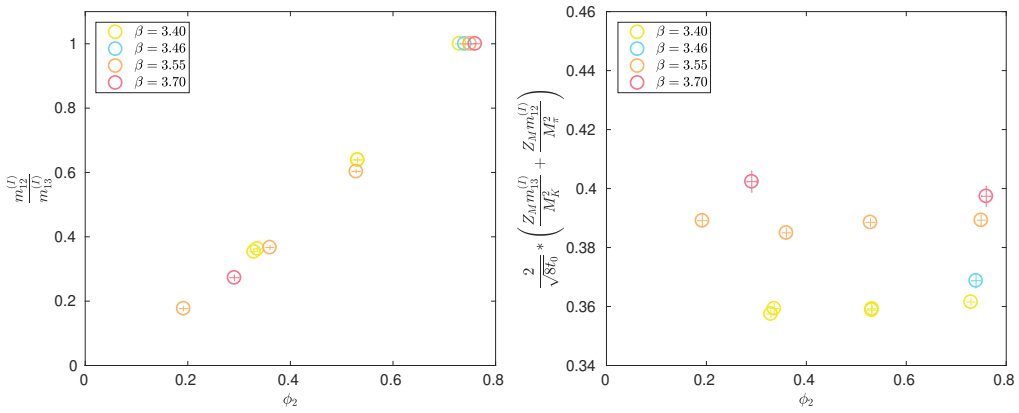

Figure 5.5: Illustration of light quark mass dependence in the mixed action for various values of β: In the left panel, the ratio $\frac{m_{12}^R}{m_{13}^R}$, where $m_{rs}^R = \frac{\mu_r^R + \mu_s^R}{2}$, indicates the presence of mild lattice artifacts. In the right panel, we use the combination in the lhs of eq. (5.19) and confirm that its dependence on ϕ_2 is suppressed.

Given that eq. (5.19) strongly constraints the approach to the physical point, we consider the first combined fit as our preferred analysis. The other functional form is used to assess the systematic effects.

In table 5.3 we show the results for the light and the strange RGI quark masses after the physical and continuum extrapolations. While the degenerate light quark masses are directly obtained in the extrapolation, the strange quark mass is computed as follows

$$m_s^{RGI} = 2m_{13}^{RGI} - m_{12}^{RGI}. \tag{5.20}$$

	Wilson	Wtm$^{\text{ps}}$	Wtm$^{\text{pcac}}$	Combined
m_ℓ^{RGI} [MeV]	4.676(98)(54)	4.754(102)(56)	4.763(98)(123)	4.713(95)(63)
m_s^{RGI} [MeV]	131.0(2.5)(2.4)	134.8(2.6)(3.6)	135.0(2.6)(4.0)	132.9(2.4)(2.0)

Table 5.3: Determination of the RGI quark masses obtained from the three considered approaches. The last column shows the combined result of Wilson and Wtm$^{\text{ps}}$. The first value in parentheses corresponds to the statistical error, while the second gives an approximation of the systematic uncertainty estimated by the largest difference among the variations associated to the choice of the parametrizations and of the ensembles included in the analysis.

Chapter 6

Conclusions

We have constructed a lattice QCD regularization based on a mixed action approach, aimed to profit from specific properties of the selected sea and valence actions. In this way, we obtain an additional handle on the approach towards the physical point of physical observables. While the main advantages of this setup are expected to occur in the heavy-quark sector, in the present study we have performed a comprehensive analysis of the mixed action in the light sector in order to assess its viability. We have described two matching conditions of sea and valence quark masses, based on the use of the renormalized quark masses and of the pseudoscalar meson masses. The tuning to maximal twist in the first case can be performed by linearly interpolating the valence PCAC quark mass to the vanishing point. In the case of the matching with pseudoscalar meson masses, the tuning requires simulating a grid of points in the plane of the standard bare quark mass and of the twisted mass. In this way, the matching condition can be achieved through small interpolations among the grid data points. The pseudoscalar mass matching procedure is beneficial since it relies on quantities that are free from $\mathcal{O}(a)$ effects. The difference between the two matching procedures reduces as the lattice spacing diminishes. The availability of both matching procedures is useful to explore the systematic uncertainties associated to the use of a mixed action.

We present a study of the continuum limit scaling of the PCAC quark masses and of the pseudoscalar meson decay constants in the light sector. The agreement between the unitary Wilson setup and the mixed action observed in the continuum limit extrapolation provides a strong evidence for the validity of our mixed action formalism.

We determine the physical value of the gradient flow scale t_0 as an intermediate step for the scale setting procedure. For that purpose, we combine the $SU(3)$ ChPT expressions for $f_{\pi K}$, defined in eq. (5.1), with the ratio between f_K and f_π to carry out the continuum and physical point extrapolations. To estimate the systematic uncertainties associated to the extrapolation to the physical point, we

repeat a similar analysis of the quark mass dependence of the pseudoscalar meson decay constants, by using several parametrizations based on ChPT and on a Taylor expansion around the symmetric point. We provide a determination of t_0 with full error propagation by a combined analysis of the unitarity and the mixed action setups, leading to following result

$$t_0^{\rm ph} = 0.02141(26)(29)\ {\rm fm}^2, \tag{6.1}$$

which is compatible with other lattice determinations using $N_f = 2+1$ dynamical quarks [53, 54].

The RGI quark masses are determined from $SU(3)$ ChPT extrapolations combined with the value of $t_0^{\rm ph}$ in eq. (6.1), and where the non-perturbative running of the quark mass was determined by finite-size scaling techniques [32]. We employ a combined fit of ratios of quark masses and pseudoscalar meson masses aimed to diminish the dependency on the pseudoscalar meson masses and on NLO low-energy constants of ChPT. The results for the light and strange quark masses are obtained from a combination of mixed action and unitary Wilson setup calculations

$$m_\ell^{\rm RGI} = 4.713(95)(63)\ {\rm MeV}, \qquad m_s^{\rm RGI} = 132.9(2.4)(2.0)\ {\rm MeV}, \tag{6.2}$$

where the systematic error comes from the dispersion of the results among different scale setting procedures, various choice of the renormalized quark mass parametrizations and of the ensembles included in the analysis.

Conclusions

Hemos diseñado una regularización de QCD en el retículo, basada en una acción mixta, con el objetivo de beneficiarse de los aspectos más ventajosos de ambas acciones, la del mar y la de valencia. De este modo, podemos controlar mejor la aproximación al punto físico de los observables. Aunque se prevé que la acción sea especialmente favorable en el sector de los quarks pesados, en este trabajo hemos desarrollado un análisis general de la acción mixta en el sector de los quarks ligeros para comprobar su validez. Hemos definido dos tipos diferentes de correspondencia entre las masas quarks del mar y de valencia, una basada en el uso de masas de quarks renormalizadas y la otra a través de masas de mesones pseudoescalares. En el primer caso, se puede alcanzar el punto nulo para la masa estándar interpolando a cero una serie de valores de la masa PCAC estimada en el sector de valencia. En caso de realizar la correspondencia entre acciones mediante las masas pseudoescalares de mesones se necesita realizar un conjunto de simulaciones en el plano de la masa estándar y la rotada quiralmente. De este modo, se puede imponer la igualdad entre las masas de mesones de ambos sectores mediante interpolaciones llevadas a cabo en dicho conjunto de puntos. Este último proceso resulta beneficioso teniendo en cuenta que las masas pseudoescalares de mesones carecen de efectos de discretización de $\mathcal{O}(a)$ de manera automática. Se observa que las diferencias entre ambos procedimientos se reducen conforme el espacio reticular se hace más cada vez pequeño. Estudiar ambos métodos resulta beneficioso para estimar el error sistemático asociado al proceso de ajuste entre ambos sectores.

Presentamos un estudio de la extrapolación al continuo de las masas de quark renormalizadas y de los factores de decaimiento pseudoescalares en el sector ligero. El cual permite visualizar el comportamiento de estos observables en función del paso reticular. El hecho de que tanto la acción mixta como la acción unitaria de Wilson coincidan en el limite al continuo es una prueba fehaciente del buen comportamiento de nuestra acción.

Como paso intermedio al cálculo de la escala reticular, determinamos el observable t_0 relacionado al *gradient flow* de la densidad de la acción gluónica. Para ello, combinamos la expresión de $f_{\pi K}$ en $SU(3)$ ChPT, cuya definición viene dada en la eq. (5.1), con el cociente entre f_K y f_π, de modo a constreñir su valor en la extrap-

olación al continuo y al punto físico. Para estimar la incertidumbre sistemática asociada a la extrapolación al punto físico, repetimos el análisis con diferentes formas funcionales basadas tanto en ChPT como en expansiones de Taylor en torno al punto simétrico. El resultado de la determinación de t_0 viene dado por medio de una combinación de los valores obtenidos para la acción unitaria de Wilson y nuestra acción mixta

$$t_0^{\rm ph} = 0.02141(26)(29)\ {\rm fm}^2, \tag{6.3}$$

donde el primer error corresponde al error estadístico, obtenido mediante un análisis completo del error, y el segundo a la incertidumbre sistemática. Se observa que nuestra estimación de $t_0^{\rm ph}$ es compatible con los valores obtenidos por otros grupos para $N_f = 2 + 1$ fermiones dinámicos [53, 54].

Las masas de quarks RGI vienen dadas al combinar la extrapolación al punto físico de las masas de quarks renormalizadas, mediante sus expresiones en $SU(3)$ ChPT, junto con el valor físico obtenido para $t_0^{\rm ph}$ en la eq. (6.3). Donde el *running* no perturbativo de las masas de quarks ha sido estimado mediante técnicas de volumen finito [32]. Para efectuar la extrapolación al punto físico, llevamos a cabo un proceso optimización donde se combinan cocientes entre las masas de quark renormalizadas y las masas pseudoescalares de los mesones. De este modo se consigue reducir la dependencia de las formas funcionales en las masas de mesones y en las constantes de baja energía de ChPT en NLO.

Los resultados para las masas RGI ligera y estraña se obtienen también combinando ambas regularizaciones

$$m_\ell^{\rm RGI} = 4.713(95)(63)\ {\rm MeV}, \qquad m_s^{\rm RGI} = 132.9(2.4)(2.0)\ {\rm MeV}, \tag{6.4}$$

donde el error sistemático viene dado por la dispersión de los resultados obtenidos tras repetir el análisis implementando ciertas variaciones: distintas parametrizaciones para fijar la escala reticular, diferentes parametrizaciones de las masas de quarks y diferentes subconjuntos de ensembles analizados.

Acknowledgments

First, I would like to specially thank my supervisor Gregorio Herdoiza, for the countless hours employed in my training and continuous encouragement and support. I will miss his enthusiasm and patience during the long discussions we had in the last years. I would like to extend gratitude to the current and former members of the lattice gauge theory group at IFT, for their support, guidance and for sharing their experience with me. I am also very thankful to my advisor during my stay at the University of Edinburgh, Antonin Portelli, for the trust placed on me, his helpful advices and supervision. He ensured that the visit was very productive.

I wish to thank our CLS colleagues for sharing the gauge configuration ensembles used in this study. In particular, I would like to express my gratitude to Mattia Bruno for useful discussions and for providing valuable input for the analyses, always willing to answer any questions about his previous analyses. His implementation of the error propagation has been an essential starting point for my own research work during this thesis.

I want to thank my parents and sister, for their enormous support and motivation, from the beginning of my University stage up to now. Special thanks to Maria, who has endured with me all the stressful moments during the last years. I would also like to mention my uncles: Jose and Chari, for supporting me during the first years in Madrid, when I needed it the most.

Appendix A

Gamma matrices

The Gamma or Dirac matrices are a set of 4×4 matrices that fulfill the following anti-commutation relation

$$\{\gamma_\mu, \gamma_\nu\} = \gamma_\mu\gamma_\nu - \gamma_\nu\gamma_\mu = 2g_{\mu\nu}\mathbb{1}, \tag{A.1}$$

$g_{\mu\nu}$ indicates the metric tensor, which defines the inner product in the 4-dimensional space-time. The definition of the gamma matrices in Minkowski and Euclidean space depends on the metric tensor. Along this work, we use the metric $\eta_{\mu\nu} = \text{diag}\,(1, -1, -1, -1)$ for a Minkowski space, while in Euclidean space $g_{\mu\nu}$ is the 4×4 identity matrix.

The representation of the gamma matrices is defined by its metric. From eq. (A.1), one obtains the relation between the Euclidean and Minkowski representations

$$\gamma_i^{(E)} = -i\gamma_i^{(M)}, \quad \forall_{i=1,2,3}, \tag{A.2}$$

$$\gamma_0^{(E)} = \gamma_0^{(M)}, \tag{A.3}$$

where the superindex denotes the manifold.

Gamma matrices fulfill the following properties:

$$\cdot \text{ Traceless:} \qquad \text{Tr}\,[\gamma_\mu] = 0, \tag{A.4}$$

$$\cdot \text{ Hermitian:} \qquad \gamma_\mu^\dagger = \gamma_\mu, \tag{A.5}$$

$$\cdot \text{ Involutory:} \qquad \gamma_\mu^2 = \mathbb{1}. \tag{A.6}$$

It is useful to define γ_5 in Minkowski and Euclidean spaces

$$\gamma_5^{(M)} = i\gamma_0^{(M)}\gamma_1^{(M)}\gamma_2^{(M)}\gamma_3^{(M)}, \tag{A.7}$$

$$\gamma_5^{(E)} = \gamma_0^{(E)}\gamma_1^{(E)}\gamma_2^{(E)}\gamma_3^{(M)}, \tag{A.8}$$

States	J^{PC}	Γ
Scalar	0^{++}	$\mathbb{1}$, γ_4
Pseudoscalar	0^{-+}	γ_5, $\gamma_4\gamma_5$
Vector	1^{--}	γ_i, $\gamma_4\gamma_i$
Axial	1^{++}	$\gamma_i\gamma_5$
Tensor	1^{+-}	$\gamma_i\gamma_j$

Table A.1: Dirac structures of some of the most common meson operators. Their quantum numbers are given by the total angular momentum J, the parity P and the charge C.

which also obeys the previous properties detailed in eqs. (A.4) to (A.6). In particular, γ_5 anticommutates with the rest of the gamma matrices

$$\{\gamma_5, \gamma_\mu\} = 0. \tag{A.9}$$

As stated in Subsection 2.3.2, a different combination of gamma matrices leads to different quantum numbers in the meson local interpolator. Table A.1 shows the most common choices.

Appendix B

Global symmetries and flavor matrices

The massless Lagrangian of QCD (1.2) is invariant under the group $U(N_f) \times U(N_f) = SU(N_f)_L \times SU(N_f)_R \times U_V(1) \times U_A(1)$.

The symmetry $SU(N_f)_L \times SU(N_f)_R$, called chiral symmetry, is defined by the invariance that the free massless QCD Lagrangian exhibits with respect to independent rotations over spinors expressed in the left-handed and right-handed basis $\left\{\psi^L, \psi^R\right\}$. In this basis, both spinor components completely decouple from each other as follows

$$\overline{\psi} D_0 \psi \longrightarrow \overline{\psi}^L D_0 \psi^L + \overline{\psi}^R D_0 \psi^R. \tag{B.1}$$

Projecting the spinor over $P^{R/L}$ gives rise to the left- and right-handed components [1]

$$\begin{aligned} \psi^R &= P^R \psi = \frac{1}{2}\left(\mathbb{1} + \gamma_5\right)\psi, \qquad & \psi^L &= P^L \psi = \frac{1}{2}\left(\mathbb{1} - \gamma_5\right)\psi, \\ \overline{\psi}^R &= \overline{\psi} P^L = \overline{\psi}\frac{1}{2}\left(\mathbb{1} - \gamma_5\right), \qquad & \overline{\psi}^L &= \overline{\psi} P^R = \overline{\psi}\frac{1}{2}\left(\mathbb{1} + \gamma_5\right), \end{aligned} \tag{B.2}$$

where the $SU(N_f)_L \times SU(N_f)_R$ transformation that leaves the massless Lagrangian invariant is given by

$$\begin{aligned} \psi^{R/L} &\longrightarrow \psi^{R/L\prime} = e^{\pm i\alpha}\psi^{R/L}, \\ \overline{\psi}^{R/L} &\longrightarrow \overline{\psi}^{R/L\prime} = \overline{\psi}^{R/L} e^{\pm i\alpha}, \end{aligned} \tag{B.3}$$

in the case of a single flavor $N_f = 1$.

[1] Dirac and flavor component are expressed matricially while space-time coordinates and color indices are omitted along this appendix.

In the standard basis $\left\{\psi, \overline{\psi}\right\}$ the transformation (B.3) for N_f flavors becomes

$$\begin{aligned} \psi &\longrightarrow \psi' = e^{i\left(\alpha_V^a T^a + \gamma_5 \alpha_A^a T^a\right)}\psi, \\ \overline{\psi} &\longrightarrow \overline{\psi}' = \overline{\psi} e^{i\left(-\alpha_V^a T^a + \gamma_5 \alpha_A^a T^a\right)}, \end{aligned} \tag{B.4}$$

in its more general expression, where T^a acts on the flavor indices of ψ. The set of transformations with $\alpha_A = 0$ gives rise to the flavor or vector symmetry, whereas the transformations obtained by setting $\alpha_V = 0$ are known as the axial transformations. Such a symmetry, denoted as $SU_V(N_f) \times SU_A(N_f)$, is explicitly broken by adding a mass term to the Dirac operator, which mixes left-handed and right-handed spinors. However, in the specific case of a degenerate mass matrix, the vector symmetry $SU_V(N_f)$ still holds.

The generators T^a, together with the identity matrix $\mathbb{1}$, provide all possible bilinear combinations in flavor space. Notice that for $SU(2)$ and $SU(3)$ the generators are the Pauli and Gell-Mann matrices respectively, up to an overall factor of one half. Defining the flavor matrix T as a generic matrix belonging to $U(N_f)$, *i.e.*, any matrix that can be expressed as

$$T = \sum_{a=1}^{N_f^2-1} \alpha^a T^a + \alpha^0 \mathbb{1}_{N_f \times N_f}, \tag{B.5}$$

we refer to charged mesons as the states $\overline{\psi} T \psi$ where T is off-diagonal. Charged mesons are formed by $\overline{q} q'$ bilinears. Conversely, neutral mesons are generated by diagonal flavor matrices whose bilinears are $\overline{q} q$. In the particular case $T = \mathbb{1}$, the resulting state is a flavor singlet.

The generators T^a must satisfy the relations:

$$\mathrm{Tr}\left[T^a T^b\right] = \frac{1}{2}\delta_{ab}, \tag{B.6}$$

$$\left[T^a, T^b\right] = i \sum_c f_{abc} T^c, \qquad f_{abc} = -2i\mathrm{Tr}\left[T^a \left[T^b, T^c\right]\right], \tag{B.7}$$

$$\left\{T^a, T^b\right\} = \frac{1}{N_f}\delta_{ab}\mathbb{1} + \sum_c d_{abc} T^c, \qquad d_{abc} = \mathrm{Tr}\left[T^a \left\{T^b, T^c\right\}\right]. \tag{B.8}$$

The unitary groups $U_V(N_f)$ and $U_A(N_f)$ are symmetries of the massless Lagrangian, meaning that it is left invariant under a generalization of the transformation (B.4)

$$\psi \longrightarrow \psi' = e^{i\left(\alpha_V^0 + \alpha_V^a T^a\right)}\psi, \qquad \overline{\psi} \longrightarrow \overline{\psi}' = \overline{\psi} e^{i\left(\alpha_V^0 - \alpha_V^a T^a\right)}, \tag{B.9}$$

$$\psi \longrightarrow \psi' = e^{i\left(\gamma_5 \alpha_A^0 + \gamma_5 \alpha_A^a T^a\right)}\psi, \qquad \overline{\psi} \longrightarrow \overline{\psi}' = \overline{\psi} e^{i\left(\gamma_5 \alpha_A^0 + \gamma_5 \alpha_A^a T^a\right)}. \tag{B.10}$$

According to Noether's theorem, every global symmetry leads to a conserved current J_μ that satisfies the continuity equation $\partial_\mu J_\mu = 0$. In particular, the symmetries detailed above lead to the conserved currents below

$$\mathcal{V}^a_\mu(x) = \overline{\psi}(x)T^a\gamma_\mu\psi(x), \qquad \mathcal{V}^0_\mu(x) = \overline{\psi}(x)\gamma_\mu\psi(x), \tag{B.11}$$

$$\mathcal{A}^a_\mu(x) = \overline{\psi}(x)T^a\gamma_\mu\gamma_5\psi(x), \qquad \mathcal{A}^0_\mu(x) = \overline{\psi}(x)\gamma_\mu\gamma_5\psi(x), \tag{B.12}$$

where the non-singlet currents are placed on the left while on the right, the singlet case can be found.

For completeness, we gather the scalar $\mathcal{S}$, pseudoscalar $\mathcal{P}$ and tensorial $\mathcal{T}_{\mu\nu}$ bilinears

$$\mathcal{S}^a(x) = \overline{\psi}(x)T^a\psi(x), \qquad \mathcal{S}^0(x) = \overline{\psi}(x)\psi(x), \tag{B.13}$$

$$\mathcal{P}^a(x) = \overline{\psi}(x)T^a\gamma_5\psi(x), \qquad \mathcal{P}^0(x) = \overline{\psi}(x)\gamma_5\psi(x), \tag{B.14}$$

$$\mathcal{T}^a_{\mu\nu}(x) = \overline{\psi}(x)T^a\sigma_{\mu\nu}\psi(x), \qquad \mathcal{T}^0_{\mu\nu}(x) = \overline{\psi}(x)\sigma_{\mu\nu}\psi(x), \tag{B.15}$$

where $\sigma_{\mu\nu}$ is an antisymmetric tensor defined as

$$\sigma_{\mu\nu} \equiv \frac{1}{2i}\left[\gamma_\mu, \gamma_\nu\right]. \tag{B.16}$$

Not all the Lagrangian symmetries are actual symmetries of QCD. The classical symmetry $U_A(N_f)$ becomes anomalous after quantization. Conversely, the vector symmetry $U_V(N_f)$ is a true symmetry of QCD, which is conserved even in the degenerate massive Lagrangian, and its conserved quantity is the Baryon number [2]. For the general case of non-degenerate mass matrix the symmetry is broken and becomes $U_V(N_f) \longrightarrow U_V(1)\times U_V(1)\times ...\times U_V(1)$. On the lattice, the formalisms that incorporate the Wilson term, defined in eq. (2.40), break both vector and axial symmetries.

[2]Note that when weak interactions are included, the symmetry becomes anomalous.

Appendix C

Discrete transformations

Discrete symmetries describe non-continuous transformations of the fields that leave the action invariant. QCD preserves three discrete symmetries: parity, charge conjugation and time-reversal.

Parity transformation $\mathcal{P}$ consists of a reflection of the spatial coordinates with respect to the origin $(x_0, \boldsymbol{x}) \xrightarrow{\mathcal{P}} (x_0, -\boldsymbol{x})$. Quark and link fields transform as follow under parity transformations:

$$\psi(x_0, \boldsymbol{x}) \xrightarrow{\mathcal{P}} \psi(x_0, \boldsymbol{x})^{\mathcal{P}} = \gamma_4 \psi\left(x_0, \boldsymbol{x}^{\mathrm{ref}}\right), \tag{C.1}$$

$$\overline{\psi}(x_0, \boldsymbol{x}) \xrightarrow{\mathcal{P}} \overline{\psi}(x_0, \boldsymbol{x})^{\mathcal{P}} = \overline{\psi}\left(x_0, \boldsymbol{x}^{\mathrm{ref}}\right) \gamma_4, \tag{C.2}$$

$$U_i(x_0, \boldsymbol{x}) \xrightarrow{\mathcal{P}} U_i(x_0, \boldsymbol{x})^{\mathcal{P}} = U_{-i}\left(x_0, \boldsymbol{x}^{\mathrm{ref}}\right)^{\dagger}, \quad \forall_{i=1,2,3}, \tag{C.3}$$

$$U_4(x_0, \boldsymbol{x}) \xrightarrow{\mathcal{P}} U_4(x_0, \boldsymbol{x})^{\mathcal{P}} = U_4\left(x_0, \boldsymbol{x}^{\mathrm{ref}}\right). \tag{C.4}$$

The coordinate $\boldsymbol{x}^{\mathrm{ref}}$ denotes the symmetric point of $\boldsymbol{x}$ with respect to the center of the lattice in the spatial direction.

The explicit expression of the charge conjugation, which transforms particles into anti-particles, depends on the gamma matrix representation

$$\mathcal{C}\gamma_\mu\mathcal{C}^{-1} = -(\gamma_\mu)^T. \tag{C.5}$$

Charge conjugation matrix $\mathcal{C}$ is, by definition, hermitian, involutory and antisymmetric. $\mathcal{C}$ acts in the Dirac indices of the lattice fields as shown below:

$$\psi(x_0, \boldsymbol{x}) \xrightarrow{\mathcal{C}} \psi(x_0, \boldsymbol{x})^{\mathcal{C}} = \mathcal{C}^{-1}\psi(x_0, \boldsymbol{x})^T, \tag{C.6}$$

$$\overline{\psi}(x_0, \boldsymbol{x}) \xrightarrow{\mathcal{C}} \overline{\psi}(x_0, \boldsymbol{x})^{\mathcal{C}} = -\overline{\psi}(x_0, \boldsymbol{x})^T \mathcal{C}, \tag{C.7}$$

$$U_i(x_0, \boldsymbol{x}) \xrightarrow{\mathcal{C}} U_i(x_0, \boldsymbol{x})^{\mathcal{C}} = U_i(x_0, \boldsymbol{x})^*, \quad \forall_{i=1,2,3}, \tag{C.8}$$

$$U_4(x_0, \boldsymbol{x}) \xrightarrow{\mathcal{C}} U_4(x_0, \boldsymbol{x})^{\mathcal{C}} = U_4(x_0, \boldsymbol{x})^*. \tag{C.9}$$

Finally, we illustrate how the quark and gluon fields behave under a reflection in the time coordinate

$$\psi\left(x_0, \boldsymbol{x}\right) \xrightarrow{\mathcal{T}} \psi\left(x_0, \boldsymbol{x}\right)^{\mathcal{T}} = \gamma_4\gamma_5\psi\left(x_0^{\mathrm{ref}}, \boldsymbol{x}\right), \tag{C.10}$$

$$\overline{\psi}\left(x_0, \boldsymbol{x}\right) \xrightarrow{\mathcal{T}} \overline{\psi}\left(x_0, \boldsymbol{x}\right)^{\mathcal{T}} = \overline{\psi}\left(x_0^{\mathrm{ref}}, \boldsymbol{x}\right)\gamma_5\gamma_4, \tag{C.11}$$

$$U_i\left(x_0, \boldsymbol{x}\right) \xrightarrow{\mathcal{T}} U_i\left(x_0, \boldsymbol{x}\right)^{\mathcal{T}} = U_i\left(x_0^{\mathrm{ref}}, \boldsymbol{x}\right)^{\dagger}, \quad \forall_{i=1,2,3}, \tag{C.12}$$

$$U_4\left(x_0, \boldsymbol{x}\right) \xrightarrow{\mathcal{T}} U_4\left(x_0, \boldsymbol{x}\right)^{\mathcal{T}} = U_{-4}\left(x_0^{\mathrm{ref}}, \boldsymbol{x}\right). \tag{C.13}$$

Appendix D

Monte Carlo integration

Monte Carlo (MC) integration appears as an alternative numerical procedure to the quadrature methods. Deterministic methods provide a closed solution, but the convergence may be slow or even impractical for multidimensional integrals. The MC method is, by contrast, a stochastic procedure where the integral is determined by performing several evaluations of the integrand.

In the MC approach, an integration of the function $f(x)$, in the domain $\mathcal{D}$, is related to the expectation value of this function

$$I = \mathbb{E}\left[f(X)\right] = \int f(x)\omega(x)dx, \tag{D.1}$$

whose distribution is given by a uniform probability density function (PDF) $\omega(x) = 1$ in such domain. A simple average of the function evaluated over a set of independent and identically distributed points X_i, generated according to $\omega(x)$, leads to an unbiased estimator of the integral above

$$\hat{I} = \frac{1}{N}\sum_{i=1}^{N} f(X_i). \tag{D.2}$$

An integral over some function $f(x)$ can be estimated through the estimator $\hat{I}$ by sampling points along a uniform random variable. However, a better convergence can be achieved by factorizing the function wisely into a new function and a non-uniform PDF, $f_1(x)\omega_1(x) = f_2(x)\omega_2(x)$, so that I remains invariant. In this way, the variance of the estimator (D.2) could be reduced

$$\mathrm{Var}\left[\hat{I}\right] = \frac{1}{N}\left(\int f^2(x)\omega(x)dx - I^2\right), \tag{D.3}$$

if the factorization is chosen to minimize the first term in the equation above. This last approach is known as importance sampling.

It can be easily proved that an optimal value of the PDF

$$\omega_{\text{opt}}(x) = \frac{f(x)\omega(x)}{I}, \tag{D.4}$$

leads to a vanishing variance (D.3), meaning that a single sample would provide a proper estimation of the integral. Although $\omega_{\text{opt}}(x)$ is not known a priori, the use of an approximation could already provide an effective way to determine the integral.

Appendix E

Topological charge

The topological charge Q is an integer number that characterizes the various topological sectors appearing in configuration space. Different topological sectors refer to distinctive domains of the configuration space which are not easily accessible from other domains in a Markov Chain.

As explained in Appendix B, the flavor singlet axial transformation is a symmetry of the Lagrangian in the classical theory but it is broken in QCD after quantization. Since the integrand of the path integral must fulfill the classical symmetries, the origin of the anomaly proceeds from the non-invariance of the measure.

The transformation of the fermion integration measure under a singlet local axial transformation in eq. (B.10) is given by the *Fujikawa method* [88, 89]. The Jacobian of this transformation is obtained by expressing the fermion fields in terms of the set of eigenvectors of the Dirac operator, $\{\varphi_i \mid D\varphi_i = \lambda_i\varphi_i\}$, leading to

$$\mathcal{D}\left[\psi', \overline{\psi'}\right] = e^{-2ia\mathrm{Tr}[T]\int d^4x\ \alpha_A^0(x)\sum\limits_i \varphi_i^\dagger(x)\gamma_5\varphi_i(x)}\mathcal{D}\left[\psi, \overline{\psi}\right]. \tag{E.1}$$

Notice that any non-singlet axial transformation cancels the anomaly since the matrix is traceless in this case.

A non-zero argument in the exponential in equation (E.1) implies the loss of unitarity, meaning that the whole configuration space cannot be explored through smooth local transformations. The topological charge Q defined through

$$Q = -\int d^4x\ \sum_i \varphi_i^\dagger(x)\gamma_5\varphi_i(x), \tag{E.2}$$

measures the extent of this effect.

The naive lattice computation of the topological charge is ambiguous, since it contains power divergences. In practice, we compute Q in terms of the gradient

flow

$$Q = -\frac{a^4}{32\pi^2} \sum_x \epsilon_{\mu\nu\alpha\beta} \mathrm{tr}\left[G_{\mu\nu}(x, t_w) G_{\alpha\beta}(x, t_w)\right], \tag{E.3}$$

where $G_{\mu\nu}(x, t_w)$ is the strength tensor at a given flow time t_w. $G_{\mu\nu}(x, t_w)$ can be interpreted as a gradient flow evolution of $F_{\mu\nu}(x)$ up to $t_w > 0$. Furthermore, through the so-called *Index Theorem*, the topological charge can be expressed in terms of the fermionic zero modes by applying γ_5-hermiticity on D [90]

$$Q = \lambda_{0^+} - \lambda_{0^-}, \tag{E.4}$$

where the quantities $\lambda_{0^{+/-}}$ denote the zero-modes of positive and negative chirality, respectively.

Appendix F

ChPT functional forms

The NLO $SU(3)$ ChPT equations for the pseudoscalar meson decay constants, written in terms of the renormalized quark masses [82], are adapted in a suitable way to the chiral trajectory used in our setup

$$f_\pi = f_0 \left[1 + \frac{2B_0}{f_0^2} \left(8 m_\ell L_5 + 8 \left(2m_\ell + m_s \right) L_4 \right) - \frac{1}{16\pi^2 f_0^2} \left(2\mu_\pi + \mu_K \right) \right], \tag{F.1}$$

$$f_K = f_0 \left[1 + \frac{2B_0}{f_0^2} \left(4 \left(m_\ell + m_s \right) L_5 + 8 \left(2m_\ell + m_s \right) L_4 \right) - \frac{1}{16\pi^2 f_0^2} \left(\frac{3}{4}\mu_\pi + \frac{3}{2}\mu_K + \frac{3}{4}\mu_\eta \right) \right], \tag{F.2}$$

$$\mu_{\rm ps} = M_{\rm ps}^2 \ln \left(\frac{M_{\rm ps}^2}{\Lambda} \right), \tag{F.3}$$

where the low-energy couplings L_i are renormalized with the scale Λ and the parameter B_0 is related to the chiral condensate Σ_0 as follows

$$B_0 = 2 \frac{\Sigma_0}{f_0^2}. \tag{F.4}$$

The decay constant of $SU(3)$ in the chiral limit, f_0, is normalized according to the physical value, shown in eq. (5.5). In the expressions (F.1) and (F.2), quark masses are expressed in terms of the meson masses in t_0 units through the use of LO relations

$$M_\pi^2 = 2B_0 m_\ell, \quad M_K^2 = B_0 \left(m_\ell + m_s \right), \quad M_\eta^2 = \frac{2}{3} B_0 \left(m_\ell + 2m_s \right). \tag{F.5}$$

Eqs. (5.7) and (5.8) are obtained after rearranging the quark masses and multiplying by $\sqrt{8t_0}$, where the parameters read

$$p_1 = \sqrt{8t_0} f_0 \left(1 + \frac{2L_4}{t_0 f_0^2}\phi_4\right), \tag{F.6}$$

$$p_2 = \sqrt{8t_0} f_0 \frac{L_5}{t_0 f_0^2}, \tag{F.7}$$

$$p_3 = -\sqrt{8t_0} f_0, \tag{F.8}$$

and K has been defined as

$$K = \frac{1}{8t_0}\frac{1}{16\pi^2 f_0^2}. \tag{F.9}$$

To minimize the number of fitting parameters $8t_0 f_0^2$ can be replaced by $f_{\pi K}^2$. This is possible since K is a parameter appearing at NLO and the effect of replacing $8t_0 f_0^2$ by $f_{\pi K}^2$ becomes a NNLO effect.

Besides, since the computation of the LECs is not our final goal, the renormalization scale is set to $\Lambda = \frac{1}{\sqrt{8t_0^{\rm ph}}}$ in a way that the chiral logarithms simplify to

$$\mathcal{L}_{\rm ps} = \phi_{\rm ps} \ln\left(\phi_{\rm ps}\right), \quad \phi_{\rm ps} = 8t_0 M_{\rm ps}^2, \quad {\rm ps} = \pi, K, \eta. \tag{F.10}$$

The squared eta meson mass ϕ_η in t_0 units can be related to the pion and kaon masses in ChPT

$$\phi_\eta = 8t_0 M_\eta^2 = 8t_0 \frac{4M_K^2 - M_\pi^2}{3} = \frac{4\phi 4 - 3\phi_2}{3}. \tag{F.11}$$

The same strategy is pursued for the quark masses. ChPT $SU(3)$ equations at NLO are derived from [87] for m_{12}^R and m_{13}^R, defined in eqs. (3.38) and (3.39)

$$m_{12}^R = \frac{M_\pi^2}{2B_0}\left[1 - \frac{16}{f_0^2}\left((2L_6 - L_4)\left(M_\pi^2 + 2M_K^2\right) + (2L_8 - L_5)\, M_\pi^2\right) - \frac{1}{16\pi^2 f_0^2}\left(\mu_\pi - \frac{1}{3}\mu_\eta\right)\right], \tag{F.12}$$

$$m_{13}^R = \frac{M_K^2}{2B_0}\left[1 - \frac{8}{f_0^2}\left((4L_6 + 2L_8 - 2L_4 - L_5)\left(M_\pi^2 + 2M_K^2\right) + (-2L_8 + L_5)\, M_\pi^2\right) - \frac{1}{16\pi^2 f_0^2}\frac{2}{3}\mu_\eta\right]. \tag{F.13}$$

After rewriting the equations (F.12) and (F.13) in a similar fashion to those of the decay constants, the resulting equations are presented in eqs. (5.15) and (5.16).

The fit parameters are now given by

$$q_1 = \frac{1}{2B_0\sqrt{8t_0}}\left(1 - \frac{4}{t_0 f_0^2}\left(2L_6 - L_4\right)\phi_4\right), \tag{F.14}$$

$$q_2 = -\frac{1}{2B_0\sqrt{8t_0}}\frac{2}{t_0 f_0^2}\left(2L_8 - L_5\right), \tag{F.15}$$

$$q_3 = -\frac{1}{2B_0\sqrt{8t_0}}. \tag{F.16}$$

Appendix G

Tables

label	t_0/a^2	aM_π	aM_K	$am_{12}^{(I)}$	$am_{13}^{(I)}$	f_π^R	f_K^R
H101	2.8585(87)	0.18045(115)	0.18045(115)	0.008892(113)	0.008892(113)	0.06323(53)	0.06323(53)
H102r001	2.8824(127)	0.15397(139)	0.19127(118)	0.006420(122)	0.010052(121)	0.05982(77)	0.06329(53)
H102r002	2.8837(108)	0.15387(149)	0.19126(114)	0.006463(128)	0.010054(127)	0.06109(76)	0.06414(55)
H105	2.8841(107)	0.12216(170)	0.20236(118)	0.004003(117)	0.011284(125)	0.05830(179)	0.06508(53)
H105r005	2.9080(193)	0.12283(177)	0.20117(126)	0.004018(149)	0.011149(149)	0.05731(105)	0.06449(75)
H400	3.6581(160)	0.15952(103)	0.15952(103)	0.007815(132)	0.007815(132)	0.05633(102)	0.05633(102)
N202	5.1626(200)	0.13428(82)	0.13428(82)	0.006850(87)	0.006850(87)	0.04833(34)	0.04833(34)
N203	5.1394(121)	0.11279(97)	0.14424(75)	0.004796(90)	0.007938(88)	0.04667(39)	0.04935(31)
N200	5.1558(112)	0.09276(118)	0.15093(73)	0.003181(83)	0.008649(81)	0.04451(28)	0.04923(31)
D200	5.1723(118)	0.06717(166)	0.15729(69)	0.001625(79)	0.009448(83)	0.04267(43)	0.04962(38)
N300	8.5938(377)	0.10407(62)	0.10407(62)	0.005270(85)	0.005270(85)	0.03766(44)	0.03766(44)
J303	8.6390(402)	0.06315(114)	0.11903(59)	0.001919(91)	0.007048(101)	0.03401(68)	0.03856(98)

Table G.1: Results computed in the Wilson regularization. Values of t_0, pseudoscalar masses, improved PCAC quark masses and renormalized decay constants in lattice units. The values are shifted to $\phi_4 = 1.117(12)$.

label	t_0/a^2	aM_π	aM_K	$am_{12}^{(I)}$	$am_{13}^{(I)}$	f_π^R	f_K^R
H101	2.8585(87)	0.18046(115)	0.18046(115)	0.006591(81)	0.006591(81)	0.06722(35)	0.06722(35)
H102r001	2.8824(127)	0.15398(139)	0.19128(121)	0.004745(83)	0.007422(87)	0.06447(43)	0.06802(34)
H102r002	2.8837(108)	0.15387(143)	0.19126(115)	0.004734(91)	0.007413(93)	0.06459(40)	0.06812(39)
H105	2.8841(107)	0.12217(174)	0.20237(120)	0.002940(86)	0.008316(92)	0.06190(48)	0.06876(38)
H105r005	2.9080(193)	0.12284(181)	0.20118(121)	0.003007(80)	0.008285(89)	0.06187(48)	0.06813(52)
H400	3.6581(160)	0.15953(105)	0.15953(105)	0.005913(82)	0.005913(82)	0.05915(43)	0.05915(43)
N202	5.1626(200)	0.13428(79)	0.13428(79)	0.005228(62)	0.005228(62)	0.04989(24)	0.04989(24)
N203	5.1394(121)	0.11280(102)	0.14425(78)	0.003640(69)	0.006036(66)	0.04820(33)	0.05089(28)
N200	5.1558(112)	0.09276(116)	0.15105(72)	0.002420(64)	0.006598(65)	0.04589(34)	0.05085(37)
D200	5.1723(118)	0.06717(168)	0.15729(68)	0.001282(61)	0.007249(51)	0.04452(54)	0.05097(60)
N300	8.5938(377)	0.10408(68)	0.10408(68)	0.004132(67)	0.004132(67)	0.03801(46)	0.03801(46)
J303	8.6390(402)	0.06313(120)	0.11901(61)	0.001512(61)	0.005542(71)	0.03520(36)	0.03947(62)

Table G.2: Results computed in the mixed action regularization matched through pseudoscalar masses. Values of t_0, pseudoscalar masses, improved and renormalized PCAC quark masses and renormalized decay constants in lattice units. The values are shifted to $\phi_4 = 1.117(12)$.

label	t_0/a^2	aM_π	aM_K	$am_{12}^{(I)}$	$am_{13}^{(I)}$	f_π^R	f_K^R
H101	2.8585(87)	0.18224(122)	0.18224(122)	0.006726(86)	0.006726(86)	0.06738(35)	0.06738(35)
H102r001	2.8824(127)	0.15572(150)	0.19333(120)	0.004857(92)	0.007604(92)	0.06462(50)	0.06823(34)
H102r002	2.8837(108)	0.15629(150)	0.19351(122)	0.004889(97)	0.007605(96)	0.06479(39)	0.06834(43)
H105	2.8841(107)	0.12392(166)	0.20404(119)	0.003028(89)	0.008535(95)	0.06205(48)	0.06894(38)
H105r005	2.9080(193)	0.12349(248)	0.20263(155)	0.003039(113)	0.008433(113)	0.06191(51)	0.06826(58)
H400	3.6581(160)	0.16004(127)	0.16004(127)	0.005952(101)	0.005952(101)	0.05920(45)	0.05920(45)
N202	5.1626(200)	0.13484(85)	0.13484(85)	0.005273(67)	0.005273(67)	0.04994(23)	0.04994(23)
N203	5.1394(121)	0.11357(109)	0.14502(84)	0.003692(70)	0.006110(67)	0.04827(32)	0.05096(28)
N200	5.1558(112)	0.09329(115)	0.15165(74)	0.002449(64)	0.006658(62)	0.04593(32)	0.05091(36)
D200	5.1723(118)	0.06633(168)	0.15732(88)	0.001251(61)	0.007273(64)	0.04449(55)	0.05095(61)
N300	8.5938(377)	0.10406(79)	0.10406(79)	0.004131(66)	0.004131(66)	0.03801(44)	0.03801(44)
J303	8.6390(402)	0.06299(154)	0.11887(79)	0.001504(71)	0.005524(79)	0.03519(38)	0.03946(59)

Table G.3: Results computed in the mixed action regularization matched through PCAC masses. Values of t_0, pseudoscalar masses, improved and renormalized PCAC quark masses and renormalized decay constants in lattice units. The values are shifted to $\phi_4 = 1.117(12)$.

Bibliography

[1] M. Gell-Mann, *A schematic model of baryons and mesons*, *Phys. Lett.* **8** (1964) 214-215.

[2] O. W. Greenberg, *Spin and Unitary-Spin Independence in a Paraquark Model of Baryons and Mesons*, *Phys. Rev. Lett.* **13** (1964) 598.

[3] M. Y. Han and Y. Nambu, *Three-Triplet Model with Double SU(3) Symmetry*, *Phys. Rev.* **139** (1965) B1006.

[4] H. Fritzsch, M. Gell-Mann and H. Leutwyler, *Advantages of the Color Octet Gluon Picture*, *Phys. Lett.* **B47** (1973) 365.

[5] K. G. Wilson, *Confinement of Quarks*, *Phys. Rev.* **D10** (1974) 2445–2459.

[6] H. D. Politzer, *Reliable Perturbative Results for Strong Interactions?*, *Phys. Rev. Lett.* **30** (1973) 1346

[7] D. J. Gross and F. Wilczek, *Asymptotically Free Gauge Theories. I*, *Phys. Rev. Lett.* **30** (1973) 1343.

[8] **BESIII Collaboration**, M. Ablikim, M. N. Achasov, X. C. Ai et al., *Observation of a Charged Charmoniumlike Structure in $e^+e^- \to \pi^+\pi^- J/\psi$ at $\sqrt{s} = 4.26$ GeV*, *Phys. Rev. Lett.* **110** (2013) 252001, [1303.5949].

[9] **LHCb Collaboration**, R. Aaij, B. Adeva, M. Adinolfi et al., *Observation of $J/\psi p$ resonances consistent with pentaquark states in $\Lambda_b^0 \to J/\psi K^- p$ decays*, *Phys. Rev. Lett.* **115** (2015) 072001, [1507.03414].

[10] R. P. Feynman, *Space-Time Approach to Non-Relativistic Quantum Mechanics*, *Rev. Mod. Phys.* **20** (1948) 367.

[11] T. Matthews and A. Salam, *The Green's functions of quantised fields*, *Nuovo Cimento* **12**, 563 (1954) 108.

[12] T. Matthews and A. Salam, *Propagators of quantized field*, *Nuovo Cimento* **2**, 120 (1955) 108.

[13] L. Giusti, T. Harris, A. Nada and S. Schaefer, *Frequency-splitting estimators of single-propagator traces*, *Eur. Phys. J.* **C79** (2019) no.7, 586, [1903.10447].

[14] H. B. Nielsen and M. Ninomiya, *Absence of neutrinos on a lattice: proof by homotopy theory*, *Nuclear Physics* **B185** (1981) 20-40.

[15] H. B. Nielsen and M. Ninomiya, *No Go Theorem for Regularizing Chiral Fermions*, *Phys. Lett.* **B105** (1981) 219.

[16] P. H. Ginsparg and K. G. Wilson, *A remnant of chiral symmetry on the lattice*, *Phys. Rev.* **D25** (1982) 2649.

[17] H. Neuberger, *Exactly massless quarks on the lattice*, *Phys. Lett.* **B417** (1998) 141-144, [hep-lat/9707022].

[18] D. B. Kaplan, *A Method for Simulating Chiral Fermions on the Lattice*, *Phys. Lett.* **B288** (1992) 342-347, [hep-lat/9206013].

[19] S. Aoki, *New phase structure for lattice QCD with Wilson fermions*, *Phys. Rev.* **D30**, 120 (1984) 2653.

[20] R. Frezzotti, P. A. Grassi, S. Sint and P. Weisz, A Local formulation of lattice QCD without unphysical fermion zero modes, *Nucl. Phys. Proc. Suppl.* **83** (2000) 941–946, [hep-lat/9909003].

[21] **ALPHA Collaboration**, R. Frezzotti, P. A. Grassi, S. Sint and P. Weisz, *Lattice QCD with a chirally twisted mass term*, *JHEP* **0108** (2001) 058, [hep-lat/0101001].

[22] R. Frezzotti and G. Rossi, *Chirally improving Wilson fermions. 1. O(a) improvement*, *JHEP* **0408** (2004) 007, [hep-lat/0306014].

[23] R. Frezzotti and G. Rossi, *Chirally improving Wilson fermions II. Four-quark operators*, *JHEP* **0410** (2004) 070, [hep-lat/0407002].

[24] C. Pena, S. Sint, A. Vladikas, *Twisted mass QCD and lattice approaches to the* $\Delta I = 1/2$, *JHEP* **09** (2004) 069, [hep-lat/0405028].

[25] A. Shindler, *Twisted mass lattice QCD*, *Phys. Rept.* 461 (2008) 37, [0707.4093].

[26] S. Sint, *Lattice QCD with a chiral twist*, *Perspectives in Lattice QCD* (2007) pp. 169-208, [hep-lat/0702008].

[27] R. Frezzotti and G. Rossi, *Twisted-mass lattice QCD with mass non-degenerate quarks*, *Nucl. Phys. Proc. Suppl.* **128** (2004) 193, [hep-lat/0311008v2].

[28] K. Symanzik, *Continuum Limit and Improved Action in Lattice Theories. 1. Principles and phi**4 Theory*, *Nucl. Phys.* **B226** (1983) 187-204.

[29] K. Symanzik, *Schrodinger Representation and Casimir Effect in Renormalizable Quantum Field Theory* , *Nucl. Phys.* **B190** (1981) 1-44.

[30] M. Lüscher, R. Narayanan, P. Weisz and U. Wolff, *The Schrodinger functional: A Renormalizable probe for nonAbelian gauge theories*, *Nucl. Phys.* **B384** (1992) 168-228, [hep-lat/9207009].

[31] G. M. de Divitiis, P. Fritzsch, J. Heitger et al., *Non-perturbative determination of improvement coefficients b_m and $b_A - b_P$ and normalisation factor $Z_m * Z_P/Z_A$ with $N_f = 3$ Wilson fermions*, *Eur. Phys. J.* **C79** (2019) 797, [1906.03445].

[32] I. Campos, P. Fritzsch, C. Pena et al., *Non-perturbative quark mass renormalisation and running in $N_f = 3$ QCD*, *Eur. Phys. J.* **C78** (2018) no.5, 387, [1802.05243].

[33] A. Vladikas, XCIII Les Houches Summer School, Modern perspectives in lattice QCD: *Three Topics in Renormalization and Improvement*, lecture notes, Les Houches, France, August 2009.

[34] M. Bruno D. Djukanovic, G. P. Engel et al., *Simulation of QCD with $N_f = 2 + 1$ flavors of non-perturbatively improved Wilson fermions*, *JHEP* **1502**, (2015) 043, [1411.3982].

[35] M. Lüscher and F. Palombi, *Fluctuations and reweighting of the quark determinant on large lattices*, *PoS* **LATTICE2008**, (2008) 049, [0810.0946].

[36] M. Lüscher and P. Weisz, *Computation of the Action for On-Shell Improved Lattice Gauge Theories at Weak Coupling*, *Phys. Lett.* **B158** (1985) 250.

[37] M. Lüscher and P. Weisz, *On-shell improved lattice gauge theories*, *Commun. Math. Phys.* **97** (1985) 59.

[38] M. Lúscher, S. Sint, R. Sommer and P. Weisz, *Chiral symmetry and O(a) improvement in lattice QCD*, *Nucl. Phys.* **B478** (1996) 365-400.

[39] B. Sheikholeslami and R. Wohlert, *Improved continuum limit lattice action for QCD with Wilson fermions*, *Nucl. Phys.* **B259** (1985) 572.

[40] B. Alles, G. Boydan and M. D'Elia, *Hybrid Monte Carlo and topological modes of full QCD*, *Phys. Lett.* **B389**, (1996) 107-111, [hep-lat/9607049].

[41] L. Del Debbio, H. Panagopoulos and E. Vicari, *Theta dependence of $SU(N)$ gauge theories*, *JHEP* **0208**, (2002) 044, [hep-th/0204125].

[42] **MILC Collaboration**, C. Bernarda, T. Burchb, T. A. DeGrand et al. *Topological susceptibility with the improved Asqtad action*, *Phys. Rev.* **D68**, (2003) 114501, [hep-lat/0308019].

[43] **ALPHA Collaboration**, S. Schaefer, R. Sommer and F. Virotta, *Critical slowing down and error analysis in lattice QCD simulations*, *Nucl. Phys.* **B845** (2011) 93-119, [1009.5228].

[44] M. Bruno, S. Schaefer and R. Sommer, *Topological susceptibility and the sampling of field space in $N_f = 2$ lattice QCD simulations*, *JHEP* **1408** (2014) 150, [1406.5363].

[45] M. Lüscher, *Topology of Lattice Gauge Fields*, *Commun. Math. Phys.* **85** (1982) 39.

[46] A. Phillips and D. Stone, *Lattice gauge fields, principal bundles and the calculation of topological charge*, *Commun. Math. Phys.* **103** (1986) 599–636.

[47] M. Lüscher, *Topology, the Wilson flow and the HMC algorithm*, *PoS LATTICE* **2010** (2010) 015, [1009.5877].

[48] M. Lüscher and S. Schaefer, *Lattice QCD without topology barriers*, *JHEP* **1107**, (2011) 036, [1105.4749].

[49] M. Lüscher and S. Schaefer, *Lattice QCD with open boundary conditions and twisted-mass reweighting* , *Comput. Phys. Commun.* **184**, (2013) 519-528, [1206.2809].

[50] K. Osterwalder, E. Seiler, *Gauge field theories on a lattice*, *Annals Phys.* **110**, (1978) 440.

[51] A. Bussone, S. Chaves, G. Herdoíza et al., *Heavy-quark physics with a tmQCD valence action*, *PoS LATTICE* **2018** (2018) 270, [1812.01474].

[52] M. Golterman, T. Izubuchi and Y. Shamir, *The role of the double pole in lattice QCD with mixed actions*, *Phys. Rev.* **D71**, (2005) 114508, [hep-lat/0504013].

[53] S. Borsanyi, S. Dürr, Z. Fodor et al., *High-precision scale setting in lattice QCD*, *JHEP* **1209** (2012) 010, [1203.4469].

[54] M. Bruno, T. Korzec and S. Schaefer, *Setting the scale for the CLS $2+1$ flavor ensembles*, *Phys. Rev.* **D95** (2017) 074504, [1608.08900].

[55] M. Lüscher, *Properties and uses of the Wilson flow in lattice QCD*, *JHEP* **1008**, (2010) 071, [Erratum: *JHEP* **1403**, (2014) 092], [1006.4518].

[56] M. Lüscher, *Trivializing maps, the Wilson flow and the HMC algorithm*, *Commun. Math. Phys.* **293**, (2010) 899-919, [0907.5491].

[57] **ALPHA Collaboration**, J. Bulava, M. Della Morte, J. Heitger and C. Wittemeier, *Non-perturbative improvement of the axial current in Nf=3 lattice QCD with Wilson fermions and tree-level improved gauge action*, *Nucl. Phys.* **B896** (2015) 555-568, [1502.04999].

[58] T. Bhattacharya, R. Gupta, W. Lee, S. R. Sharpe and J. M. Wu, *Improved bilinears in lattice QCD with non-degenerate quarks*, *Phys. Rev.* **D73** (2006) 034504, [hep-lat/0511014].

[59] M. Dalla Brida, T. Korzec, S. Sint and P. Vilaseca, *High precision renormalization of the flavour non-singlet Noether currents in lattice QCD with Wilson quarks*, *Eur. Phys. J.* **C79** (2019) 23, [1808.09236].

[60] Y. Taniguchi, A. Ukawa, *Perturbative calculation of improvement coefficients to $\mathcal{O}(g^2a)$ for bilinear quark operators in lattice QCD*, *Phys. Rev.* **D58** (1998) 114503, [hep-lat/9806015].

[61] M. Bruno, *The energy scale of the 3-flavour Lambda parameter*, *Doctoral dissertation*, Humboldt-Universität zu Berlin (2015).

[62] G. Herdoíza, C. Pena, D. Preti, J. A. Romero and J. Ugarrio, *A tmQCD mixed-action approach to flavour physics*, *EPJ Web Conf.* **175** (2018) 13018, [1711.06017].

[63] A. Bussone, G. Herdoíza, C. Pena et al., *Matching of $N_f = 2+1$ CLS ensembles to a tmQCD valence sector*, *PoS LATTICE* **2018** (2019) 318, [1903.00286].

[64] T. A. DeGrand, *A Conditioning Technique for Matrix Inversion for Wilson Fermions*, *Comput. Phys. Commun.* **52** (1988) 161–164.

[65] M. Hasenbusch *Speeding up the Hybrid-Monte-Carlo algorithm for dynamical fermions,Phys. Lett.*, *Phys. Lett.* **B519** (2001) 177–182, [hep-lat/0107019].

[66] M. Creutz, *Monte Carlo study of quantized SU(2) gauge theory*, *Phys. Rev.* **D21**, (1980) 2308.

[67] S. L. Adler, *An Overrelaxation Method for the Monte Carlo Evaluation of the Partition Function for Multiquadratic Actions*, *Phys. Rev.* **D23**, (1981) 2901.

[68] C. Whitmer, *Over-relaxation methods for Monte Carlo simulations of quadratic and multiquadratic actions*, *Phys. Rev.* **D29**, (1984) 306.

[69] S. Duane, A. D. Kennedy, B. J. Pendleton and D. Roweth, *Hybrid Monte Carlo*, *Phys. Lett.* **B195**, (1987) 216.

[70] S. Gottlieb, W. Liu, D. Toussaint, R. L. Renken and R. L. Sugar, *Hybrid-molecular-dynamics algorithms for the numerical simulation of quantum chromodynamics*, *Phys. Rev.* **D35**, (1987) 2531.

[71] A. D. Kennedy and P. Rossi, *Classical mechanics on group manifolds and applications to hybrid Monte Carlo*, *Nucl. Phys.* **B327**, (1989) 782.

[72] G. M. de Divitiis, R. Petronzio and N. Tantalo, *Distance preconditioning for lattice Dirac operators*, *Phys. Letter.* **B692** (2010) 157-160, [1006.4028].

[73] S. Collins, K. Eckert, J. Heitger, S. Hofmann and W. Soeldner, *Charmed pseudoscalar decay constants on three-flavour CLS ensembles with open boundaries*, *PoS LATTICE* **2016** (2016), [1701.05502].

[74] S. Gusken, *A Study of smearing techniques for hadron correlation functions*, *Nucl. Phys. Proc. Suppl.* **17** (1990) 361-364.

[75] F. Virotta, *Critical slowing down and error analysis of lattice QCD simulations*, *Doctoral dissertation*, Humboldt-Universität zu Berlin (2012).

[76] **ALPHA Collaboration**, U. Wolff, *Monte carlo errors with less errors*, *Comput. Phys. Commun.* **156** (2004) 143-153, [hep-lat/0306017].

[77] S. Lottini and R. Sommer, Lattice Practices 2014: *Data analysis in Lattice Field Theory*, lecture notes, DESY Zeuthen and HU Berlin, Zeuthen, March 2014.

[78] N. Madras and A. D. Sokal, *The pivot algorithm: A highly efficient Monte Carlo method for the self-avoiding walk*, *J. Stat. Phys.* **50** (1988) 109.

[79] M. Bruno, I. Campos, P. Fritzsch et al., *Light quark masses in $N_f = 2 + 1$ lattice QCD with Wilson fermions*, [1911.08025].

[80] S. Aoki, Y. Aoki, D. Becirevic et al., *Review of lattice results concerning low-energy particle physics*, *Eur. Phys. J.* **C77** (2017) no.2, 112, [1607.00299].

[81] **Particle Data Group Collaboration**, K. A. Olive et al., *Review of Particle Physics*, *Chin. Phys.* **C38** (2014) 090001.

[82] S. Aoki, Y. Aoki, D. Becirevic et al., *FLAG Review 2019*, [1902.08191].

[83] G. Rupak and N. Shoresh, *Chiral perturbation theory for the Wilson lattice action*, *Phys. Rev. D* **66** (2002) 054503, [hep-lat/0201019].

[84] O. Bär, G. Rupak and N. Shoresh, *Chiral perturbation theory at $\mathcal{O}(a^2)$ for lattice QCD*, *Phys. Rev. D* **70** (2004) 034508, [hep-lat/0306021].

[85] W. Bietenholz, V. Bornyakov, M. Göckeler et al., *Flavour blindness and patterns of flavour symmetry breaking in lattice simulations of up, down and strange quarks*, *Phys. Rev. D* **84** (2011) 054509, [1102.5300].

[86] J. Gasser and H. Leutwyler, *Quark masses*, *Phys. Rept.* **87** (1982) 77.

[87] C. Allton, D. J. Antonio and Y. Aoki, *Physical Results from $2 + 1$ Flavor Domain Wall QCD and $SU(2)$ Chiral Perturbation Theory*, *Phys. Rev. D* **78** (2008) 114509, [0804.0473].

[88] K. Fujikawa, *Path Integral Measure for Gauge Invariant Fermion Theories*, *Phys. Rev. Lett.* **42** (1979) 1195-1198.

[89] K. Fujikawa, *Path Integral for Gauge Theories with Fermions*, *Phys. Rev.* **D21** (1980) 2848, [Erratum: *Phys.Rev.* **D22**, (1980) 1499].

[90] M. F. Atiyah and I. M. Singer, *The Index of Elliptic Operators: V*, *Annals of Mathematics*, Second Series, **93** (1971) 139–149. **D22**, (1980) 1499].